DETECTORES DE SEMICONDUCTOR:

CALIBRACIÓN Y APLICACIONES A LA DOSIMETRIA IN VIVO EN PACIENTES SOMETIDOS A TRATAMIENTOS CON RADIOTERAPIA EXTERNA

Núria Jornet i Sala

Barcelona, Julio 2001

DETECTORES DE SEMICONDUCTOR: CALIBRACIÓN Y APLICACIONES A LA DOSIMETRIA IN VIVO EN PACIENTES SOMETIDOS A TRATAMIENTOS CON RADIOTERAPIA EXTERNA

Memoria presentada por Núria Jornet i Sala para optar al grado de Doctor en Física por la Universidad Autónoma de Barcelona,

Trabajo realizado en el Servei de Radiofísica i Radioprotecció del Hospital de la Santa Creu i Sant Pau de Barcelona bajo la dirección de la Dra. Montserrat Ribas, directora del Servei de Radiofísica i Radioprotecció del Hospital de la Santa Creu i Sant Pau y la tutoría del Profesor Francisco Fernández, Catedrático del área de Física Atómica, Molecular y Nuclear del departamento de Ciencias Físicas de la Universidad Autónoma de Barcelona.

Barcelona, 11 Mayo 2001.

Dra. Montserrat Ribas Dr. Francisco Fernandez

Agraïments

A en Xevi que m'ha animat i ajudat durant tot el temps que he treballat amb la tesi.

A la Dra Montserrat Ribas, sense el seu suport i ànim aquesta tesi no hagués estat possible. Amb ella he compartit moltes hores de mesures a l'accelerador i de discussió sobre els resultats dels experiments.

Al Professor Francisco Fernandez pel seu interés en la tesi i que ha fet possible que aquesta tesi que va començar com un projecte s'hagi dut a terme.

A la Teresa Eudaldo pel seu recolçament i pels seus inestimables comentaris sobre els treballs.

A en Pablo Carrasco pels seus comentaris sobre la tesi.

A totes les persones que composen el Servei de Radiofísica així com al equip del Servei de Radioterapia, especialment al Dr. Jordi Craven-Bartle, el seu director, pel interès en la posta en marxa del control de qualitat mitjançant la dosimetría *in vivo* amb detectors de semiconductor. Vull agraïr la col·laboració de tot el personal tècnic i mencionar especialment a l'Eulàlia Rial i a la Dolors Oller que son les infermeres que van participar inicialment en les mesures *in vivo*.

A la Dra. Mª Amor Duch y a la Dra. Mercé Ginjaume, per la seva colaboració en la validació dels algoritmes de càlcul mitjançant la mesura de la dosis amb dosímetres TL així com pel seus comentaris sobre la metodologia de calibració.

Al Dr. Göran Rikner que em va animar a escriure el meu primer article.

A totes les persones que de alguna manera han cooperat en la realització d'aquest treball.

Al Fons d'Investigació Sanitaria (projectes nº 94/0030-02 i nº 98/0047-02) per a la seva participació econòmica en aquest treball.

Als meus pares

FE DE ERRATAS

Capítulo 2, página 13: corriente inversa debida **a los** portadores minoritarios

Capítulo 2, página 15: En un diodo de tipo p (**unión N^+ P**) la región N está mucho más dopada que la región P.

Capítulo 2, fig. 2.2

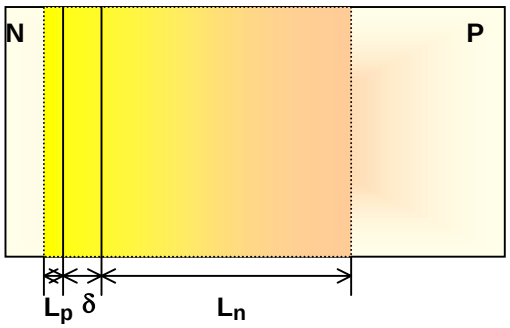

Fig. 2.2 Volumen de detección de un diodo tipo p.

Capítulo 2, página 16: La corriente adicional $\mathbf{I_L}$ se crea dentro de la zona de transición y dentro de la zona P de espesor $\mathbf{L_n}$.

Capítulo 2, página 23: La cámara cilíndrica tiene un factor (sobra la referencia a la cámara plano paralela).

Capítulo 2, página 33 (apartado 2.3.2): El primero, calcula la dosis **a plano medio**

Capítulo 3, tabla 3.2 (pie de tabla): diode calibrated to give dose at the depth of dose maximum, **1.4 cm** from entrance and exit relatively

Capítulo 6, página 113: The diodes are inserted in a plastic water phantom **at 10 cm depth** with their flat surface facing the beam. The source surface distance is then varied from 80 cm (**0.56 mGy/pulse**) to **(0.23 mGy/pulse**).

Capítulo 7, página 127: Esta asimetría tiene como consecuencia que el diodo **sobrestima** la dosis en este porcentaje…

ÍNDICE

CAPÍTULO 1

INTRODUCCIÓN

1.1 La radioterapia dentro de las distintas modalidades terapéuticas del tratamiento del cancer

La terapia génica, que consiste en introducir un gen activo en una célula para corregir una anomalía metabólica o para generar una nueva función, ha abierto nuevas posibilidades en el tratamiento del cáncer. Sin embargo, el progreso en este tipo de terapia se ve limitado por las técnicas de transferencia genética de las que se dispone en la actualidad. Debido a esto, muchas aplicaciones de la terapia génica son de difícil aplicación clínica con la tecnología actual. Por tanto, la radioterapia, la quimioterapia y la cirugía siguen siendo los tratamientos de elección en la mayoría de cánceres. El objetivo de la radioterapia con fin curativo es administrar una dosis tan alta como sea necesaria al tejido afectado de cáncer, protegiendo a su vez al máximo los tejidos sanos circundantes para causar los mínimos efectos secundarios al paciente tratado.

Desde el descubrimiento de los RX en 1895 se han utilizado las radiaciones ionizantes para el tratamiento del cáncer. Existen dos modalidades de Radioterapia: La Teleterapia y la Braquiterapia. La Braquiterapia consiste en administrar la dosis necesaria de radiación introduciendo las fuentes radioactivas en contacto con el tumor aprovechando una cavidad natural del organismo o directamente en el tejido afecto. En Teleterapia el tratamiento consiste en la irradiación del paciente con uno o varios haces de radiación externos (principalmente fotones y electrones) que provienen bien sea de un acelerador lineal o de una unidad de Co-60. Las direcciones de los haces de tratamiento, así como sus puertas de entrada, se escogen de tal manera que la irradiación del tejido afecto sea lo más homogénea posible y que el daño a órganos

críticos y tejidos sanos sea mínimo. La radioterapia conformada, que consiste en adaptar la forma del campo de radiación a las proyecciones geométricas del volumen que se quiere tratar, ha permitido aumentar las dosis al tumor sin aumentar las dosis al tejido sano circundante.

En esta última década, el desarrollo de la terapia con modulación de intensidad y la planificación inversa permite mejorar de forma significativa las distribuciones de dosis adaptándolas aún más al volumen que se quiere tratar reduciendo la dosis en los tejidos sanos circundantes.

Todos los procedimientos, cada vez más complejos, en la planificación y en la ejecución de los tratamientos con radioterapia contribuyen a aumentar la incertidumbre global en las distribuciones de dosis. El control de calidad, es por tanto, de vital importancia. El control de calidad durante la irradiación del paciente se puede desglosar en dos tipos de verificaciones: la verificación geométrica y la verificación dosimétrica

1.2 Verificación de los tratamientos con radioterapia externa

1.2.1 Verificación geométrica

La planificación de un tratamiento de radioterapia precisa de una representación de la anatomía del paciente así como de la delimitación de la zona que se quiere irradiar, ya sea el tumor o el lecho tumoral. Actualmente, esta información se obtiene a partir de imágenes de tomografía computarizada (TC), que permiten una reconstrucción tridimensional de la anatomía del paciente. A partir de estas imágenes se definirá el volumen que se quiere tratar, *planning target volume* (PTV) y se diseñarán los campos de irradiación necesarios para irradiar homogéneamente el PTV protegiendo tanto como sea posible los tejidos y órganos sanos circundantes. Las técnicas actuales de escalada de dosis van asociadas a una reducción de los PTV de tal manera que un error en el posicionamiento o en la forma de los campos de irradiación comportaría una subdosificación del PTV o una sobredosificación de los órganos o tejidos circundantes.

Las películas radiográficas de verificación o las imágenes adquiridas con un *electronic portal imaging device* (EPID) permiten verificar la forma y la localización del campo de tratamiento a partir de referencias óseas y compararlo con los campos planificados. Existen diversos estudios publicados que comparan las placas de simulación o las radiografias reconstruidas digitalmente (DRR), cuando se trata de una planificación virtual, con las placas de verificación o las imágenes del EPID así como trabajos que estudian la variabilidad diaria del volumen irradiado [1-4].

1.2.2 Verificación dosimétrica

La precisión en la dosis administrada juntamente con la precisión en la balística del tratamiento, es decir, que los campos de irradiación abarquen correctamente el PTV, son piezas clave en el éxito o fracaso de un tratamiento con radioterapia.

La relación entre la dosis administrada y su efecto biológico viene descrita por las curvas dosis-respuesta para el tumor y para los órganos o tejidos críticos. Normalmente, una dosis alta implica un buen control tumoral; sin embargo, el aumento de dosis está limitado por la tolerancia de los tejidos sanos que se irradian al mismo tiempo.

La precisión necesaria en la dosis administrada viene determinada por las curvas dosis-respuesta medidas clínicamente. El ICRU 24 [5] recomendaba una precisión de un ±5% en la dosis administrada al PTV basándose en la experiencia clínica disponible en 1975.

Posteriormente, en 1983, Goitein propuso considerar la incertidumbre de un 5% como 1,5 veces la desviación estándar (DE) [6]. Más tarde Brahme, basándose en modelos radiobiológicos calculó cual era la precisión con la que se tenía que administrar la dosis y llegó a la conclusión que para la mayoría de tumores, para obtener una desviación estándar absoluta menor de un 10% en la probabilidad de control tumoral, la desviación estándar en la dosis media administrada al PTV debía ser menor de un 5% [7,8]. Esta desviación se calcula como la combinación de las incertidumbres aleatorias y sistemáticas. Finalmente Mijnheer *et alt.* [9] proponen una desviación absoluta máxima de un 3.5 % en la dosis administrada en los tratamientos con finalidad radical.

La correspondencia entre la dosis prescrita y la dosis administrada al paciente sólo puede verificarse por medio de la dosimetría *in vivo*, es decir, medidas de dosis durante el tratamiento.

El primero en utilizar la dosimetría *in vivo* fue Sievert en el año 1932. Utilizaba pequeñas cámaras de ionización colocadas en cavidades fácilmente accesibles como el recto, la vagina, la cavidad oral o la vejiga y de esta manera realizaba medidas rutinarias.

En los primeros tiempos de la radioterapia, con equipos de RX de 200 kV, los cálculos de la dosis eran inciertos y la dosimetría se basaba en medidas efectuadas en la piel y en el centro del campo. La cámara de ionización era el dosímetro por excelencia, pero debido a la dificultad de su posicionamiento para realizar medidas *in vivo* y principalmente por el peligro potencial de electrocución del paciente, se dejaron de hacer medidas de dosis durante los tratamientos.

En los años sesenta y setenta, gracias a la introducción de los dosímetros basados en la termoluminescencia (TLD) para medir la dosis absorbida en radioterapia, se le da un nuevo impulso a la dosimetría *in vivo*. En el año 1976 Rudén, evalúa el uso de los TLD para la dosimetría *in vivo* [10].

Posteriormente, en los años ochenta, a raíz de los trabajos publicados por Rikner y Grussell [11-16] sobre la utilización de detectores de semiconductor, diodos, para la medida de la dosis, se empieza a investigar la posibilidad de utilizar este tipo de detectores para la dosimetría *in vivo* [17-25]. La ventaja de los diodos sobre los TLD es que los primeros son de lectura inmediata. Esto permite, en el caso de que se detecte una diferencia entre la dosis medida por el detector y la dosis prescrita, comprobar todos los parámetros del tratamiento mientras el paciente aún está en la sala de tratamiento.

Aunque en la actualidad los diodos y los TLD son los detectores más utilizados para la dosimetría *in vivo*, se están estudiando otros métodos alternativos como la utilización de los EPID [26-31], de centelleadores plásticos, detectores de alanina y de diamante [32].

1.3 Finalidades de la dosimetria *in vivo*.

Las medidas de dosis *in vivo* se realizan con dos finalidades. En primer lugar, se utilizan como una parte de los programas de control de calidad en radioterapia. Se compara la dosis medida con la dosis esperada, según la planificación del tratamiento, en el mismo punto. En segundo lugar, se utilizan para conocer la dosis recibida en un punto en donde no es posible determinarla con precisión por los sistemas informáticos habituales de planificación en radioterapia (PRT). Este sería el caso de la dosimetría en técnicas especiales tales como la irradiación corporal total (ICT) y la irradiación de piel total (IPT).

La dosimetría *in vivo*, como parte del control de calidad de los tratamientos estándar, permite tanto detectar errores humanos tales como intercambiar una técnica de tratamiento a distancia fuente piel constante (DFP) por una técnica isocéntrica, inexactitudes en la toma del contorno del paciente, etc., como detectar problemas técnicos como, por ejemplo, que la tasa de dosis del acelerador no sea estable. Así, Bascuas *et alt*. [33] averiguaron que las diferencias encontradas entre la dosis medida y la dosis prescrita eran debidas a una variación en la recombinación de iones en las cámaras monitoras del acelerador y variaciones en la cantidad de electrones dispersados que incidían en las paredes de estas cámaras cuando se variaba la energía, la posición del brazo o la tasa de dosis.

Dependiendo del tipo de errores que se quieren detectar se realizarán medidas en la entrada de los haces de tratamiento exclusivamente o bien medidas combinadas entrada/salida. Las medidas en la entrada permiten detectar errores tales como variaciones en la tasa de dosis de las unidades de tratamiento, cálculos erróneos de la dosis de entrada por el planificador, errores en la transcripción de datos de la planificación a la hoja de tratamiento y/o errores en la ejecución del tratamiento (DFP, filtros en cuña, protecciones, energía, tiempo o unidades monitor, tamaño de campo). Las medidas de dosis combinadas permiten, además, detectar variaciones en el grosor del paciente y errores inherentes a los modelos de cálculo de dosis del planificador (i.e. correcciones por heterogeneidad). Existen distintos grupos que han publicado los errores que han detectado mediante dosimetria *in vivo* en series de pacientes para distintas localizaciones [18-23, 34-39].

Las técnicas especiales reciben este nombre porque se apartan de las técnicas estándar de tratamiento. En el caso de la ICT [40] y de la IPT cada centro diseña la técnica en función de sus posibilidades tecnológicas para conseguir una distribución de dosis homogénea en el paciente y que la dosis en los órganos de riesgo no supere sus niveles de tolerancia. Como la técnica estará condicionada por los recursos y equipamiento de cada centro (tamaño del *bunker*, tipo de haz de radiación, etc.), la mayoría de sistemas de planificación comercializados no disponen de ninguna opción para el cálculo de dosis en este tipo de tratamientos de forma fiable. Se ha de tener en cuenta, también, que como son tratamientos de larga duración (5 o 6 minutos de irradiación cuando se utiliza una técnica fraccionada o casi una hora si se administra toda la dosis en una sesión) los movimientos del paciente no son despreciables. Por todas estas razones, la monitorización de la dosis mediante dosimetría *in vivo* es imprescindible para conocer la dosis en los puntos de interés, sobre todo en los pulmones, donde las curvas dosis-efecto son muy pronunciadas y un exceso de dosis podría inducir una neumonitis intersticial radiógena.

1.4 Objetivos de este estudio

El objetivo de este estudio es la calibración de diodos, para ser utilizados en dosimetria *in vivo* en haces de fotones de alta energía, en diversas situaciones, la mayoría de ellas no descritas en la literatura:

En primer lugar se calibra un conjunto de diodos para determinar la dosis entrada y salida en la técnica específica de ICT (capítulo 3). Se hace especial hincapié en la calibración de los diodos detrás de protecciones a pulmón de transmisión parcial.

En el capítulo 4 se desarrolla un algoritmo de cálculo para calcular las dosis a plano medio a partir de las dosis *in vivo* en ICT. Se presentan resultados en una serie de pacientes. Se comprueba la aplicabilidad de este algoritmo en presencia de heterogeneidades (pulmón) y detrás de protecciones de transmisión parcial. Se compara este algoritmo con el algoritmo propuesto por Rizzoti *et alt.* [41].

La calibración de diodos para altas energías de RX en técnicas estándar de tratamiento se trata en los capítulos 5 y 6. En el capítulo 5 se comparan dos tipos de diodos diseñados para trabajar con RX de 16-25 MV. En el capítulo 6 se amplía esta

comparación a 4 tipos de diodos comercializados y también se presenta la calibración de un diodo para trabajar con haces de RX de energías comprendidas entre 4-8 MV. Este capítulo corresponde a la recopilación de la experiencia del Hospital de la Santa Creu i Sant Pau en la calibración de diodos para medir la dosis in vivo a la entrada en técnicas estándar así como en la implementación de la dosimetría in vivo en la rutina clínica. Esta recopilación hace inevitable que se repitan, aunque con más detalle, algunos de los procedimientos de calibración citados en capítulos anteriores.

Ha sido también objetivo del capítulo 5 matizar una tesis propuesta por G. Rikner y E. Russell [11, 13, 14, 16] que hace referencia a la inferioridad desde el punto de vista dosimétrico de los diodos tipo n, en un nuevo diodo n comercializado por Pecitron en 1997.

1.5 Bibliografía

[1] J. M. Balter, H. M. Sandler, K. Lam, R. L. Bree, A. S. Llichter y R. K. Ten Haken. **Measurement of prostate movement over the course of routine radiotherapy using implanted markers.** Int.J. Radiat. Oncol. Biol. Phys. 31: 113-118, 1995.

[2] C. J. Beard, P. Kijewski, M. Bussière, R. Gelman, D. Gladstone, K. Shaffer, M. Plunkett, P. Costello y C.N. Coleman. **Analysis of prostate and seminal vesicle motion: Implications for treatment planning**. Int. J. Radiat. Oncol. Biol. Phys. 34: 321-332, 1996.

[3] E. Melian, G. J. Kutcher, S. A. Leibel, M. Zelefsky, B. Baldwin y Z. Fuks. **Variation in prostate position: quantification and implications for three-dimensional conformal treatment planning**. Int. J. Radiat. Oncol. Biol. Phys. 38: 73-81, 1997.

[4] J. C. Roeske, J. D. Forman, C. F. Mesina, T. He, C. A. Pelizzari, E. Fontenla, S. Vijayakumar y G. T. Y. Chen. **Evaluation of changes in the size and location of the prostate, seminal vesicles, bladder and rectum during a course of external beam radiation therapy**. Int. J. Radiat. Oncol. Biol. Phys. 33: 1321-1329, 1995.

[5] ICRU report 24. **Determination of absorbed dose in a patient irradiated by means of X or gamma rays in radiotherapy procedures**. Technical report, International Commission on Radiotherapy Units and Measurements, 1976.

[6] M. Goitein. **Nonstandard deviations**. Med. Phys., 709-711, 1983.

[7] A. Brahme. **Dosimetric precision requirements in radiation therapy**. Acta Radiol Oncol, 23:379-391 1984.

[8] A. Brahme. **Accuracy requirements and quality assurance of external beam therapy with photons and electrons**. Acta Oncologica, suppl. nº 1, capítulo 2: 9-15, 1988.

[9] B. J. Mijnheer, J. J. Battermann and A. Wambersie. **What degree of accuracy is required and can be achieved in photon and neutron therapy?** Radiother. Oncol, 8:237-252, 1998.

[10] B. I. Rudén. **Evaluation of the clinical use of TLD**. Acta Radiol. Ther. Phys. Biol., 15: 447-464, 1976.

[11] G. Rikner. **Silicon diodes as detectors in relative dosimetry of photon, electron and proton radiation fields**. PhD Tesis, Uppsala University, Suecia, 1983.

[12] G. Rikner y E. Grusell. **General specifications for silicon semiconductors for use in radiation dosimetry**. Phys. Med. Biol., 32: 1109-1117, 1987.

[13] G. Rikner y E. Grusell. **Effects of radiation damage on p-type silicon detectors. Phys. Med. Biol.**, 28: 1261-1267, 1983.

[14] E. Grusell y G. Rikner. **Radiation damage induced dose rate non-linearity in an n-type silicon detector**. Acta Radiol. Oncol. 23: 465-469,1984.

[15] E. Grusell y G. Rikner**. Evaluation of temperature effects in p-type silicon detectors**. Phys. Med. Biol. 38: 785-792, 1986.

[16] E. Grusell y G. Rikner. **Linearity with dose rate of low resistivity p-type silicon semiconductor detectors**. Phys. Med. Biol. 38: 785-792, 1993.

[17] S. Heukelom, J.H. Lanson y B.J. Mijnheer. **Comparison of entrance and exit dose measurements using ionization chambers and silicon diodes**. Phys. Med. Biol. 36: 47-59, 1991.

[18] S. Heukelom, J.H. Lanson y B.J. Mijnheer. ***In vivo* dosimetry during pelvic treatments**. Radiother. Oncol. 25: 111-120, 1992.

[19] M. Essers, R. Keus, J.H. Lanson y B.J. Mijnheer. **Dosimetric control of conformal treatment of parotid gland tumors**. Radiother. Oncol., 32: 154-162, 1994.

[20] M. Essers, J.H. Lanson, G. Leunens, T. Schnabel y B.J. Mijnheer. **The accuracy of CT-based inhomogeneity corrections and *in vivo* dosimetry for the treatment of lung cancer**. Radiother. Oncol., 37: 199-208, 1995.

[21] M. Essers, J.H. Lanson y B.J. Mijnheer. ***In vivo* dosimetry during conformal therapy of prostatic cancer**. Radiother. Oncol., 29: 271-279, 1993.

[22] G. Leunens, A. Dutreix, E. Van der Schueren. **Quality assurance in radiotherapy by *in vivo* dosimetry. 1. Entrance dose measurements, a reliable procedure**. Radiother. Oncol. 17; 141-151, 1990.

[23] G. Leunens, A. Dutreix, E. Van der Schueren. **Quality assurance in radiotherapy by *in vivo* dosimetry. 2. Determination of the target absorbed dose**. Radiother. Oncol. 19; 73-87, 1990.

[24] J. Van Dam y G. Marinello. **Methods for *in vivo* dosimetry in external radiotherapy**. Physics for clinical radiotherapy. Booklet nº 1 ESTRO, 1994.

[25] N. Jornet**. Calibració d'un conjunt de díodes per a la dosimetria *in vivo***. Treball de recerca, Barcelona, 1996.

[26] M. Kroonwijk, K. L. Pasma, S. Quint, P. C. M. Koper, A. G. Visser y V. J. M. Heijmen**. *In vivo* dosimetry for prostate cancer patients using an electronic portal imaging device (EPID): detection of internal organ motion.** Radiother. Oncol. 49: 125-132, 1998.

[27] K. L. Pasma, M. Droonwijk, S. Quint, A. G. Visser y V. J. M. Heijmen**. Transit dosimetry with an electronic portal imaging device (EPID) for 115 prostate cancer patients.** Int. J. Radiat. Oncol. Bio. Phys.,

[28] K. L. Pasma, B. J. M. Heijmen, M. Kroonwijk y A. G. Visser**. Portal dose image (PDI) prediction for dosimetric treatment verification in radiotherapy I: An algorithm for open beams**. Med. Phys., 25: 830-840, 1998.

[29] R. Boellaard, M. van Herk y B. J. Mijnheer. **A convolution model to convert transmission dose images to exit dose distributions**. Med. Phys., 24: 189-199, 1997.

[30] R. Boellaard, M. van Herk, H. Uiterwaal y B. J. Mijnheer. **New method to obtain the midplane dose using portal *in vivo* dosimetry**. Int. J. Radiat. Oncol. Biol. Phys., 41: 465-474, 1998.

[31] R. Boellaard, M. van Herk, H. Uiterwaal y B. J. Mijnheer. **First clinical tests using a liquid-filled electronic portal imaging device and a convolution model for the verification of the midplane dose**. Radiother. Oncol., 47:303-312, 1998.

[32] G. Garavaglia, K. A. Johansson, G. Leunens, B. J. Mijnheer. **The role of *in vivo* dosimetry**. Radiother. Oncol. 29: 281-282, 1993.

[33] J. L. Bascuas, J. Chavaudra. G. Vauthier y J. Dutreix. **Interêt des mesures *in vivo* systematiques en radiotherapie**. J. Radiol. Electrol. 58: 701-708,1977.

[34] C. Fiorino, D. Corletto, P. Mangili et al. **Quality Assurance by systematic *in vivo* dosimetry: results on a large cohort of patients**. Radiother. Oncol. 56: 85-95, 2000.

[35] S. Heukelom, J. H. Lanson, G. Van Tienhoven y B. J. Mijnheer**. *In vivo* dosimetry during tangential breast treatment**. Radiother. Oncol. 22: 269-279, 1991.

[36] S. Heukelom, J. H. Lanson y B. J. Mijnheer. **Quality assurance of the simultaneous boost technique for prostatic cancer: dosimetric aspects.** Radiother. Oncol. 30: 74-82, 1994.

[37] B. J. Mijnheer, S. Heukelom, J. H. Lanson, L. J. Van Battum, N. A. M. Van Bree y G. Van Tienhoven**. Should inhomogeneity corrections be applied during treatment planning of tangential breast irradiation?** Radiother. Oncol. 22: 239-244, 1991.

[38] A. Noel, P. Aletti, P. Bey y L. Malissard. **Detection of errors in individual patients in radiotherapy by systematic *in vivo* dosimetry**. Radiother. Oncol. 34: 144-151, 1995.

[39] J. T. Shakeshaft, H. M. Morgan, P.D. Simpson. ***In vivo* dosimetry using diodes as a quality control tool: experience of 2 years and 2000 patients**. Br. J. Radiol. 72: 891-895, 1999.

[40] F. Sánchez-Doblado, U. Quast, R. Arráns, L. Errazquin, B. Sánchez-Nieto y J. A. Terrón. **Total body irradiation prior to bone marrow transplantation**. EBMT, Sevilla, 1995.

[41] G. Rizzotti, C. Compri y G. F. Garussi. **Dose evaluation to patients irradiated by Co-60 beams, by means of direct measurements on the incident and on the exit surfaces**. Radiother. Oncol. 3: 279-283, 1985.

CAPÍTULO 2

MATERIAL I MÉTODO

2.1 Introducción

Dado que la teoría de semiconductores, y en particular la de diodos de unión, está ampliamente descrita en multitud de trabajos [1-4] y no es objetivo de está tesis profundizar en ella, sólo se tratarán los aspectos relevantes relacionados con el objetivo de la misma, es decir, la utilización de los diodos como detectores de radiación ionizante.

2.1.1 El diodo como detector de radiación.

Cuando se expone un diodo a una radiación electromagnética de longitud de onda suficiente para que la energía transportada por un fotón sea superior a la energía mínima necesaria para crear un par electrón-hueco, las interacciones de los fotones con la red cristalina producirán un aumento en el número de portadores minoritarios que atraviesan la unión. Estos portadores crearán una corriente adicional I_L (intensidad de corriente de ionización). El valor de esta corriente depende del número de pares electrón-hueco creados por unidad de tiempo, y por tanto del número de fotones incidentes por unidad de tiempo. Por lo tanto, midiendo el valor de esta corriente, o de una cantidad relacionada, se puede obtener una indicación de la tasa de dosis a la que ha sido irradiado el diodo [1].

En la figura 2.1 se puede ver la intensidad de corriente en función de la tensión aplicada cuando la unión está o no está irradiada. La corriente de fugas (corriente inversa debida portadores minoritarios) en el diodo polarizado inversamente

experimenta una gran variación dependiendo de que dicho diodo se encuentre irradiado o no. Esta variación de la corriente inversa es la que se utiliza como señal de detección. En el caso de los diodos utilizados para dosimetría *in vivo* en nuestro ámbito este voltaje es cero, ya que los diodos operan cortocircuitados. La energía media necesaria para crear un par electrón-hueco es de unos 3.6 eV. Esta energía es superior a la energía del *gap* ya que una parte de esta energía se cede al electrón en forma de energía cinética y otra parte cederá energía a los fonones de la red cristalina.

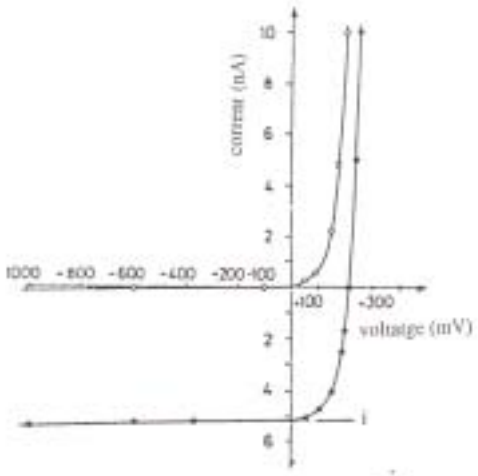

Fig. 2.1 Características de un diodo trabajando cuando se irradia (•) y cuando no se irradia (o).

Para que exista esta corriente suplementaria (I_L), es necesario que los portadores de carga minoritarios creados puedan atravesar la unión. Es, pues, necesario que sean creados en la zona de transición o suficientemente cerca de tal manera que puedan llegar a ella antes de desaparecer por recombinación o por captura de alguno de los defectos de la red cristalina.

Es pues necesario, definir una vida media τ de los portadores minoritarios dentro de su medio:

- τ_p vida media de los huecos dentro de la región N (en donde los huecos son minoritarios).
- τ_n vida media de los electrones dentro de la región P (en donde los electrones son minoritarios).

Y una longitud de difusión **L**:

- L_p longitud de difusión de los huecos dentro de la región N.

- $\mathbf{L_n}$ longitud de difusión de los electrones dentro de la región P.

La ley de Fick liga estas magnitudes con la movilidad (μ) y la temperatura absoluta **T**.

$$L_p = (k \cdot T \cdot \mu_p \cdot \tau_p \cdot e^{-1})^{\frac{1}{2}} \qquad \text{Ec. 2.1}$$

en donde **e** es la carga del electrón y **k** una constante.
La misma expresión substituyendo la p por la n puede aplicarse para $\mathbf{L_n}$.

El volumen útil dentro del cual todos los pares electron-hueco creados contribuirán a la corriente $\mathbf{I_L}$ está limitado por las longitudes $\mathbf{L_p}$ y $\mathbf{L_n}$ desde las superficies que delimitan la zona de transición de espesor δ. El espesor del volumen de detección viene dado por la siguiente expresión:

$$\text{Volumen de detección} = A \cdot (L_p + L_n + \delta) \qquad \text{Ec. 2.2}$$

En donde A es la superficie de la unión.

La intensidad de corriente de ionización $\mathbf{I_L}$ depende del número **g** de portadores de carga minoritarios, creados en exceso por la irradiación, por unidad de tiempo y de volumen.

$$I_L = e \cdot g \cdot A \cdot (L_p + L_n + \delta) \qquad \text{Ec. 2.3}$$

En un diodo de tipo p (unión P^+N) la región N está mucho más dopada que la región P. Por lo tanto en un diodo de tipo p la probabilidad de que un hueco de la región N (portador minoritario) se recombine es más grande que la probabilidad de recombinación de un electrón en la región P, ya que en la región N hay muchas más trampas e impurezas y los huecos son capturados justo después de su creación. En consecuencia, la vida media de un hueco en la zona N (τ_p) es mucho más pequeña que la de un electrón libre dentro de la zona P (τ_n). Esto implica que $\mathbf{L_p} >> \mathbf{L_n}$ (fig. 2.2).

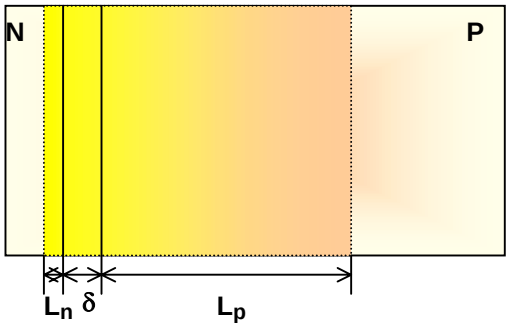

Fig. 2.2 Volumen de detección de un diodo tipo p.

Por tanto, en un diodo de tipo p, la contribución de los huecos a la corriente de ionización es prácticamente despreciable. La corriente adicional $\mathbf{I_L}$ se crea dentro de la zona de transición y dentro de la zona P de espesor $\mathbf{L_p}$. En general esta última es mucho más grande que δ. Esto explica que las uniones N^+P reciban el nombre de diodos tipo p y las uniones P^+N reciban el nombre de diodos tipos n.

2.1.2 Efecto de las radiaciones de alta energía sobre el diodo

La dosimetría de las radiaciones ionizantes con diodos se basa en la creación de pares electrón-hueco dentro del volumen de detección del detector. Por tanto, la sensibilidad del diodo depende de las dimensiones del volumen efectivo de detección.

La excitación de los electrones de las capas externas de los átomos y la ionización de los mismos es, de hecho, la principal manifestación de la interacción radiación-semiconductor. Pero, cuando la radiación incidente está constituida por partículas de alta energía también se deben considerar las interacciones de la radiación con los átomos de Silicio que se traducen en un desplazamientos de los mismos creando vacíos (lagunas) o parejas atómicas intersticiales dentro de la red. Estas dislocaciones modifican las propiedades del cristal y actúan como trampas o centros de recombinación. Un efecto bien conocido de estas modificaciones es la pérdida de sensibilidad de este tipo de detectores a medida que son irradiados. Esto se debe a que se produce una disminución en la longitud de difusión y por tanto en el volumen efectivo de detección.

2.2 Material

En este apartado se describe brevemente el material utilizado en los distintos artículos de los que se compone este trabajo de investigación.

2.2.1 Sistemas de detección

2.2.1.1 Sistema de dosimetría in vivo mediante detectores de semiconductor

El sistema de dosimetría *in vivo* se compone de un electrométro y de diversos tipos de detectores de semiconductor (diodos).

Electrómetro

El electrómetro utilizado es el DPD510 comercializado por Scanditronix. Es un electrómetro de 10 canales.

Para medidas de precisión es tan importante el electrómetro como los diodos. Para minimizar las corrientes de fuga, los diodos no se polarizan. Sin voltaje de polarización externo, se puede medir la respuesta del diodo en cortocircuito (corriente) o con el circuito abierto (voltaje). El electrómetro utilizado opera en modo corriente, de esta forma tenemos una relación lineal entre la carga generada y la dosis. Al operar cortocircuitado el electrómetro debe tener una impedancia muy baja, en este caso cero. Como la señal del diodo es alta el electrómetro no necesita tener una ganancia demasiado alta. En la figura 2.3 se representa el diagrama de un electrómetro operando de la manera descrita.

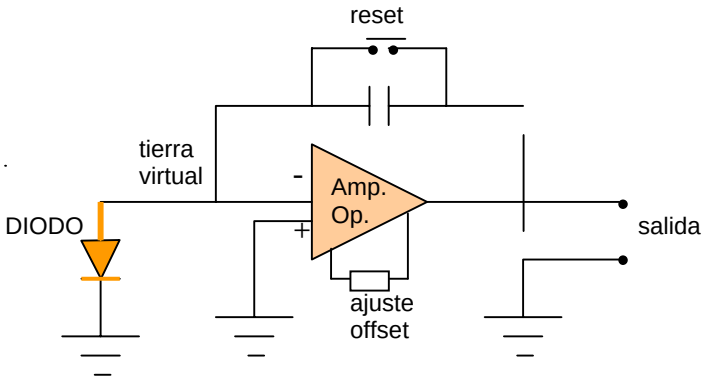

Fig. 2.3 Diagrama de un electrómetro operando en modo de cortocircuito apropiado para la medida de la dosis utilizando diodos.

En la tabla 2.1 se resumen las características de medida del electrómetro DPD510 suministradas por el fabricante.

Tabla 2.1 Características de medida del DPD510 (Scanditronix)

Característica	Valor
Modalidades de medida	Dosis absoluta, tasa de dosis
Unidades disponibles	Gy o rads
Rangos de medida	1mGy hasta 20 Gy
	(cambio de rango automático)
Resolución	0,001 Gy

Detectores de semiconductor (diodos)

En el desarrollo de los diversos artículos se han utilizado diversos tipos de diodos comercializados para dosimetría *in vivo*. Un diodo consiste de un chip de silicio (el diodo propiamente dicho) y de un capuchón. Este capuchón además de proteger el diodo, que es muy frágil, garantiza que el diodo mida en condiciones de equilibrio electrónico. Esta es la razón por la que una misma casa comercial ofrece distintos detectores adaptados a distintos rangos de energías (fig. 2.4). La única diferencia entre estos detectores es su capuchón de equilibrio electrónico.

Fig. 2.4. Fotografía de los distintos tipos de diodos que ofrece Scanditronix. De izquierda a derecha EDD2 (haces de electrones), EDE5 (Co-60), EDP0 (dosis piel), EDP10 (RX 4-8 MV), EDP15 (6-12 MV), EDP20 (RX 8-16 MV), EDP30 (RX 16-25 MV).

Cuando se utilizan diodos como dosímetros se debe tener en cuenta los distintos factores que tienen influencia sobre su respuesta:

A*. *Factores que modifican la respuesta del diodo debidos a la naturaleza del mismo (chip de Silicio):

- La energía del haz de fotones. El número atómico del silicio (Z=14) es más alto que el del tejido blando ($Z_{efectiva} \approx 7$) y por tanto, el número de electrones creados por efecto fotoeléctrico será más alto en el silicio que en el tejido blando cuando la energía varía.

- La tasa de dosis. A tasas de dosis altas los centros de recombinación estarán ocupados y por tanto, se tendrá una menor tasa de recombinación, induciendo, por tanto, una mayor respuesta del diodo a estas tasas.

- La temperatura. Cuando se aumenta la temperatura, algunos electrones que están atrapados en centros de recombinación, que están dentro del *gap*, tienen suficiente energía para pasar a la banda de conducción y contribuir a la respuesta del diodo. Por tanto, la sensibilidad del diodo aumenta al aumentar la temperatura. Este efecto es menos pronunciado para un diodo no irradiado (menor número de centros de recombinación) y aumenta a medida que el diodo acumula dosis. Sin embargo, el cambio de sensibilidad en función de la temperatura tiende a estabilizarse a medida que la dosis acumulada aumenta.

- El tipo. Los diodos tipo n son unas 4-5 veces más sensibles que los diodos tipo p. El tipo de diodo también se ha asociado a la dependencia de la sensibilidad con la tasa de dosis [5, 6].

- El nivel de dopaje. Afectará también la sensibilidad del diodo y está relacionado con la dependencia de la sensibilidad con la tasa de dosis y de la variación de esta sensibilidad con la dosis acumulada [7, 8].

- Dosis acumulada. Tal y como se ha explicado en el apartado 2.1.2 la radiación es la causa también de la creación de nuevos centros de recombinación. Por tanto, a medida que la dosis acumulada aumenta, los centros de recombinación aumentan y la sensibilidad del diodo disminuye. Esta disminución es muy pronunciada con los primeros Gy y se suaviza a medida que la dosis acumulada aumenta. Debido a

esto, los diodos se suministran preirradiados. Se intenta así que los diodos tengan una respuesta independiente de la dosis acumulada.

La dosis acumulada puede también modificar la respuesta del diodo en función de la energía y de la tasa de dosis.

B. ***Factores que modifican la respuesta del diodo debidos al capuchón de equilibrio electrónico****:*

- El ángulo de incidencia de la radiación sobre el diodo. La forma del capuchón de equilibrio electrónico determina la dependencia angular de la respuesta del diodo. De esta manera un diodo con capuchón cilíndrico tiene una dependencia angular muy distinta a la de otro con un capuchón semiesférico.

- Contaminación electrónica. Si el capuchón de equilibrio electrónico no tiene un espesor equivalente agua igual al de la profundidad del máximo de dosis absorbida para la energía de fotones utilizada, el diodo sobrestimará la dosis debido a que detectará electrones que la cámara de referencia situada a la profundidad del máximo de dosis no detectará.

Para la elaboración de este trabajo se ha utilizado un tipo de diodo para haces de RX entre 4 y 6 MV (tabla 2.2) y cuatro tipos de diodos distintos diseñados para trabajar en haces de RX de alta energía (entre 16-25 MV) (tabla 2.3). En las tablas 2.2 y 2.3 se detallan las características técnicas más relevantes de cada uno de estos diodos proporcionadas por el fabricante. La figura 2.5 muestra la fotografía de este conjunto de diodos.

Fig. 2.5 De izquierda a derecha EDP10, EDP30, P30, isorad-p, QED.

Tabla 2.2 Características técnicas de los diodos utilizados en haces de RX de 6 MV según el fabricante

	EDP 10 (Scanditronix)
Tipo	p
Forma del capuchón de equilibrio electrónico	Semiesférico
Composición del capuchón de equilibrio electrónico	Epoxi 0,75 mm de acero inoxidable
Espesor equivalente agua del capuchón de equilibrio electrónico	10 mm
Resistividad	0,2 ohm·cm
Sensibilidad	40 nC/Gy
Espesor del volumen de detección	60 μm
Area efectiva de detección	1,76 mm^2
Preirradiación	Electrones de 10 MeV 8 kGy

Tabla 2.3 Características técnicas de los diodos utilizados en haces de RX de 18 MV según el fabricante

	EDP 30 (Scanditronix)	P30 (Precitron)	**QED** 1116 (Sun Nuclear)	**Isorad-p** 1164 (Sun Nuclear)
Tipo	p	n	p	p
Forma del capuchón de equilibrio electrónico	Semiesférico	Semiesférico	Semiesférico	Cilíndrico
Composición del capuchón de equilibrio electrónico	1mm de Tantalio	0,5 mm poliacetal 1,6 mm tungsteno 2,4 mm epoxi	0,7 mm epoxi 3,4 mm Cu	1,3 mm tungsteno
Espesor equivalente agua del capuchón de equilibrio electrónico	30 mm	30 mm	30 mm	25,8 mm
Resistividad	0,2 Ohms·cm	-	0,8 Ohms·cm	0,8 Ohms·cm
Sensibilidad	40 nC/Gy	150-300 nC/Gy	40 nC/Gy	40 nC/Gy
Espesor del volumen de detección	60 μm	100 μm	50 μm	50 μm
Area efectiva de detección	1,76 mm^2	6,8 mm^2	2,65 mm^2	2,72 mm^2
Preirradiación	Electrones de 10 MeV 8 kGy	Electrones de 10 MeV 25 kGy	Electrones de 10 MeV 10 kGy	Electrones de 10 MeV 10 kGy

2.2.1.2 Sistema ionométrico

Los diodos se calibran comparando su respuesta con la dosis determinada con un sistema ionométrico. Este sistema consta de:

Un electrómetro de la firma Nuclear Enterprise (N.E.) modelo DOSELEADER conectado a una cámara de ionización cilíndrica de tipo dedal de 0,6 cm^3 modelo N.E. 2571.

Tanto la cámara cilíndrica como la cámara plano-paralela conectadas al electrómetro tienen un factor de calibración trazable al Laboratorio Oficial de Metrología en España (CIEMAT). Para la determinación de la dosis absoluta se sigue el Protocolo Español elaborado por el comité de Dosimetría en Radioterapia de la SEFM [9, 10].

Se trabaja con el electrómetro midiendo carga ya que el laboratorio de metrología da el factor de calibración del conjunto cámara-electrómetro en mGy/nC.

2.2.1.3 Emulsiones fotográficas y filmdensitómetro

Para estudiar la perturbación causada por los diodos a una cierta profundidad dentro del paciente se utilizan las emulsiones radiográficas. En particular se utilizan las películas X-Omat V. Esta película se suministra en un embalaje de papel (ready-pack) y es sensible a la irradiación directa con rayos X. Son películas de emulsión doble.

El densitómetro utilizado para leer las películas es de la firma comercial Scanditronix. Este densitómetro automático forma parte del equipo analizador de campos de irradiación RFA-300. El densitómetro se monta sobre el maniquí de agua, ajustándose en el soporte del detector y tiene la posibilidad de moverse en el plano x-y mediante un servosistema.

Previo a su utilización, este sistema ha sido sometido a pruebas de aceptación y calibrado [11].

2.2.1.4 Sistema de detección mediante detectores termoluminiscentes

Los detectores termoluminiscentes se utilizan para comprobar los algoritmos de cálculo de dosis a plano medio. La calibración de los detectores termoluminiscentes (detectores o dosímetros TL) con haces de fotones y electrones de alta energía se ha realizado comparando la respuesta termoluminescente de los dosímetros con los valores de dosis de referencia proporcionados por un sistema ionométrico con un factor de calibración trazable al laboratorio de referencia Español (CIEMAT). En el Laboratorio de Dosimetría y Calibración del Instituto de Técnicas Energéticas de la Universidad Politécnica de Catalunya (INTE-UPC) se ha realizado la lectura de los dosímetros, así como irradiaciones periódicas con haces de Cs-137 para la asignación de factores de calibración individuales para cada detector y el control de estabilidad de los mismos[12-15].

El sistema dosímetrico termoluminiscente consta de:

- Cristales de fluoruro de litio de dimensiones 3,1 x 3,1 x 0,9 mm^3 del tipo LiF TLD 700 (Harshaw). La utilización de Li-7 elimina la posible contribución neutrónica.

- Lector semiautomático modelo Rialto (Vinten). Este lector consta de dos canales independientes de lectura, carrusel para 30 dosímetros y sistema de calentamiento por resistencia.

- Horno de borrado de PTW. Su ciclo de borrado está controlado por un microprocesador.

El proceso de lectura de los dosímetros TL se lleva a cabo de la forma siguiente: Antes de cada irradiación tiene lugar un tratamiento de borrado en el horno, primero a 400ºC durante una hora y luego a 100ºC durante dos horas.

Después de la irradiación, la lectura de los dosímetros tiene dos partes: una zona de precalentamiento a 135ºC y 10s y una zona de lectura de 135ºC a 270ºC con una velocidad de calentamiento de 25ºC/s durante 12s.

Con el fin de mejorar la precisión de la lectura se calibra cada detector TL independientemente, se le asigna un factor de calibración individual y se realizan controles de estabilidad del sistema dosimétrico con una fuente de Cs-137 periódicamente. La incertidumbre en la determinación de la dosis con estos dosímetros es de un 3% (1 DE).

2.2.2 Maniquíes

Para la calibración de diodos se utilizan maniquíes sólidos de láminas (poliestireno y *plastic water*). Los maniquíes utilizados disponen de láminas con una hendidura para poder insertar las cámaras de ionización.

Para estudiar como influye la temperatura en la respuesta del diodo se utiliza un maniquí de agua y por último, para verificar los algoritmos de dosis a plano medio a partir de medidas *in vivo*, se utiliza un maniquí antropomórfico tipo Rando-Alderson.

2.2.2.1 Maniquíes de poliestireno

Se utilizan dos maniquíes de láminas de poliestireno blanco. Las láminas tienen una superficie de 30 x 30 cm^2 en el primero y de 50 x 50 cm^2 en el segundo y grosores de 1 mm, 4 mm y 5 mm. Se pueden conseguir maniquíes de distintos espesores apilando distintos números de láminas. Estas láminas han sido mecanizadas en el propio hospital. En la figura 2.6 se muestra uno de los maniquíes de poliestireno. Se dispone de láminas especiales para la inserción de la cámara cilíndrica (fig. 2.6) y para un diodo (fig. 2.7).

Fig. 2.6 Maniquí de láminas de poliestireno con la lámina de inserción para una cámara cilíndrica de 0.6cc.

Fig. 2.7 Lámina de inserción para un diodo semiesférico.

El espesor equivalente agua de distintos grosores de poliestireno se obtiene de la aplicación de la siguiente expresión:

$$e_{agua} = e_{poliestireno} \cdot \rho_{poliestireno} \cdot \frac{\eta_{poliestireno}}{\eta_{agua}} \qquad \text{Ec. 2.4}$$

En donde: e es el espesor, ρ es la densidad másica y η es el número de electrones por unidad de masa.

Sustituyendo ρ y η por sus valores se obtiene el siguiente factor de conversión:

$$e_{agua} = e_{poliestireno} \cdot 1{,}0372 \qquad \text{Ec. 2.5}$$

Se considera que aplicando este factor de escala no es necesario aplicar un factor de conversión dosis poliestireno-dosis agua.

2.2.2.2 Maniquí de "plastic water"

A partir del año 1998 se dispone en el Servicio de un maniquí de láminas de *plastic water* (CIRS). Este maniquí es tejido equivalente y por tanto equivalente al agua. Las láminas tienen una superficie de 30 x 30 cm^2 y grosores que varían entre 1 mm y 6 cm. En la figura 2.8 se muestra un maniquí de láminas de *plastic water* así como la lámina de inserción para una cámara cilíndrica.

Fig. 2.8 Maniquí de láminas de *plastic water*.

Para el maniquí de *plastic water* el factor de escala es 1 y el factor de conversión dosis *plastic water*-dosis agua es 0,996 para los haces de RX de 18 MV y de 1.004 para los haces de RX de 6 MV [16]. Por lo tanto, se considera este maniquí como equivalente agua y la dosis medida en él con la cámara de ionización es la dosis agua a la profundidad de medida.

2.2.2.3 Maniquí de agua

El maniquí utilizado, que se ha fabricado en el propio centro, tiene las siguientes dimensiones: 24 x 42 x 7,5 cm^3. Dispone de un termostato que permite variar la temperatura y de un agitador para asegurar que esta sea uniforme. Este maniquí dispone de una lámina de metacrilato de 2 mm de grosor en contacto con el agua (fig. 2.9), en donde se fijan los diodos, que no pueden estar en contacto directo con el agua.

Fig. 2.9 Maniquí de agua con el montaje experimental para medir la influencia de la temperatura en la respuesta del diodo.

2.2.2.4 Maniquí antropomórfico

Para verificar los algoritmos de cálculo de dosis a plano medio a partir de las medidas *in vivo* a la entrada y a la salida del haz de radiación, previo a su utilización sobre pacientes, se ha utilizado un maniquí antropomórfico tipo Rando Alderson (fig. 2.10). Este maniquí ha sido cedido por el Servicio de Oncología Radioterápica del Hospital Clínico de Barcelona.

Este maniquí comprende cabeza, tronco y abdomen. Se presenta en secciones de 2.5 cm de espesor. Cada una de estas secciones dispone de alojamientos de 0,5 cm de diámetro que permiten la inserción de dosímetros TL (cristales). Estos alojamientos están distribuidos uniformemente y separados 3 cm los unos de los otros.

Fig. 2.10 Fotografía del maniquí Rando Alderson.

2.2.3 Equipo de irradiación

Para la realización de estos trabajos se utiliza un acelerador lineal de electrones con finalidad médica (Varian, modelo Clinac 1800) instalado en el Servicio de Oncología Radioterápica del Hospital de la Santa Creu i Sant Pau (fig. 2.11).

Fig. 2.11 Fotografía del acelerador Clinac 1800 (Varian).

Este acelerador de electrones permite trabajar con distintas energías de electrones (4, 6, 9, 12, 16 MeV) y con haces de RX de dos energías (6 MV y 18 MV). En la tabla 2.4 se indican los índices de calidad de los haces de RX y las energías en la superficie (E_0) de los haces de electrones.

Tabla 2.4 Calidad de los distintos haces de radiación del acelerador lineal Clinac 1800 del Hospital de la Santa Creu i Sant Pau de Barcelona

	energía nominal	**Indice de calidad J_{100}/J_{200}**	**E_0 (MeV)**
RX	6 MV	1,73	-
	18 MV	1,50	-
electrones	4 MeV	-	3,4 MeV
	6 MeV	-	5,7 MeV
	9 MeV	-	8,3 MeV
	12 MeV	-	10,9 MeV
	16 MeV	-	15,7 MeV

Este acelerador permite seleccionar diversos valores de la tasa de dosis (UM/min) (80, 160, 240, 320, 400 UM/min). Es importante señalar que al variar el valor de la tasa de dosis se está modificando la cantidad de pulsos por unidad de tiempo, y no la dosis por pulso, que en este tipo de aceleradores es constante.

Cuando se trabaja con RX, el sistema de colimación del acelerador permite obtener haces de radiación de sección rectangular variable (de 1 x 1 cm^2 hasta 40 x 40 cm^2 a 100 cm de la fuente de irradiación). Se pueden conformar los campos mediante bloques de *cerrobend* que se disponen sobre una bandeja de polimetilmetacrilato (PMMA) (fig. 2.12) y que se ancla al portabandejas del acelerador. Este acelerador dispone de 4 cuñas físicas (15º, 30º, 45º, 60º), como la que se muestra en la figura 2.13.

Fig. 2.12 Bloque de cerrobend montado sobre la bandeja de PMMA.

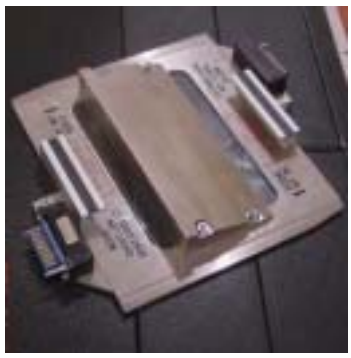

Fig. 2.13 Cuña de 45º

Cuando se trabaja con haces de electrones es necesario utilizar un sistema de colimación adicional. Este tipo de acelerador utiliza conos como colimación adicional (fig. 2.14). Se dispone de 5 conos que definen campos de irradiación que van desde 5 x 5 cm^2 hasta 25 x 25 cm^2 en incrementos de 5 cm. Se pueden obtener otros tamaños o formas de campo colocando bloques de *cerrobend* de un centímetro de grosor en la base del cono (fig. 2.15).

Fig. 2.14 Cabezal del acelerador con un cono de electrones.

Fig. 2.15 *Cerrobend* para configurar el campo de electrones.

2.3 Método

La metodología está ampliamente descrita en cada uno de los artículos que componen este trabajo, sin embargo en este apartado se describen brevemente el procedimiento de calibración así como los modelos de cálculo de dosis a plano medio a partir de las medidas *in vivo*.

2.3.1 Calibración

La calibración de los diodos consta de dos partes bien diferenciadas. La primera es la calibración en condiciones de referencia. La segunda, la determinación de los factores de corrección cuando las condiciones de irradiación difieren de las condiciones de referencia.

En el caso de la calibración para técnicas estándar de tratamiento las condiciones de referencia son: DFS = 100 cm, campo 10 x 10 cm^2 definido en el isocentro, tasa de dosis 240 UM/min y sin ningún accesorio entre la fuente y la superficie del maniquí.

Para la calibración para la técnica de ICT las condiciones en nuestro centro son: DFS = 405 cm, campo máximo (40 x 40 cm^2 definido en el isocentro), tasa de dosis 400 UM/min, una lámina de 1 cm de grosor de polimetilmetacrilato (PMMA) (*spoiler)* interpuesto entre la fuente y el maniquí.

Se define la dosis entrada como la dosis a la profundidad del máximo de dosis (d_{max}) y la dosis salida, por simetría, como la dosis a d_{max} desde la superficie de salida del haz de radiación (fig. 2.16). Se definen pues, dos factores de calibración: un factor de calibración entrada ($F_{cal,en}$) y un factor de calibración salida ($F_{cal,ex}$) . Para la técnica de ICT se definen también un factor de calibración entrada y otro salida detrás de las protecciones parciales de *cerrobend* ($F_{cal,en,cer}$ $F_{cal,ex,cer}$).

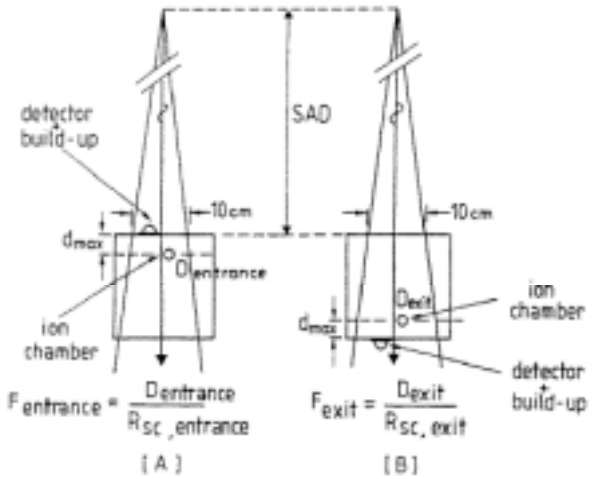

Fig. 2.16 Esquema del dispositivo experimental para determinar el factor de calibración entrada [A] ($F_{cal,en}$) y el factor de calibración salida [B] ($F_{cal,ex}$). Tomado de J. Van Dam y G. Marinello [17].

Los diodos se calibran comparando su respuesta con la dosis determinada con la cámara de ionización cilíndrica situada en el centro del campo y a la profundidad del máximo de dosis. El factor de calibración se define como:

$$F_{cal} = \frac{D_{ci}}{L_{diodo}}$$

Donde D_{ci} es la dosis determinada por la cámara de ionización y L_{diodo} es la lectura del diodo.

Puesto que la sensibilidad de los diodos depende de la tasa de dosis, de la energía y de la temperatura, cuando las condiciones de medida difieran de las condiciones de calibración se deberán aplicar factores de corrección para obtener la dosis a partir de la lectura del diodo (ver capítulo 6). Así, se deberían determinar los factores de corrección por tamaño de campo (FC_{campo}), por bandeja ($FC_{bandeja}$), por distancia de la superficie a la fuente (FC_{DFS}), por cuña ($FC_{cuña}$), por temperatura (FC_{temp}) y por ángulo de incidencia del rayo central del haz sobre el diodo($FC_{ángulo}$). Estos factores se consideran independientes entre sí. La dosis medida por el diodo vendrá dada, entonces, por la siguiente expresión:

$$D = L \cdot F_{cal} \cdot \Pi\, CF_i \qquad \text{Ec. 2.8}$$

En donde L es la lectura del diodo, F_{cal} es su factor de calibración y $\Pi\ CF_i$ es el producto de todos los factores de corrección.

2.3.2 Algoritmos de cálculo

Para calcular la dosis a plano medio a partir de las dosis a la entrada y a la salida determinadas con los diodos se utilizan dos algoritmos de cálculo.

El primero, calcula la dosis entrada a partir de la media aritmética entre la dosis a la entrada y la dosis a la salida. Esta media se corrige por un factor CF dado que la variación de la dosis con la profundidad es exponencial y no lineal. Este algoritmo es similar al propuesto por Alan Noel [18] y correspondería a un cálculo simplificado como los propuestos por Huyskens *et alt*. [19]. Así, la dosis a plano medio se puede calcular para cada haz según la ecuación 2.9.

$$D_{1/2} = \frac{D_{en} + D_{ex}}{2} \times CF \qquad \text{Ec. 2.9}$$

El factor de corrección CF se determina experimentalmente del modo siguiente: En primer lugar, se calibran los diodos siguiendo la metodología descrita en el apartado 2.3.1, después se colocan los mismos a la entrada y a la salida de maniquíes regulares de distinto grosor con la cámara de ionización a plano medio. Se fijan las condiciones de irradiación de acuerdo con las condiciones de calibración, es decir, si

se calibra para ICT el CF se determinará a una DFS de 405 cm, con el *spoiler* interpuesto, campo máximo, mientras que si se calibra para técnicas estándar se determinará el CF a DFS de 100 cm y para distintos tamaños de campo. Se mide simultáneamente la dosis a la entrada (D_{en}), a la salida (D_{sal}) y a plano medio ($D_{1/2}$(c.i.)). El factor de corrección CF se calcula mediante la ecuación 2.10.

$$CF = \frac{D_{1/2}(c.i.)}{(D_{en} + D_{sal})/2} \qquad \text{Ec. 2.10}$$

El segundo método es el propuesto por Rizzotti *et alt*. [20]. Se determina la relación entre D_{en}, D_{ex} y $D_{1/2}$ en condiciones de ICT o para distintos tamaños de campo en condiciones estándar de tratamiento. Este método tiene la ventaja respecto del primero de no utilizar de forma explicita el grosor del paciente.

2.4 Bibliografía

[1] G. F. Knoll. **Radiation detection and measurement**. John Wile and sons. 1979.

[2] B. Grehan. **Cours de physique des semiconducteurs**. Eyrolles. 1987.

[3] G. Rikner. **Silicon diodes as detectors in relative dosimetry of photon, electron and proton radiation fields**. Tesis. Universidad de Uppsala. 1983.

[4] J. M. Taylor. **Semiconductor particle detectors**. Butterworths. 1963.

[5] G. Rikner y E. Grusell. **Effects of radiation damage on p-type silicon detectors.** Phys. Med. Biol., 28, 1261-1267, 1983.

[6] E. Grusell y G. Rikner**. Radiation damage induced dose rate nonlinearity in a n-type silicon detector.** Acta Radiol. Oncol., 23, 465-469, 1984.

[7] E. Grusell y G. Rikner. **Linearity with dose rate of low resistivity p-type silicon semiconductor detectors.** Phys. Med. Biol., 38, 785-792, 1993.

[8] D. Wilkins, X. Allen Li, J. Cygler y L. Gerig. **The effect of dose rate dependence of p-type silicon detectors on linac relative dosimetry.** Med. Phys., 24 (6), 879-881, 1997.

[9] SEFM (Sociedad Española de Física Médica). **Procedimientos recomendados para la dosimetría de fotones y electrones de energías comprendidas entre 1 MeV y 50 MeV en radioterapia de haces externos**. 1984.

[10] SEFM (Sociedad Española de Física Médica). **Suplemento al documento SEFM nº 1: Procedimientos recomendados para la dosimetría de fotones y electrones de energías comprendidas entre 1 MeV y 50 MeV en radioterapia de haces externos**. 1987.

[11] Mª D. Carabante, T. Eudaldo, M. Ribas y N. Jornet. **Puesta en marcha de un filmdensitómetro para la verificación de los campos de irradiación**. Oncología, 20(2), 71-77. 1996.

[12] M.A. Duch, N. Jornet, M. Ginjaume, M. Ribas y X. Ortega. **A comparison of two *in vivo* dosimetry procedures in total body irradiation technique**. Med. Biol. Eng. Com., Vol. 35, supplement part 2, 1038. 1997.

[13] M. Ginjaume, X. Ortega, M.A. Duch, N. Jornet y A. Sánchez-Reyes. **Characteristics of LiF:Mg,Cu,P for Clinical applications**. Radiat. Prot. Dosim., Vol. 85, nº1-4, 389-391. 1999.

[14] M.A. Duch, M. Ginjaume, H.. Chakkor, X. Ortega, N. Jornet y M. Ribas. **Thermoluminescense dosimetry applied to "*in vivo*" dose measurements for total body irradiation technique**. Radiother. Oncol., 47, 319-324. 1998.

[15] M.A. Duch. **Desarrollo de técnicas dosimétricas para su aplicación en dosimetria "*in vivo*" en terapia de alta energía**. Tesis Doctoral. INTE, UPC. Barcelona, 1998.

[16] N. Jornet, T. Eudaldo, Mª D. Carabante y M. Ribas. **Dosimetric Evaluation of a plastic water phantom for high energy photon beam use**. Radiother. Oncol., 51, supplement 1, S40.1999.

[17] J. Van Dam y G. Marinello. **Methods for *in vivo* dosimetry in external radiotherapy**. Physics for clinical radiotherapy. Booklet nº 1 ESTRO, 1994.

[18] A. Noel, P. Alletti, P. Bey y L. Malissard. **Detection of errors in individual patients in radiotherapy by systematic *in vivo* dosimetry**. Radiother. Oncol. 34:144-151. 1995.

[19] D. Huyskens, J. Van Dam y A. Dutreix. **Midplane dose determination using *in vivo* dose measurements in combination with portal imaging.** Phys. Med. Biol. 39: 1089-1101. 1994.

[20] A. Rizzotti, C. Compri, G.F. Garussi. **Dose evaluation to patients irradiatied by Co-60 beams, by means of in direct measurement on the incident and on the exit surfaces.** Radiother. Oncol. 34: 144-151. 1985.

CAPÍTULO 3

CALIBRATION OF SEMICONDUCTOR DETECTORS FOR DOSE ASSESSMENT IN TOTAL BODY IRRADIATION

N. Jornet, M. Ribas and T. Eudaldo

Radiother. Oncol. 38: 247-251, 1996.

Financiado por el F.I.S.S. expediente nº 94/0030-02

The aim of this paper is to discuss the measurements that were carried out to implement "in vivo dosimetry" with EDP-30 diodes, in total body irradiation (TBI) techniques. Exit calibrations and calibrations behind cerrobend protection blocks showed the importance of calibrating diodes in all relevant clinical conditions. Special attention was given to calibration of diodes behind cerrobend blocks. Dependence of the calibration factors on the thickness of the shielding blocks was therefore studied. This dependence was again studied adding a wax cap to the diode and the ionisation chamber was placed at the same depth that the measuring point of the diode. Temperature dependence in diode sensitivity and dependence on accumulated dose for diodes response and for temperature correction factors were studied.

3.1 Introduction

High dose total body irradiation (TBI) with a megavoltage photon beam prior to bone marrow transplant has been performed in our hospital since September 1993. A hyperfractionated technique is used so that six fractions of 2.25 Gy are delivered twice a day over 3 days.

The aim of this work is to describe the measurements we made to calibrate EDP-30 diodes in order to implement in vivo dosimetry for a TBI assessment of dose. Special emphasis was put in the calibration below the cerrobend blocks as we found a 30% change in calibration factors, which was greater than we expected from bibliographic references of EDP-10 and EDP-20 diodes, about which much has been written.

In a separate paper the algorithm that is used to derive the midplane dose as well as the results of patient dose measurements using this method will be described

3.2 Material

TBI is performed using the 18 X-Ray beam generated by Varian Clinac-1800 linear accelerator. Customized lung blocks which allow partial transmission are being used to assure a maximum lung dose of 10 ± 0.5 Gy. The collimator is opened to its maximum field size which is 40 * 40 cm^2 at the isocenter and is rotated 45º. The source-skin distance is set to 405 cm. We interpose a 1 cm thick lucite screen called Spoiler between the source and the patient (40-50 cm from the patient) with two purposes: firstly, to raise skin-dose and secondly, to hold the lung shields. This irradiation technique is the same as that used at the "Hôpital Cantonal Universitaire" in Geneva, Switzerland (5).

Ten EDP-30 diodes (Scanditronix) connected to the DPD-510 electrometer are used. Each diode is encapsulated by a hemi-spherical build-up cap of 1 mm of tantalum stated to be equivalent to approximately 3 cm water for 16-25 MV X-rays.

All calibration measurements were performed with a polystyrene phantom consisting of slabs with an area of 30 x 30 cm^2 . A 0.6 cc cylindrical chamber (type NE 2505/3A) connected to an Ionex 2500/3 electrometer was inserted in a special slab made for this purpose. This ionisation chamber has an exposure calibration factor traceable to the National Standard Dosimetry Laboratory in Spain and was used to determine absolute

dose values.

To determine the temperature correction factor we used a water phantom equipped with a thermostat.

3.3 Method and results

3.3.1 Initial tests

When a new diode is received it is subjected to the following tests

Determination of diode build-up cap thickness

Measurements are made at standard calibration conditions (i.e. SSD=100 cm, field 10x10 cm^2) to find the real build up of EDP 30. Slabs of 4mm and 1 mm of polystyrene are used to cover the diodes till dose maximum is reached. Air gaps are eliminated by using a special slab with a hole to insert the diode.

Knowing that for our 18 MV X-rays the dose maximum at standard calibration conditions is found at 35 mm water depth, from table 3.1, it can be seen that the water equivalent build-up cap thickness of our detectors is about 14 mm instead of the 30 mm marketed by Scanditronix. This has also been observed by A. Noel (priv. commun.) and admitted by Scanditronix.

Table 3.1 Build-up cap determination for EDP-30

Bolus equivalent Water thickness (mm)	**Diode 3** (Gy)	**Diode 5** (Gy)
Without bolus	1.980	1.995
0.6	2.026	2.059
5.8	2.132	2.162
13.1	2.197	2.232
17.2	2.212	2.245
21.4	2.216	2.251
23.4	2.212	2.249
29.7	2.204	2.240
33.8	2.194	2.229
42.1	2.166	2.202

Posterior response verification

Posterior response is tested by placing the diode at a 180º angle at the entry surface and covering it with a bolus of 35 mm water equivalent to guarantee electronic equilibrium at standard calibration conditions. The diodes are inserted in the special slab to avoid air gaps. Measurements were made at standard calibration conditions. Their response is then compared with that of the diode placed at a 0º angle at the entry surface in full electronic equilibrium.

A ratio between the obtained and the expected response of about 0.73 is obtained.

Linearity correction factor

As EDP-30 diodes are being used only for TBI treatments, the linearity of the diode-electrometer system signal with dose is checked in TBI conditions in the range of doses that our detectors read in a clinical situation; from 0.3 Gy to 1.5 Gy.

The signal of the diode-electrometer system is linear with the delivered dose within 1% over the useful range in TBI. Uncertainties due to the non-linearity of the diode-electrometer system can therefore be ignored.

3.3.2 Calibration procedure

Once the diodes have passed the previous tests we proceed to their calibration for TBI technique. Calibration implies the determination of the "calibration factors" of each individual diode and the determination of correction factors that are needed to calculate the absorbed dose when measuring and calibration conditions, differ. In fact, for TBI only three correction factors are of any interest: dose rate correction factor, temperature correction factor and directionality correction factor. Therefore, to determine the dose measured with the diode we should apply the following equation:

$$\text{dose (Gy)} = \text{diode reading} \times F_{cal} \times F_{correction} \qquad \text{Ec. 3.1}$$

$$F_{correction} = F_{dose\ rate} \times F_{direct.} \times F_{temp} \qquad \text{Ec. 3.2}$$

3.3.2.1 Determination of calibration factors

The calibration factor of each individual diode is determined in TBI reference conditions (SSD = 405 cm, field 40 x 40 cm^2 at the isocenter, spoiler in position). For this purpose we use the polystyrene phantom with a total thickness of 20 cm equivalent water. The diodes are taped to the anterior slab of the polystyrene phantom forming a circle of 10 cm diameter centered on the beam axis and the ionisation chamber is placed at the depth of dose maximum at the beam axis. The deviation resulting from not calibrating the diodes one by one at the beam axis is of the order of the reproducibility error (< 0.5%) and therefore not taken into consideration.

The signal of each diode is then compared to the absorbed dose determined with the ionisation chamber. Spanish Dosimetry Protocol (8) includes the application of a displacement factor for the ionisation chamber. This factor is applied only on exit dose measurements. For entrance dose, as measurements are not performed on the exponential part of the curve but at the depth of dose maximum, this factor is not applied (2). The calibration factor (F_{cal}) is determined as the ratio of the absorbed dose determined with the ionisation chamber (IC) and the diode reading in TBI conditions.

$$F_{cal} = \frac{\text{absorbed dose ic}}{\text{diode reading}} \qquad \text{Ec. 3.3}$$

The entrance dose is defined as the dose at the point along the central axis of the beam at a distance d_{max} from the entrance surface of the phantom; d_{max} is equal to the depth of dose maximum in the phantom (1). In TBI reference conditions d_{max} is equal to 14 mm. As the build-up cap of the diodes is about 14 mm the measuring point of the diode and the ionisation chamber are at the same depth.

Calibration is done at room temperature which is about 22.5ºC. Temperature inside the accelerator room is controlled by means of a thermostat so temperature variations are usually inferior to 0.5ºC, and no temperature corrections are made.

As a change in the calibration factor can be expected when the irradiation conditions described are changed due to the fact that diode sensitivity depends on dose rate and on directionality (1, 2, 4, 6), four different calibrations are made:

- Entrance (F_{en})
- Exit (F_{ex})
- Entrance behind cerrobend shielding blocks ($F_{en,cer}$)
- Exit behind cerrobend shielding blocks ($F_{ex,cer}$)

By making these four different calibrations we avoid applying the dose rate correction factor and the directionnality correction factor. Therefore, to obtain the dose from the reading of the diode we should multiply this reading by the appropriate calibration factor and by the temperature correction factor.

Entrance calibration (F_{en})

F_{cal} described previously is now F_{en}

Exit calibration (F_{ex})

To calibrate in exit conditions, the polystyrene phantom is turned so the exit dose is then defined as the dose at -14 mm from the exit surface at the beam axis. A depth of 1.4 cm is largely sufficient in TBI geometry to assure conditions of electronic equilibrium in the backward direction.

Dependence on phantom thickness

Measurements of exit calibration factor with different phantom thickness (10, 20, 30 cm, SSD= 405 cm.) were performed to assess the independence of exit calibration factor on patient thickness.

Comparing the reading of the diode positioned on the phantom exit surface with the dose measured with the ionisation chamber at the exit point we never obtain differences greater than 0.5 %. As the experimental error is of the same order, the exit calibration factor can be considered independent of phantom thickness.

Calibration behind cerrobend shielding blocks ($F_{en,cer}$, $F_{ex,cer}$)

To calibrate behind the cerrobend shielding, we attach one cerrobend block of the same thickness to be used in the treatment (3 cm) onto the spoiler. This block is rectangular (12 cm high and 7 cm wide). The four detectors to be used in the treatment to assess lung dose are placed behind this protection and the same entrance and exit calibration procedure is followed.

Dependence on the thickness of the cerrobend block

Dependence on the thickness of the cerrobend block of $F_{en,cer}$ and $F_{ex,cer}$ was tested calibrating some diodes behind blocks of thicknesses ranging from 0 to 4 cm. Ratios between calibration factors with and without cerrobend blocks are shown in table 3.2.

Table 3.2 Variation of calibration factors depending on cerrobend thickness

Entrance factors

Thickness (cm)	$F_{en,cer}/F_{en}$ [a]	$F_{en,cer}/F_{en}$ [b]	$F_{en,cer}/F_{en}$ [c]
0	1.000	1.000	1.000
1	1.100	1.159	1.009
2	1.214	1.338	1.013
3	1.334	1.562	1.022
4	1.450	1.817	1.031

Exit factors

Thickness (cm)	$F_{ex,cer}/F_{ex}$ [a]	$F_{ex,cer}/F_{ex}$ [c]
0	1.000	1.000
1	0.986	0.990
2	0.961	0.970
3	0.930	0.950
4	0.905	0.934

Study of variation of entrance and exit factors behind cerrobend blocks when changing block thickness. [a] diode calibrated to give dose at the depht of dose maximum, 1.2 cm from entrance and for exit respectively. [b] diode calibrated to give dose at the depht of dose maximum without cerrobend. The diode has an additional cap of 16 mm water equivalent thickness to give a total build-up of 30 mm.
[c] diode calibrated to give dose at 3 cm depht from entrance and exit respectively. The diode has the additional cap on.

Calibration behind cerrobend blocks of different thickness introducing an additional build-up cap of wax (16 mm equivalent water) was done, so the diode had a total build-up cap of 30 mm equivalent water. The ionisation chamber was left at 14 mm from surface. The same was done with the ionisation chamber at 30 mm equivalent water depth. This was

also made for exit factors. Results of this are also shown in table 3.2.

The following ratios, F_{ex}/F_{en}, $F_{en,cer}/F_{en}$ and $F_{ex,cer}/F_{en}$, were calculated. For these set of diodes instead of using different ratios for each different diode we could use the media as the standard deviation of the individual values is significantly lower than the deviation of the individual readings. So for that set it was found: F_{ex}/F_{en}=0.761±0.003, $F_{en,cer}/F_{en}$ =1.298±0.004 and $F_{ex,cer}/F_{en}$ =0.772±0.008.

3.3.2.2 Correction factors

Temperature correction factor

The influence of temperature on the diode signal was studied as this correction factor is not negligible for the TBI treatment condition (7, 9).

A water phantom equipped with a thermostat was used. The diodes were taped on a thin slab of perspex which was in contact with the water. The temperature, measured with a digital thermistor provided with an immersion probe, was slowly increased from 22ºC to 32ºC (the average skin temperature). The sensitivity of the diodes was determined at different temperatures and expressed relative to that of 22.5ºC. Each temperature was maintained approximately 20 min in order to reach full thermal equilibrium between the surface of the phantom and the diodes. This experience was done first when we received the diodes, and then, some time after of use.

The response is found to increase linearly with temperature. Sensitivity varies between 0.16 and 0.29% per ºC when they are new and between 0.23 and 0.3 % depending on the diode itself per ºC when the dose accumulated is of about 1 KGy.

During all dose determinations with a diode, the measurements were accompanied by a simultaneous dose determination with the ionisation chamber so the output variation of the accelerator could then be ignored [1].

3.3.2.3 Calibration frequency

Calibration factors were checked weekly, before each TBI. After 60 TBI (i.e. between 0.9

and 1 KGy) an increase of calibration factor with accumulated dose of about 8 to 11% was observed for all diodes as the dose build up. The increase rate was higher for the first Grays than for the last ones.

From weekly calibration we saw that there was a small, almost linear increase in the value of the ratios F_{ex}/F_{en}, $F_{en,cer}/F_{en}$ and $F_{ex,cer}/F_{en}$ amounting to approximately 2 % between the first and last calibration for all diodes. It would then be possible to use these ratios for weekly calibrations over a month, after which, a constancy check should be made (2).

3.4 Discussion

For dose assessment in TBI techniques by means of in vivo dosimetry, calibration factors should be determined for diodes in all relevant clinical conditions.

In fact, if entrance calibration factors were used for diodes positioned on the exit surface, dose would be overestimated in approximately 25%. Testing the directional dependence of these diodes at standard calibration conditions a 0.73 factor between the prescribed dose and that of the diode is found. That is in agreement with the F_{ex}/F_{en} ratio that we find at TBI conditions, 0.761. For EDP-10 F_{ex}/F_{en} varies from 1.04 to 1.11 (3) and for EDP-20 it is of the order of 0.98 (A. Noel, priv. commun.). Thus ratios which are higher than expected from the literature and for older diodes are found.

If entrance calibration factors were used instead of entrance calibration factors behind lung block protections, there would be an underestimation of dose in approximately 30-35%. Other authors have repported a decrease of the diode response behind wedges (1,2) or when the SSD varies (2,9) for EDP-10 and EDP-20. However, we obtained higher dose underestimation percentages than those obtained by them. This can be due to the different design of EDP-30, as these diodes were designed to assure small field disturbance and small field size dependence. Behind cerrobend blocks there is an increase of secondary particles and with this new design and this small build-up cap the electronic and the low energy X-rays contamination could influence the diode response due to the interphase tantalum-semiconductor.

From table 3.2 it can be seen that to avoid different calibration factors for each different block thickness, EDP-30 should be calibrated behind cerrobend blocks with a total build up

similar to that marketed by Scanditronix and with the ionisation chamber at the same depth. For exit calibration factor we do not observe any improvement when adding this additional build-up cap calibrating with the ionisation chamber at 30 mm depth. It can seen that once we have reached the electronic equilibrium, both with the chamber and with the diode, the obtained ratios are compatible with those reported for other diodes by Van Dam and al. (9).

The dependence on temperature is similar to that found by other authors (4,7,9). Temperature correction factor must be determined separately for all diodes. A detector calibrated at room temperature 22.5ºC will overestimate the dose on the patient by about 2-3% if no correction factor is applied. As this correction factor may vary with integrated dose it should be controlled after some time in use.

As the sensitivity of diodes changes with accumulated dose the entry calibration factor in TBI conditions should be checked before every TBI treatment against an ionisation chamber when they are new, and after some time of use the calibrations can be spaced out.

Once we have the ratios: F_{ex}/F_{en}, $F_{en,cer}/F_{en}$ and $F_{ex,cer}/F_{en}$, and after having studied how they change with accumulated dose during a year and a half of use we have decided to check entry calibration factors once a week, and ratios once a month.

References

1. Heukelom, S., Lanson, J.H., Minjnheer, B.J. Comparison of entrance and exit dose measurements using ionization chambers and silicon diodes. Phys. Med. Biol., Vol 36: 47-49, 1991.

2. Leuens, G., van Dam, J., Dutreix, A., van der Shueren, E. Quality assurance in radiotherapy by in vivo dosimetry. 1. Entrance dose measurements, a reliable procedure. Radiother. Oncol., 17: 141-151, 1990.

3. Leuens, G., van Dam, J., Dutreix, A., van der Shueren, E. Quality assurance in radiotherapy by in vivo dosimetry. 2. Determination of the target absorbed dose. Radiother. Oncol., 19: 73-87, 1990.

4. Nilsson, B., Rudén, B.I., Sorcini, B. Characteristics on silicon diodes as patients dosemeters in external radiation therapy. Radiother. Oncol., 11: 279-288, 1988.

5. Miralbell, R., Rouzaud, M., Grob, E., Nouet, P., Bieri, S., Majno, S., Botteron, P., Montero, M., Precoma, J.C. Can an optimized total body irradiation technique be fast and reproducible?. Int. J. Radiat. Oncol. Biol. Phys., vol 29: 1167-1173, 1994.

6. Rikner, G., Grusell, E. Patient dose measurements in photon fields by means of silicon semiconductor detectors. Med. Phys. 14: 870-873, 1987.

7. Rikner, E., Grussell, E. Evaluation of temperature effects in p-type silicon detectors. Phys. Med. Biol. vol 31: 527-534, 1986.

8. Sociedad Española de Física Médica (S.E.F.M.). Procedimientos recomendados para la dosimetria de fotones y electrones de energías comprendidas entre 1 MeV y 50 MeV en radioterapia de haces externos, 1984.

9. Van Dam, J., Leuens, G., Dutreix, A. Correlation between temperature and dose rate

dependence of semiconductor response; influence of accumulated dose. Radiother. Oncol., 19: 345-351, 1990.

CAPÍTULO 4

MIDPLANE DOSE DETERMINATION DURING TOTAL BODY IRRADIATION USING IN VIVO DOSIMETRY

Montserrat Ribas, Núria Jornet, Teresa Eudaldo, Dolores Carabante, M.Amor Duch, Mercè Ginjaume, Gerardo Gómez de Segura, Francisco Sánchez-Doblado.
Radiother. Oncol. 49: 91-98, 1998.

Parcialmente financiado por el F.I.S. expediente nº 94/0030-02

Background and Purpose

During TBI techniques an accurate determination of the dose distribution is very difficult when using commercial treatment planning systems. In order to determine the midplane dose, an algorithm was developed, based on the use of in vivo dosimetry.

Material and Methods

Scanditronix EDP-30 diodes were placed at the entrance and the exit surface for in vivo dosimetry. The proposed algorithm was validated firstly in a regular and homogeneous phantom of different thickness with an ionisation chamber and TL dosimeters, and secondly, in an Alderson anthropomorphic phantom with TL dosimeters. In this study, in vivo measurements were evaluated in 60 patients and furthermore, in 20 of them, the midplane dose calculated with this algorithm was compared with the method described by Rizzotti A, Compri C, Garusi GF. Dose evaluation to patients irradiated by ^{60}Co beams, by means of direct measurement on the incident and on the exit surfaces. Radiother. Oncol. 1985;3;279-283.

Results

No differences were found between the two methods. The differences between dose values calculated with both methods and dose values

measured with the ionisation chamber and TL dosimeters were within a ± 2% and a ±4%, respectively, in the regular and homogeneous phantom, and within a ±2% in the Alderson phantom. The used algorithm showed to be useful to calculate midplane dose when hetereogeneities as lungs were present. Even when partial transmission blocks were used to reduce dose to lungs, the algorithm, with modified correction factors gave midplane lung dose in the Alderson phantom within a 1.3% of the measurements with TL dosimeters. For 360 patients' measurements in each A-P and P-A field, the relative deviations were analysed between the measured and calculated entrance, exit dose and midplane dose and the prescribed dose, always applying the temperature correction factor. These deviations at the entrance dose were within ±4%. Greater deviations were found for the exit dose measurements. Deviations larger than ±10%, corresponded in general to obese patients, with a thickness over 25 cm. The relative deviations between the total received and prescribed midplane dose in 60 patients were within ±3%.

Conclusions

The results indicate excellent correspondence between the total prescribed and calculated midplane dose using this algorithm while also no significant differences were found when the Rizzotti method was used. Comparison between doses measured with TL dosimeters in the core of the Alderson phantom lungs and doses calculated from in vivo measurements showed that the proposed algorithm could be used in the presence of heteogeneities even when partial transmission blocks were used. The temperature correction factor must be applied in order to avoid a 2-3% dose overestimation.

4.1 Introduction

Since the early applications of total body irradiation (TBI) prior to bone marrow transplantation in the seventies, haematologists, immunologists, radiotherapists and medical physicists have been trying to increase the success of the treatments. Improvement requires an understanding of all the clinical, biological and physical aspects.

The techniques and dosimetry of radiation treatments are more controllable than many other variables associated with clinical trials. However, regardless of the TBI technique used, limitations of the available input data and inherent problems with dose calculation algorithms, make accurate determination of TBI dose distributions very difficult when using most commercial treatment planning systems. Consequently, it is difficult to predict the actual dose delivered to the patient under the sometimes special circumstances required for TBI. Therefore, some authors [1,2] recommend the use of in vivo dosimetry for the determination of the actual dose to patients undergoing TBI treatments.

The accuracy in the determination of an administrated dose in this technique as well as in standard radiotherapy has to be high. The estimated accuracy required should be stated and as good as possible [3], preferably below ±5% (1 s.d.).

For this reason, an in vivo dosimetry procedure was started in our hospital in September 1993, with the aim of determining the dose prescribed to the midplane along the central axis of the beam which corresponds to umbilicus level, as well as the dose to lungs considered organs at risk for this technique.

The purpose of this study was, therefore, firstly to develop an algorithm for dose calculation in TBI techniques using direct measurements carried out with diodes placed on the entrance and the exit surfaces during treatment. Secondly, the accuracy of the dose calculation procedure for this technique was investigated using regular and anthropomorphic phantoms. Thirdly, the proposed algorithm was compared with the method described by Rizzotti et al. [4].

The proposed algorithm has been shown to be useful for calculating the dose to the lungs. Partial transmission lung shields are used for half of each treatment session.

The quality of the beam changes behind those blocks, so special diode calibration [5] and a modification of the correction factors employed in this algorithm were needed to calculate the dose to the lung core under these conditions.

The doses obtained by in vivo dosimetry using the proposed algorithm were compared with the prescribed midplane dose for a series of 60 patients. Midplane doses were also calculated using the Rizzotti method for a selection of 20 patients. The deviations from the prescribed dose using both methods are compared.

4.2 Material and methods

In our centre the TBI technique consists of a set of parallel opposed anterior - posterior fields using a horizontal 18 MV X-ray beam generated by a Varian Clinac 1800 linear accelerator. This technique is the same as that used at the “Hôpital Cantonal Universitaire” in Geneva, Switzerland [6] and is described in a previous paper [3]. A total dose of 13.5 Gy is delivered by a hyperfractionated technique, with six fractions of 2.25 Gy twice a day, over three days. The dose in the lungs is reduced to 10.5 ± 0.5 Gy with partial transmission cerrobend blocks (3 cm thick) which are fixed to the spoiler. Although both anterior and posterior fields are treated in every session, lung blocks are used in an alternative fashion: anterior blocks are used in the first, third, and fifth treatment fractions, while posterior blocks are used during the second, fourth, and sixth fractions. If, according to the in vivo dose measurements, a lung dose higher or lower than previously specified is predicted, the lung blocking time is corrected. The dose rate is 25.26 cGy/min at midplane for a standard thickness of 20 cm. One session lasts approximately 30 min, from the moment that the patient goes into the treatment room up to the moment he/she goes out.

In order to determine, the dose administrated to patients in any point along the beam’s central axis, as well as the dose at midplane inside lungs, by means of in vivo dosimetry with diodes placed at the entrance and the exit surface, the following methodology was chosen:

4.2.1 Calibration of the equipment

p-type EDP-30 silicon diodes (Scanditronix) are used as dosimeters connected to a DPD-510 electrometer (Scanditronix). The calibration of these diodes is performed against a 0.6cm^3 cylindrical chamber (NE 2571) connected to a Doseleader electrometer (NE). A polystyrene phantom (30 x 30 x 20 cm^3) is used to calibrate the diodes. The calibration procedure as well as the determination of correction factors was described in a previous paper [5].

4.2.2 Development of the calculation method for target dose determination on the beam axis

Using combined entrance and exit dose measurements (D_{en}, D_{ex}), one can estimate the dose delivered to a point placed in the target volume. Different algorithms have been proposed to determinate midplane dose in recent literature [7,8]. In TBI treatments, most centres choose a midplane point along the central beam axis as the point where the dose is prescribed. In our centre the midplane dose ($D_{1/2}$) is estimated by taking the arithmetical mean of the entrance and the exit dose corrected by a factor, CF, since the dose variation with depth is not linear but exponential. This algorithm is similar to the one proposed by Noel et al. [8] and would correspond to a simplified calculation such as those proposed by Huyskens et al. [7].

Therefore the midplane dose ($D_{1/2}$) can be expressed for each radiation treatment beam as:

$$D_{1/2} = \frac{D_{en} + D_{ex}}{2} \times CF \qquad \text{Ec. 4.1}$$

The theoretical CF (CF_{theor}) is given by the expression:

$$CFtheor = \frac{PDD(e/2)}{\frac{PDD(ecal) + PDD(e - ecal)}{2}} \qquad \text{Ec. 4.2}$$

Where PDD corresponds to percentage depth dose measured in TBI conditions using a microchamber type RK 85-05 (0.120cm^3) connected to a radiation field analyser RFA-300 (scanning volume 49.5 x 49.5 x 49.5 cm^3). PDD is normalized at the depth of

calibration. e_{cal} is the depth of calibration corresponding to the depth of dose maximum in TBI conditions without partial shielding blocks (14 mm of water). By definition PDD (e_{cal})=1, e is the thickness of the patient and e/2 is midthickness.

The validity of the formula proposed for CF, Ec. 4.2, was investigated in a homogeneous polystyrene phantom (fig 4.1a) in which the entrance and exit diodes and the ionisation chamber at midplane along the central axis were simultaneously positioned. The positioning of detectors was carefully carried out in order to avoid the shadowing effect, which was 3% at 5 cm depth.

Therefore, the experimental CF (CF_{exp}) is given by the expression:

$$CFexp=\frac{D1/2}{\frac{Den+Dex}{2}} \qquad \text{Ec. 4.3}$$

$D_{1/2}$ was determined with the ionisation chamber placed at midplane for different phantom thicknesses. The readings of the ionisation chamber were converted to dose values by applying the Spanish Dosimetry Protocol [9].

Behind the partial transmission blocks used to reduce dose to lungs, different CF (CF'_{theor}, CF'_{exp}) were determined as a different PDD referred as PDD' was measured (Fig. 4.2). CF'_{theor} was calculated using Ec. 4.2. It was then compared with CF'_{exp} (fig 4.1b).

The theoretical and experimental CF data were compared and the difference between them was less than 1% without transmission blocks and 2% with transmission blocks (fig. 4.1). These differences may be due to a rise in the response of the entrance diode when it approaches the spoiler, to a small dependence of the exit calibration factor on phantom thickness that was not taken into consideration [5], or to the difference in exit dose when using a semi-infinite phantom or a finite one. The experimental CF will be used for the calculation algorithm so all these factors will be taken into account. From here on, CF_{exp} will be referred to as CF.

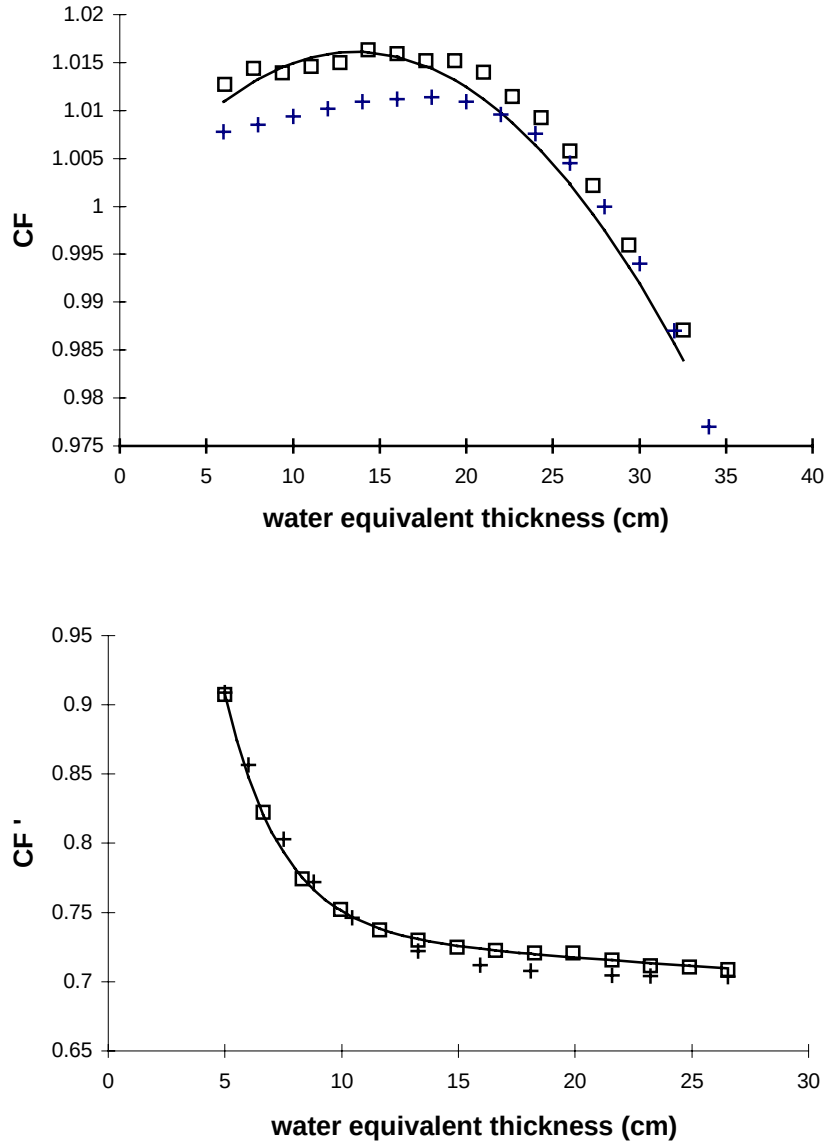

Fig. 4.1 (a) Correction factor (CF) as a function of thickness used in Ec. 4.1 for dose calculation from in vivo measurements in our TBI technique. (b) Correction factor (CF') when partial transmission blocks are used. CF_{theor} (+) and CF_{exp} (□) are shown as well the fitted model of CF_{exp}

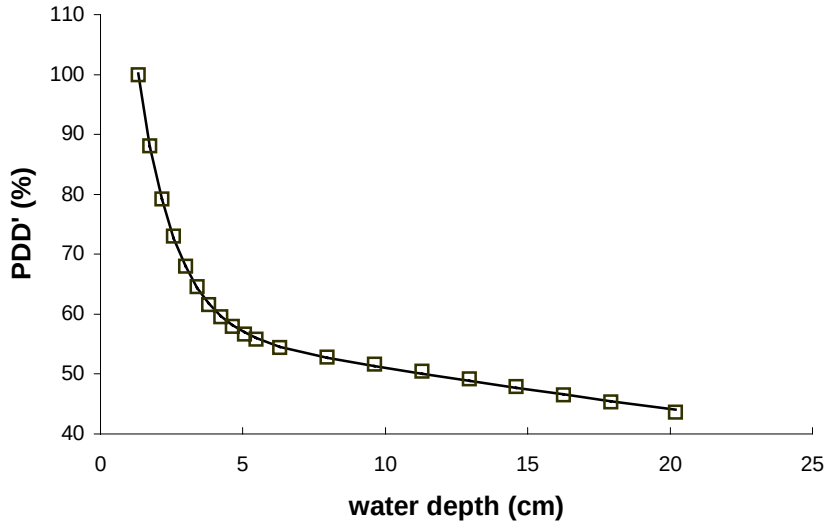

Fig. 4.2 PDD in TBI conditions under a partial transmission block (3 cm thick cerrobend block allowing for a 32% transmission), experimental data and the fitted model are shown.

When heterogeneities are present (lungs) water equivalent thickness, instead of the total_thickness of the patient at the level where the diodes are placed, was used to calculate CF. The ratio between exit and entrance dose measured with the diodes is taken as PDD(e-e_{cal}), then e can be found from the PDDs curves.

The conversion of midplane dose to dose at any other point along the central axis is performed using the PDD corresponding to TBI conditions. Then, to find the dose at any point along the central axis the following expression is applied:

$$D(z) = D_{1/2} \times \frac{PDD(z)}{PDD(e/2)} \qquad \text{Ec. 4.4}$$

Where $D_{1/2}$ is given by Ec. 4.1.

The midplane dose along the central beam axis can also be deduced using the method proposed by Rizzotti and al. [4]. The relation between D_{en}, D_{ex} and $D_{1/2}$ was determined in TBI conditions using polystyrene phantoms of different thickness with the ionisation chamber placed at midplane and two diodes, one placed at the entrance surface and the other at the exit surface. All detectors were placed along the central axis of the beam. The relation between D_{ex}/D_{en} and $D_{1/2}/D_{en}$ was first determined

without partial shielding blocks (fig. 4.3a) and then with partial shielding blocks (fig. 4.3b). This method has the advantage of not using the patient thickness explicitly.

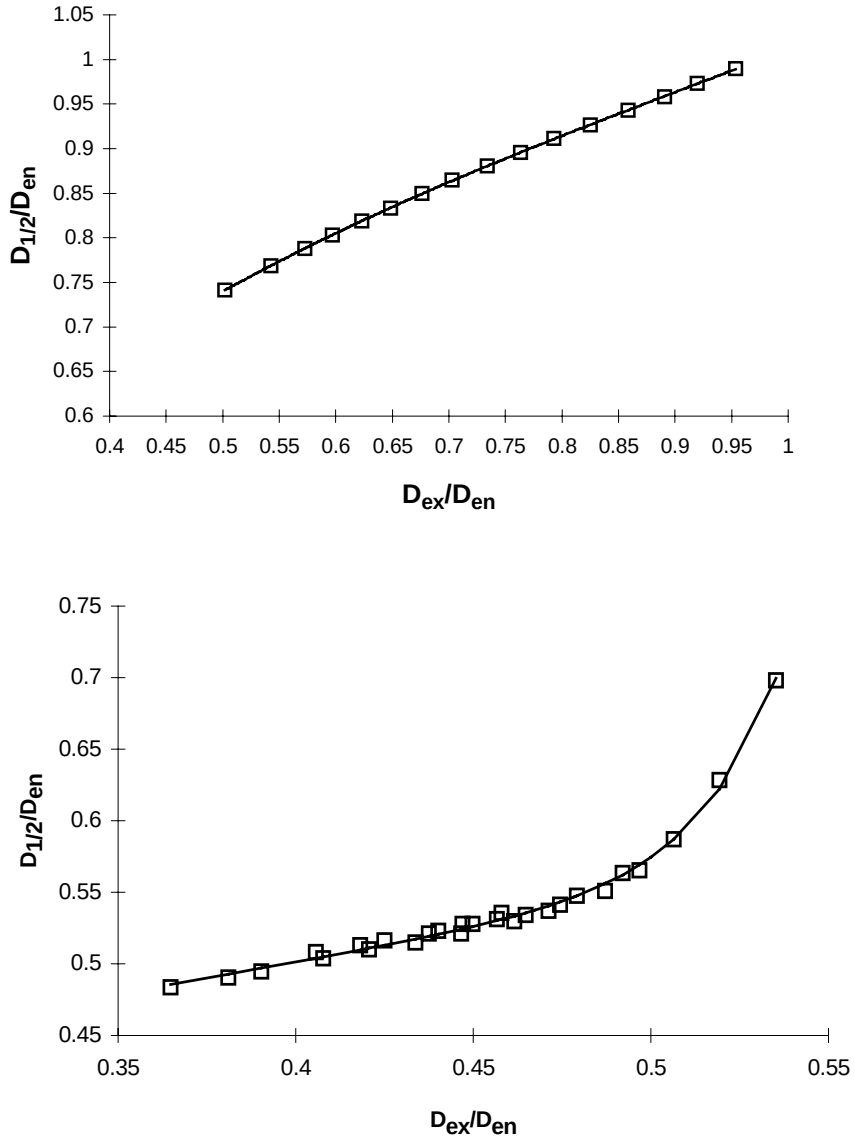

Fig. 4.3 (a) Experimental D1/2 /Den as a function of D_{ex}/D_{en}. $D_{1/2}$ was determined placing an ionisation chamber at the midplane while D_{en} and D_{ex} were determined placing one diode on the entrance surface and the other at the exit surface of the phantom. The fitted model is also shown. (b) Idem under partial transmission blocks.

4.2.3 Verification on phantoms of the dose calculation algorithm for in vivo dosimetry, with an ionisation chamber and TL dosimeters

To validate our algorithm in TBI conditions, two kinds of phantoms were used, one regular and homogeneous and the other anthropomorphic.

4.2.3.1 Homogeneous and regular phantom

Measurements were made on polystyrene phantoms of different thickness (10, 20, and 30 cm) with and without partial transmission blocks. Diodes were placed on entrance and exit sites on the central axis. The ionisation chamber and TLD chips were inserted in special slabs made for this purpose which were placed at several depths in the phantoms. The dose, calculated from the readings of the diodes using Ec. 4.4 (where $D_{1/2}$ was calculated using Ec. 4.1 or the Rizzotti method) was compared with the dose measured with the ionisation chamber and the TL dosimeters placed at the depth of interest.

The TL detectors used in this study were LiF chips type TLD-700 (3.1 x 3.1 x 0.9 mm^3) from Harshaw. Before each irradiation, a standard annealing procedure was carried out in a PTW microprocessor-controlled annealing oven: 400ºC for 1 hour, followed by 100ºC for two hours. The detectors were read out with a commercial semi-automatic Vinten Rialto TLD reader. The heating cycle had two parts: a preheat zone of 135ºC for 10 s, and a reading zone from 135ºC to 270ºC with a linear heating rate of 25ºC/s for 12 s. To improve the dosimetric accuracy, individual calibration factors were established for each detector [10,11], and stability checks were performed periodically at the INTE Secondary Standard Calibration Laboratory with a cesium-137 beam. In this way, the relative statistical uncertainty obtained never exceeded 3%.

4.2.3.2 Anthropomorphic phantom

In this case, an Alderson anthropomorphic phantom sliced into 2.5 cm thick transverse sections, each containing a matrix of 5 mm diameter holes spaced 3 cm apart, was employed. The anthropomorphic part of the phantom extended from the head to the iliac crest. During the irradiation, the Alderson phantom was held in the same standing position as patients in such a way that the umbilical section was aligned on the central

axis. This section is 22 cm thick and along its axis it has three TLD inserts at 4.5, 10 and 19 cm depth. Three TLD dosimeters were loaded into each insert. TLD's were also inserted at midplane in the lungs. Only the right lung was shielded with a partial transmission block.

Diodes were placed at the entrance and the exit surfaces on the phantom along the central beam axis as well as on one of the slices containing the lungs (22.1 cm thick). Doses calculated using the two algorithms, the one based on the arithmetical mean of entrance and exit doses and that used by Rizzotti, are compared with TLD doses at midplane and at other depths along the central axis and also at midplane of the lungs.

4.2.3.3 Measurement procedure in patients

In vivo dosimetry is performed on every patient and at each treatment session by using diodes placed on the skin at the entrance and exit surfaces on different anatomical sites: central axis (abdomen) and off-axis (head-front, neck, mediastinum, lungs, thigh and leg). The diodes are positioned by a technician and remain in the same points throughout the session. In this study only the measurements along central axis are evaluated.

In each session, the skin temperature of the patient is taken before the treatment starts by fixing a contact thermometer on the skin. In the first treatment session, after completion of the treatment set-up, the patient diameter along the beam axis is checked using a calliper.

For each patient the theoretical entrance and exit dose are calculated by the expressions:

$$\mathrm{Den}=\frac{2.25\mathrm{Gy}/2}{\mathrm{PDD}(\mathrm{e}/2)}\times 100 \qquad \text{Ec. 4.5}$$

$$\mathrm{Dex}=\mathrm{Den}\times\frac{\mathrm{PDD}(\mathrm{e}-\mathrm{ecal})}{100} \qquad \text{Ec. 4.6}$$

All the in vivo dose measurements are performed by a physicist. When discrepancies of more than ±5% on entrance dose are found, a check of the treatment set-up is performed with the patient still in treatment position. All calculations of midplane dose are also made by a physicist.

Twenty patients with diameters along central beam axis ranging from 15 to 34 cm were chosen to compare the dose at midplane calculated using the two methods, that based on the arithmetical mean of the entrance and exit dose that is used in routine in our institution, and that proposed by Rizzotti et al.

4.3 Results

4.3.1 Dose comparison: phantom dose vs. dose calculation

The results of the regular and homogeneous phantom dose comparison with ionisation chamber and TL dosimeters are summarised in Table 4.1.The comparison between results with TLD and dose calculated for all depths along the central beam axis in the Alderson phantom are shown in Table 4.2. While the comparison between dose measured inside the lungs with TLD and dose calculated from in vivo entrance and exit measurements with and without partial shielding blocks are shown in Table 4.3.

Table 4.1 Dose comparison in an homogeneous regular phantom

Water depth (cm)	D_m/D_1		D'_m/D'_1		$D_m/D_{rizzotti}$		$D'_m/D'_{rizzotti}$	
	IC	TLD	IC	TLD	IC	TLD	IC	TLD
Phantom thickness: 10 cm								
1.7	1.013	1.028	1.037	0.956	1.013	1.028	1.052	0.970
5.0	1.007	1.021	1.004	0.987	1.007	1.021	1.019	1.002
7.1	1.000	1.005	1.003	0.997	1.000	1.005	1.017	1.011
Phantom thickness: 20 cm								
3.0	1.017	1.041	0.996	0.974	1.015	1.039	0.994	0.972
5.0	1.016	1.032	0.998	1.002	1.014	1.030	0.997	1.000
10.0	1.006	1.006	1.006	1.033	1.006	1.004	1.004	1.031
13.7	1.002	1.002	1.013	1.009	1.000	1.000	1.011	1.007
17.5	0.998	0.993	0.995	1.003	0.995	0.993	0.994	1.001
Phantom thickness: 30 cm								
3.2	1.019	1.041			1.017	1.043		
5.8	1.020	1.041			1.018	1.040		
9.5	1.014	1.004			1.011	1.000		
13.2	1.008	1.000			1.006	0.998		
17.0	1.009	0.991			1.007	0.988		
19.4	0.978				0.976			
20.7		1.025				1.023		
24.5		1.011				1.008		
26.9	1.012				1.009			

Comparison between the dose measured, D_m, with an ionisation chamber (IC) and termoluminescent dosemeters (TLD) and the dose calculated from entrance and exit in vivo measurements using Ec. 4.4, where $D_{1/2}$ can be calculated using Eq. 4.1, D_1, or Rizzotti method, $D_{rizzotti}$. D'_m, D'_1 and $D'_{rizzotti}$ refer to doses under partial transmission blocks.

Table 4.2 Anthropomorphic phantom dose comparison (central axis)

Depth (cm)	$D(TLD)/D_1$	$D(TLD)/D_{rizzotti}$
4.5	1.021±0.006	1.019±0.006
10.5	1.015±0.003	1.015±0.004
19	0.991±0.005	0.991±0.006

Comparison between dose measured with TLD placed at different depths in the abdominal slice of an Alderson rando phantom (antero-posterior diameter of 22.1 cm) and the doses calculated from entrance and exit in vivo dose measurements using Ec. 4.4 where $D_{1/2}$ can be calculated using Ec. 4.1, D_1, or Rizzotti method, $D_{rizzotti}$. The mean of measurements done on four different days as well as its standard deviation is given.

Table 4.3 Anthropomorphic phantom dose comparison (dose to the lungs)

	water

	equivalent thickness (cm)	$D(TLD)/D_1$	$D(TLD)/D_{rizzotti}$
Right lung with partial transmission block	12.2	1.013	0.952
Left lung without partial transmission block	13.2	0.993	0.993

Comparison between dose measured with TLD placed at mid-depth in a slice containing the lungs (antero-posterior diameter of 22.1cm) and the midplane dose calculated from entrance and exit in vivo dose measurements using Ec. 4.1 D_1 , or Rizzotti method, $D_{rizzoti}$.

4.3.2 Dose comparison: patient dose vs. dose calculation

Combined entrance and exit dose measurements along the central axis were performed on 60 patients. This corresponds to a total number of 360 measurements for each field A-P and P-A. The patients included in this study were both sexes and aged between 5 and 50. The central axis diameter ranged from 15.2 to 33.9 cm. Diode's readings were corrected for temperature dependence.

Differences between measured and expected doses have been plotted as frequency distribution histograms. N is the number of measurements, x the mean value and s.d. the standard deviation.

Figure 4.4 (a,b) shows the relative deviations (%) between entrance and exit doses measured and calculated, $((D_{mes} - D_{cal})/D_{cal}) \times 100$, both for A-P and P-A fields. The frequency distribution of the relative deviation between the total dose at the midplane received and prescribed for both the A-P and the P-A beams is represented in Fig. 4.4 (c). The mean and standard deviation are indicated in the figures.

Figure 4.5 shows the frequency distribution of the relative deviations between the total received dose and the prescribed dose for all patients.

Figure 4.6 shows the midplane dose for both fields calculated from in vivo measurements using Rizzotti method compared with the midplane dose calculated using Ec. 4.1.

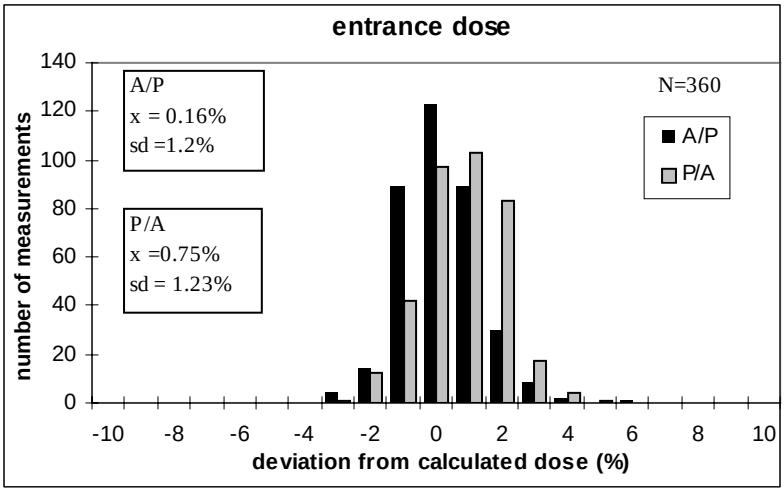

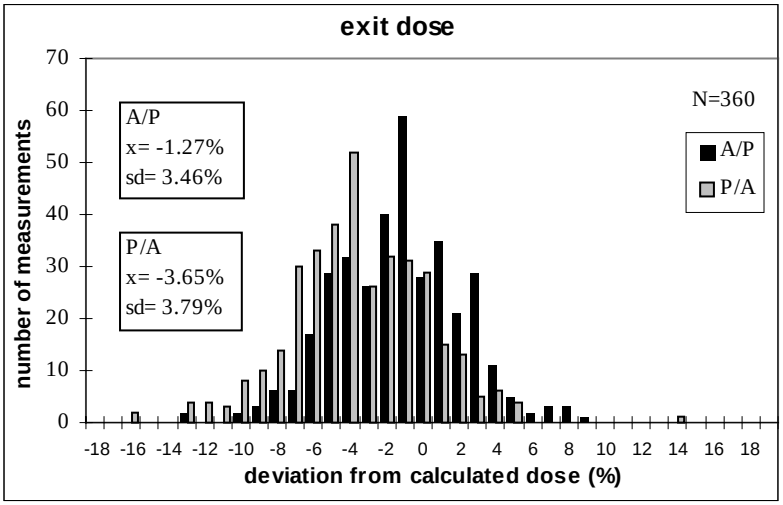

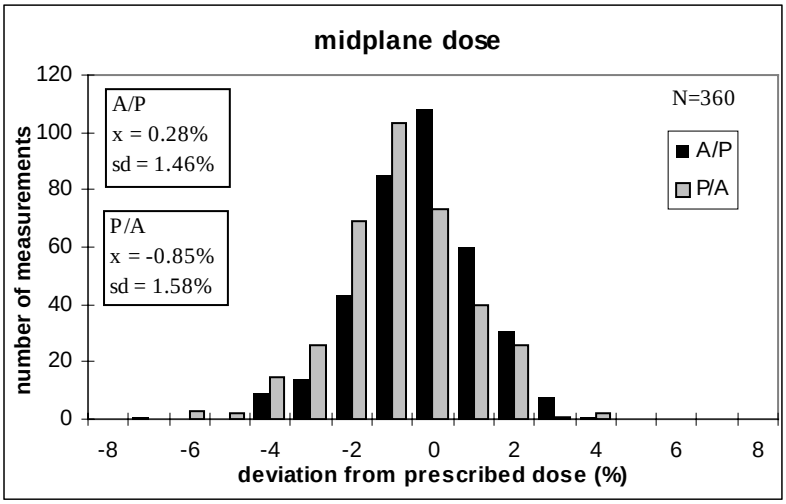

Fig. 4.4 Relative deviations (%) between the measured and the calculated entrance (a), exit (b) and midplane (c) doses for 360 measurements for the A-P and P-A field.

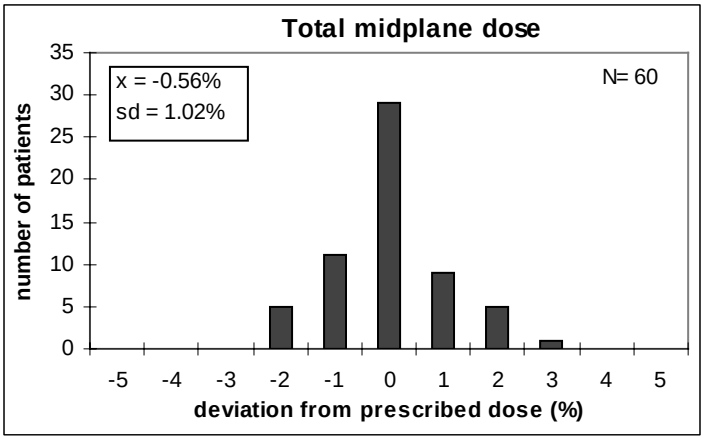

Fig. 4.5 Relative deviations (%) between the total midline dose calculated from in vivo measurements adding the A-P and P-A contributions for 60 patients.

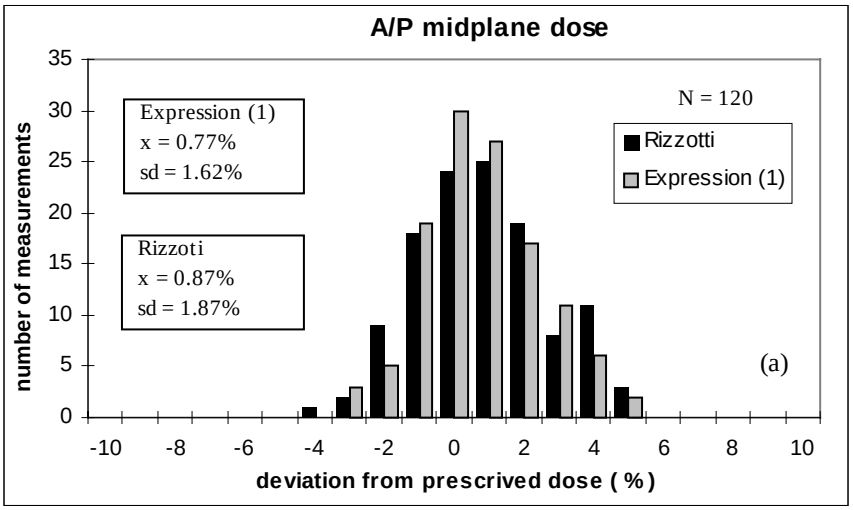

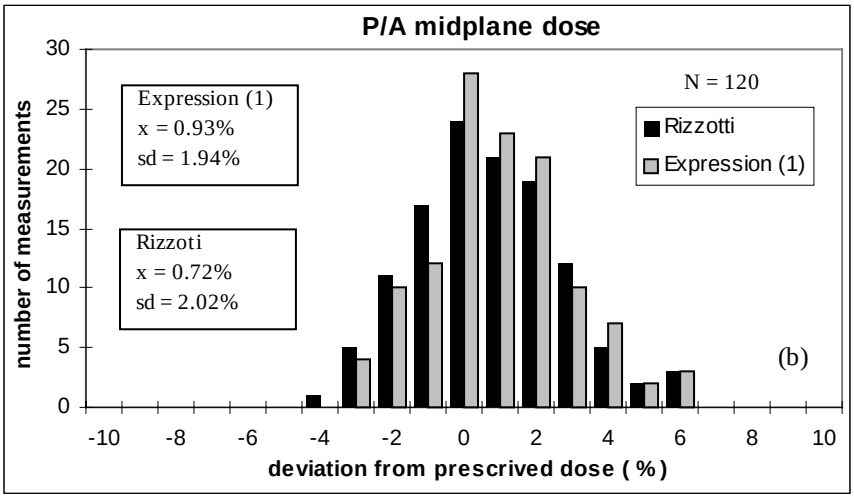

Fig. 4.6 Relative deviations (%) between the calculated midplane dose and the prescribed dose. The midplane dose was calculated from in vivo measurements using Ec. 4.1 and the Rizzotti method for 20 patients (120 measurements) for the A-P field (a) and for the P-A field (b).

4.4 Discussion

4.4.1 Dose comparison: phantom dose vs. dose calculation

The differences observed in Table 4.1 between the dose values measured with the ionisation chamber and the dose values calculated with the algorithm in routine use or with the method proposed by Rizzotti are within ±2% in most cases when using the ionization chamber and within ±3% when are determined with TLD. These deviations are of the same order as the experimental error.

It can be seen from table 4.2 that using both calculation methods the dose agrees with the dose measured with TLD within ±2%.

Table 4.3 shows that both algorithms give the same dose as that measured with TLD inside the lung when no transmission blocks are used. In this case, using or not using the water equivalent thickness of the slice on which diodes are placed, does not signify any major difference in the calculated dose using Ec. 4.1, as CF varies smoothly with *e* (from 1.015 to 0.985 between 7 cm and 32 cm). Behind the transmission blocks, CF' has to be used. Using CF instead of CF' would lead to a 24% dose overestimation. CF' depends strongly on *e*, particularly the first 10 cm, so it is important to use the equivalent water thickness. When transmission blocks are used, the measurement of CF and $D_{1/2}/D_{en}$ as a function of D_{ex}/D_{en} entrains more uncertainties than when the blocks are not present. Therefore, the dose to lungs under the blocks is given with a deviation of ±10%. More work is needed to improve accuracy.

4.4.2 Dose comparison: patient dose vs. dose calculation

The results displayed in figure 4.4 (a) show that for the A-P beam the majority of measurements have deviations from the expected dose smaller than ±2%, and that with the exception of one of those, all are included into ±4%. The one value greater than 4% was examined and it was seen that it corresponded to the thickest patient, being 33.9 cm along the central axis. For the P-A field all deviations are within the ±4% except for five measurements which correspond to the same patient. The error was attributed to the difficulties in its positioning.

In figure 4.4 (b) a broad distribution for the A-P beams ranging from -13% to 9% can be seen. It has been checked that values larger than ±10% (two measurements) are related to patients thicker than 30 cm. In this figure and for the P-A field, deviations go from –16% to 14%, with 14 measurements with a deviation higher than a 10%. The standard deviations for the exit dose are higher than those found for the entrance diode, which may be attributed to the fact that the mobility of the abdomen surface becomes pronounced in obese patients, with a thickness over 25 cm. Besides, as the exit surface of the patient is in contact with the support structure, movement of the patient could then also move exit diodes whose surface could then deviate from being perpendicular to the beam resulting in a slight underestimation of dose. This would be more pronounced for P-A beams where the abdomen surface is in contact with the support structure.

In Fig. 4.4 (c) all deviations are within ±3% with 98% of the measurements with a deviation within ±2% for the A-P beam and 92% for the P-A beam.

In Fig. 4.5 can be seen that all deviations are within ±3% and 98% of the measurements are within ±2% when the temperature correction factor is applied. It is important to note that neglecting correction factor would introduce a 2-3% systematic overestimation of dose which is also mentioned in the literature [12].

The discrepancies between measured and prescribed doses were attributed to the fact that the diodes are taped on the patient's skin from the beginning to the end of the session. Although the patient turns around from one field to the other with the diodes still in position, it is checked if they remain at the same point. In addition, for each treatment radiation field, the patient must not move for 8 to 10 minutes, which may be difficult for some patients and especially for children.

For these reasons, the level of action for TBI treatments has been set at 5% for entrance and midplane doses and at 10% for exit dose measurements.

Although the algorithm that we use is, in principle, less accurate than the Rizzoti method if real instead of equivalent thickness is used, from Fig. 4.5 it can be seen that no significant differences were found between these two methods. The proposed algorithm is preferred first for its simplicity. The on-line dose can be estimated by a very

simple calculation from in vivo entrance and exit measurements, as without applying CF the error made would be less than 3%. Secondly, an error of 10% on the exit dose would lead to a 4% error on the midplane dose using the proposed algorithm, while if the Rizzotti method was used this error would be increased to 5%. When lung partial shielding blocks are used equivalent thickness must be calculated and CF' is not negligible, so the Rizzotti method could be more appropiate.

4.5 Conclusions

A dose calculation algorithm from exit and entrance in vivo dose measurements with diodes has been developed for a TBI technique. The validity of the proposed algorithm has been checked in regular and anthropomorphic phantoms with an ionisation chamber and TLD. Almost all values are within ±3% of the measured doses. This algorithm gives also good results when heterogeneities are present (lungs), even when partial transmission shielding blocks are used. In this last case a special CF (CF') has to be used in expression (1) as the beam quality changes behind the partial transmission blocks. If CF was used instead of CF' lung would be overdosed in a 24%.

The agreement between the total prescribed midplane dose and the calculated dose, in this series of 60 patients was excellent, better than ±3%. Taking into account that the skin temperature is not the same as the temperature at which the diodes are calibrated, unless temperature correction factor is applied, the dose would be overestimated by 2-3%. The greatest deviations were found for the exit dose measurements (more for the P-A field than for the A-P field). When analysed, these measurements corresponded to patients with thicknesses greater than 30 cm. Heukelom and al. [13] reached similar conclusions for pelvic treatments. The Rizzotti method gave similar results as our routine method. Finally, these excellent results show that the proposed algorithm can be used in TBI technique, being more straightforward than the Rizzotti method.

4.6 References

[1] B.J. Mijnheer. **Possibilities and limitations of in vivo dosimetry. In: Radiation dose in radiotherapy from prescription to delivery.** IAEA-TECDOC-734, pp259-267. IAEA, Vienna, 1994.

[2] J. Van Dyk, J.M. Galvin, G.P. Glasgow and E.B. Podgorsak. **The Physical Aspects of Total and Half Body Irradiation.** AAPM Report Nº 17. 1986.

[3] F.Sánchez-Doblado, U. Quast, R. Arráns, L. Errazquin, B. Sánchez-Nieto and J.A. Terrón. **Total body irradiation prior to bone marrow transplantation. European group for Blood and Marrow Transplantation (EBMT)**. ISBN: 84-605-3132-5. 1995.

[4] A. Rizzotti, C. Compri, G.F. Garussi. **Dose evaluation to patients irradiatied by Co-60 beams, by means of direct measurements on the incident and on the exit surfaces.** Radiother. Oncol. 34: 144-151. 1985.

[5] N. Jornet, M. Ribas, and T. Eudaldo. **Calibration of semiconductor detectors for dose assessment in total body irradiation.** Radiother. Oncol. 38: 247-251. 1996.

[6] R. Miralbell, M. Rouzaud, E. Grob, P. Nouet, S. Bieri, S. Majno, P. Botteron, M. Montero y J.C. Precoma. **Can an optimized total body irradiation technique be fast and reproducible?** Int. J. Radiat. Oncol. Biol. Phys., vol 29: 1167-1173. 1994.

[7] D. Huyskens, J. van Dam, and A. Dutreix. **Midplane dose determination using *in vivo* dose measurements in combination with portal imaging.** Phys. Med. Biol. 39: 1089-1101. 1994.

[8] A. Noel, P. Alletti, P. Bey y L. Malissard. **Detection of errors in individual patients in radiotherapy by systematic in vivo dosimetry**. Radiother. Oncol. 34:144-151. 1995.

[9] Sociedad Española de Física Médica (S.E.F.M.). **Procedimientos recomendados para la dosimetria de fotones y electrones de energías comprendidas entre 1 MeV y 50 MeV en radioterapia de haces externos**, 1984.

[10] F. Sánchez-Doblado, J.A. Terrón, B. Sánchez-Nieto et al. **Verification of an on line in vivo semiconductor dosimetry system for TBI with two TLD procedures.** Radiother. Oncol. 34: 73-77. 1995.

[11] M.J. Toivonen. **Improving the accuracy of TLD systems in clinical applications.** Radiat. Prot. Dosim 47: 497-503. 1993.

[12] J. van Dam and G. Marinello. **Methods for In Vivo Dosimetry in External Radiotherapy.** Physics for Clinical Radiotherapy, Booklet Nº 1.Garant, Leuven/Apeldoorn. 1994.

[13] S. Heukelom, J.H. Lanson and B.J. Mijnheer. **In vivo dosimetry during pelvic treatment.** Radiother. Oncol. 25: 111-120. 1992.

CAPÍTULO 5

IN VIVO DOSIMETRY: INTERCOMPARISON BETWEEN p-TYPE BASED AND n-TYPE BASED DIODES FOR 16 TO 25 MV ENERGY RANGE

N. Jornet, M. Ribas, T. Eudaldo.

Med. Phys., vol 27, nº6, June 2000.

Parcialmente financiado por el F.I.S. expediente nº 98/0047-02

This paper compares two different types of diodes designed to cover the energy range from 16 to 25 MV, one n-type (P30) and the other p-type (EDP30). A 18 MV X-ray beam has been used for all tests. Signal stability post-irradiation, intrinsic precision and linearity of response with dose, antero-posterior symmetry and dose decrease under the diode were studied. Also, the water equivalent thickness of the build up caps was determined. Both types of diodes were calibrated to give entrance dose. Entrance correction factors for field size, tray, source skin distance, angle and wedge were determined. Finally, the effect of dose rate, temperature and accumulated dose on the diode's response were studied. Only P30 had full build-up for 18 MV X-rays and standard irradiation conditions. Field size correction factor was about 2-4 % for field sizes bigger than 20 x 20 cm^2 for both types of diodes. Tray correction factor was negligible for P30 while EDP30 would overestimate the dose by a 2% for a 40 x 40 cm^2 field size if the correction factor was not applied. Wedge correction factors are only relevant for the 60º wedge, being the correction factor for P30 significantly higher than for EDP30. P30 showed less temperature dependence than EDP30. Sensitivity

dependence on dose per pulse was a 1.5% higher for P30 than for EDP30 and therefore a higher SSD dependence was found for P30. The loss of sensitivity with accumulated radiation dose was only about 0.3% for P30, after 300 Gy, while amounted to 8 % for EDP30. Weighing the different correction factors for both types of diodes no conclusions about which type is better can be driven. From these results it can be also seen that the dependence of the diode response on dose rate in a pulsed beam does not seem to be associated with the fact of being n-type or p-type but could be related to the doping level of the diodes.

5.1 Introduction

In vivo dosimetry has proved to be a useful tool for quality assurance in radiotherapy [1-7]. Diodes offer an advantage over other in vivo detectors, such as TLD, in that they can measure dose on line. Nevertheless if very accurate measurements are required, each diode must be extensively calibrated before being used on the patient.

Diodes from different firms can differ in terms of type (n-type or p-type), doping level, doping process, the effective width of the sensitive volume, build up cap design, material and thickness, and preirradiation dose given to the diode.

On the one hand**,** the design of the build up cap of diodes to be used for in vivo dosimetry in high energy X-ray photon beams must be a compromise between the build-up cap thickness needed to ensure electronic equilibrium for every beam configuration (field size, source to skin distance, beam modifying devices, etc), patient comfort and avoidance of under-dosage of the target volume under the diode. On the other hand**,** the level of preirradiation influences the dose rate dependence of the diode response as well as temperature dependence and loss of sensitivity with accumulated dose [1,3,8-12].

The ideal in vivo diode for a range of X-ray energies should have small dependence (below 1%) on field size, source to skin distance (SSD), interposition of beam modifying devices such as wedges, trays, partial transmission blocks**,** and orientation of the beam. Moreover**,** correction factors should not be modified with accumulated dose. The loss of sensitivity with accumulated dose should be kept as low as possible. All these requirements must be fulfilled taking into consideration that the field perturbation caused by the diode should be minimal.

In the literature, there is very limited information about the dosimetric characteristics of in vivo diodes for 16-25 MV X-Ray beams. Moreover data on the. dosimetric characteristics of studied n-type diode has not been previously published so that the common thought that p-type diodes are more suitable for in vivo dosimetry [13] is based on references dating from mid-nineties [4,9,12,14,15] which refer to older n-type diodes. Therefore, the aim of this work was to study the dosimetric characteristics of two different types of commercial diodes (one n-type and the other p-type) designed to cover the energy range from 16 to 25 MV X-rays for in vivo dosimetry and also to

establish the differences between them. It is important to know the dosimetric characteristics of different types of diodes before choosing one type to be used in clinical routine, as the correction factors that have to be applied to the reading of the diode to give real dose differ quite a lot from type to type. It will depend on how they are to be used and on the action levels chosen by the centre which is the more appropriate type of diode.

5.2 Materials

Two types of Silicon diodes with a high doping level**,** one p-type from Scanditronix (EDP30) and one n-type from Precitron AB (P30) were used. Three diodes of each type were tested. These diodes were connected to a DPD510 ten-channel Scanditronix electrometer.

EDP30 have a thickness of the measuring volume of 60 µm and an effective detection area of 1.76 mm^2 , they are provided with a half-spherical build-up cap of 1 mm of Tantalum stated by the manufacturer to correspond to 30 mm water equivalent thickness, their resistivity is stated to be 0.2 ohms·cm and their sensitivity is about 40 nC/Gy. They have been preirradiated by the manufacturer with 10 MeV electrons up to 8 kGy.

P30 have an effective thickness of the measuring volume of 0.1 mm and an effective detection area of 6.8 mm^2 and their build-up cap is made of, from the outside in 0.5 mm Polyacetal, 1.6 mm of tungsten and 2.4 mm of epoxi, stated to correspond to 30 mm water equivalent thickness. They have a sensitivity of 150-300 nC/Gy. The manufacturer has preirradiated them with 10 MeV electrons up to 25 kGy. The manufacturer provides no information about the doping level or the resistivity of the diodes.

All measurements were performed in an 18 MV X-ray beam from a linear accelerator Clinac 1800 (Varian).

A Farmer 2571 ionisation chamber (0.6cc) connected to a Dose Leader electrometer was used as the reference dose detector. This ionisation chamber has a calibration factor traceable to the National Standard Dosimetry Laboratory in Spain.

A plastic water phantom (CIRS) (slices of area 30 x 30 cm^2 and thickness ranging from 0.1 to 5 cm) was used. This phantom has a special slab to accommodate the ionisation chamber. For the plastic water phantom and for 18 MV X-rays the scaling factor is 1 and the conversion factor dose measured in plastic water dose-to-water is 0.996 [16] so it was neglected.

To determine the influence of temperature on diode's sensitivity, a water phantom equipped with a thermostat was used.

5.3 Methods

Both sets of diodes were subjected to a set of tests that our department performs whenever a new diode is received. These initial tests consist of the measurement of:

Signal stability after irradiation: the display of the signal taken immediately after irradiation is compared with the display of the signal 5 min after the end of the irradiation.

Intrinsic precision: the mean and the standard deviation of ten readings are calculated.

Linearity of the response with dose: The response of the diode is represented as a function of dose.

Depth of the diode measuring point: The diode is fixed on the surface of the plastic water phantom with its hemispherical surface facing the gantry and covered with a special plastic water slab to avoid air gaps. Irradiations with 18 MV X-rays are performed by adding plastic water slabs over the diode until its reading reaches maximum. As the depth of dose maximum in water at these irradiation conditions is known, the water equivalent thickness of the build-up cap can be calculated.

Antero-posterior symmetry: the ratio of the diode reading when irradiated with its round side facing the accelerator collimator, and when irradiated with its flat side facing the collimator, is obtained. To fix the diode with its round build-up cap on the phantom the special slab in which the diode can be inserted is used. The diode measuring point is considered to be on its flat side and is kept at the depth of dose maximum during this test.

Dose decrease under the diode: The dose decrease at 5 cm depth under the diode is calculated by comparing two beam profiles at this depth, one measured with the diode on the surface of the phantom, and the other without the diode.

Once all these tests had been performed, the diodes were calibrated to be used in clinical practice. Calibration involves determining first the calibration factor of each diode under standard reference conditions (SSD = 100 cm; 10 x 10 cm^2 field size at the isocentre; gantry angle 0º) and then the correction factors that have to be applied when irradiation conditions differ from reference ones. For this intercomparison only entrance calibration factors and entrance correction factors were determined.

Entrance calibration factor is defined as the ratio of the dose measured by the ionisation chamber placed at the depth of dose maximum (z_{max}) in standard reference irradiation conditions and the reading of the diode on the surface of the plastic water phantom. The calibration factor is determined at 22.5ºC.

Different correction factors (table 5.1) have been measured and compared for the two types of diodes. To determine these correction factors the diode was fixed on the surface of the plastic water phantom on the field axis and the ionisation chamber, when needed, was placed at z_{max} on the field axis inside the plastic water phantom. With the exception of the correction factor when a tray is used, where two parameters are changed at the same time from reference conditions (i.e. field size and the tray), only one parameter is changed each time. For instance, to determine field size correction factor, SSD is set to 100 cm and field size is changed from 5 x 5 cm^2 to 40 x 40 cm^2.

Table 5.1. **Definition of the entrance correction factors determined**

CF	
field size	$\frac{OF_{ic}(z_{max}, SSD = 100)^1}{OF_{sc}(SSD = 100)}$
tray	$\frac{transmission\,ic(z_{max}, cxc, SSD = 100)}{transmission\,sc(cxc, SSD = 100)}$

SSD	$\frac{R_{ic}(z_{max},10x10,SSD)/R_{ic}(z_{max},10x10,SSD=100)}{R_{sc}(10x10,SSD)/R_{sc}(10x10,SSD=100)}$
wedge	$\frac{transmission\ ic(z_{max},10x10,\ SSD=100,wd)}{transmission\ sc(10x10,\ SSD=100,\ wd)}$
angle	$\frac{R_{sc}(10x10,SSD=100,0^o)}{R_{sc}(10x10,SSD=100,\theta^o)}$
temperature	$\frac{R_{sc}(22.5^oC)}{R_{sc}(T^oC)}$

[1] OF = R(c x c) / R (10 x 10)

R applies for reading, sc for semiconductor detector (diode), ic for ionization chamber, wd for wedge angle, c for field size, θ for gantry angle, and z_{max} for the depth of dose maximum.

To study the dependence of diode sensitivity on temperature ($CF_{temperature}$) the methodology described in a previous paper [17] was used.

The influence of dose rate (dose per pulse) on diode sensitivity was also studied. The diodes, and the ionisation chamber were inserted in a plastic water phantom at 10 cm depth. The diodes were placed inside the plastic water phantom with their flat surface facing the beam, so both diodes and the ionisation chamber measured at the same depth regardless of the different build-up caps of the diodes. This depth was chosen to exclude the influence of contaminating electrons. The source surface distance was, then, varied from 80 cm (0.54 mGy/pulse) to 130 cm (0.22 mGy/pulse). The field size was set so as to guarantee that the phantom was completely irradiated at any distance.

The loss of sensitivity with accumulated dose was determined for the two sets of diodes. A reading of the diode was taken after irradiations of 20 Gy with 18 MV X-rays, till the accumulated dose reached 300 Gy. A monitoring ionisation chamber was used to prevent accelerator dose fluctuations from influencing the results of this study.

5.4 Results

5.4.1 Initial tests

Results of these tests for both types of diodes are shown in table 5.2.

Table 5.2. Comparison between the results of the initial tests performed on one diode of each type

	EDP30	P30
STABILITY AFTER IRRADIATION (dif. 5 min)	-0.6%	0.3%
INTRINSEC PRECISSION (SD) (10 readings)	0.16%	0.05%
LINEALITY RESPONSE/DOSE (r^2) (range of dose studied)	1.0000E00 (0.17 Gy- 6.78 Gy)	1.0000E00 (0.17 Gy - 3.4 Gy)
DEPTH OF THE DIODE MEASUREMENT POINT	1.4 cm	3.0 cm
FRONT-BACK SYMMETRY (ratio[1])	0.752	0.851
DOSE DECREASE (under the diode) AT 5 cm DEPTH	3%	9%

where:[1] ratio refers to the ratio between the dose at the depth of dose maximum with the diode irradiated with its round size facing the collimator and the dose at the depth of dose maximum with the flat size of the diode facing the collimator.

5.4.2 Calibration factors

The entrance calibration factors for P30 and for EDP30 are 0.191 and 1.492 respectively.

5.4.3 Correction factors

5.4.3.1 Field size correction factor ($CF_{field\ size}$)

Field size correction factor for both type of diodes is shown in Fig 5.1. As can be seen**,** EDP30 would overestimate the dose by 2% for field sizes above 20x20 cm^2 while P30 would underestimate it by the same amount if the field correction factor was not applied. The accuracy in the determination of this correction factor is about 0.2 % (1 sd). The correction factor variation within the same type of diodes is 0.3 % (1 sd) for both types.

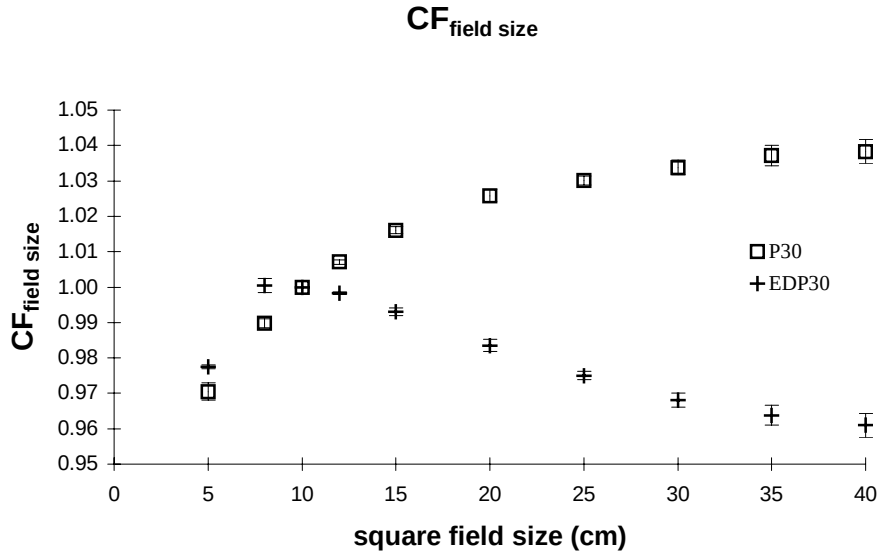

Fig. 5.1. Entrance field size correction factors ($CF_{field\ size}$) for EDP30 (+) and for P30 (□). The mean of the correction factors determined for the three diodes of each type is presented. The error bars correspond to 1sd.

5.4.3.2 Tray correction factor (CF_{tray})

From fig. 5.2. it can be seen that CF_{tray} is negligible, less than 0.5%, for P30, while EDP30 would overestimate the dose by 2% for the maximum field size if the correction factor was not applied. The uncertainty in the determination of this factor is about 0.2% (1 sd) and the factor variation within diodes of the same type is of the same order.

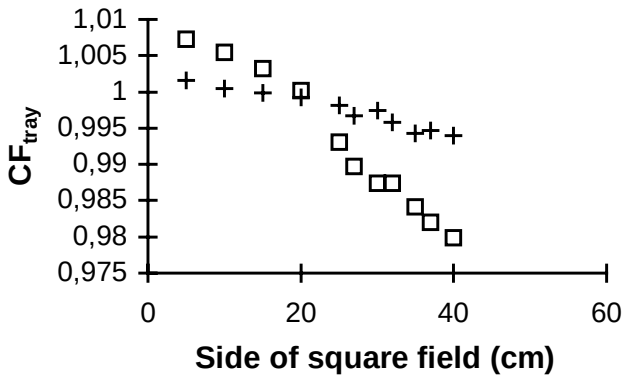

Fig. 5.2. Entrance tray correction factor (CF_{tray}) as a function of field size for EDP30 (+) and for P30 (□). The mean of the correction factors determined for the three diodes of each type is presented. The error bars correspond to 1sd.

5.4.3.3 SSD correction factor (CF_{SSD})

Fig. 5.3 shows the variation of CF_{SSD} for the two types of diodes. The accuracy in the determination of this factor is 0.3% (1 sd). For EDP30, CF_{SSD} increases by about 5% when increasing the SSD from 80 to 120 cm while it increases by about 7% for the same SSD range and for P30 diodes.

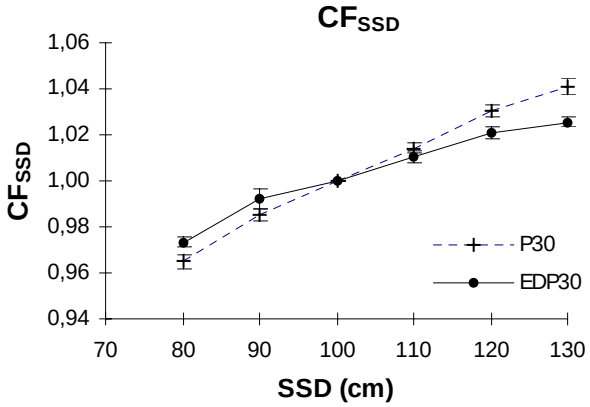

Fig. 5.3. SSD correction factor (CF_{SSD}) for EDP30 and for P30.The mean of the correction factors determined for the three diodes of each type is presented. The error bars correspond to 1sd.

5.4.3.4 Angle correction factor (CF_{angle})

Fig. 5.4.(a) and fig. 5.4.(b) show that the sensitivity of both types of diodes decreases as a function of the angle between the central beam axis and the symmetry axis of the diode (x, y axis fig 5.4). These sensitivity variations amount to 4 % for EDP30 and to 4–5% for P30 for an angle of 45º. For EDP30, the maximum difference within the same batch and for an angle of 45º is about 2% while the maximum difference between measurements for the same diode is 0.5%. For P30, the reproducibility of measurements for the same diode (0.3% as a maximum) as well as the interdiode variability (0.5% for a 45º wedge) is better than for EDP30.

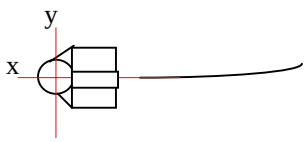

Plane containing x AXIAL
Plane containing y TILT

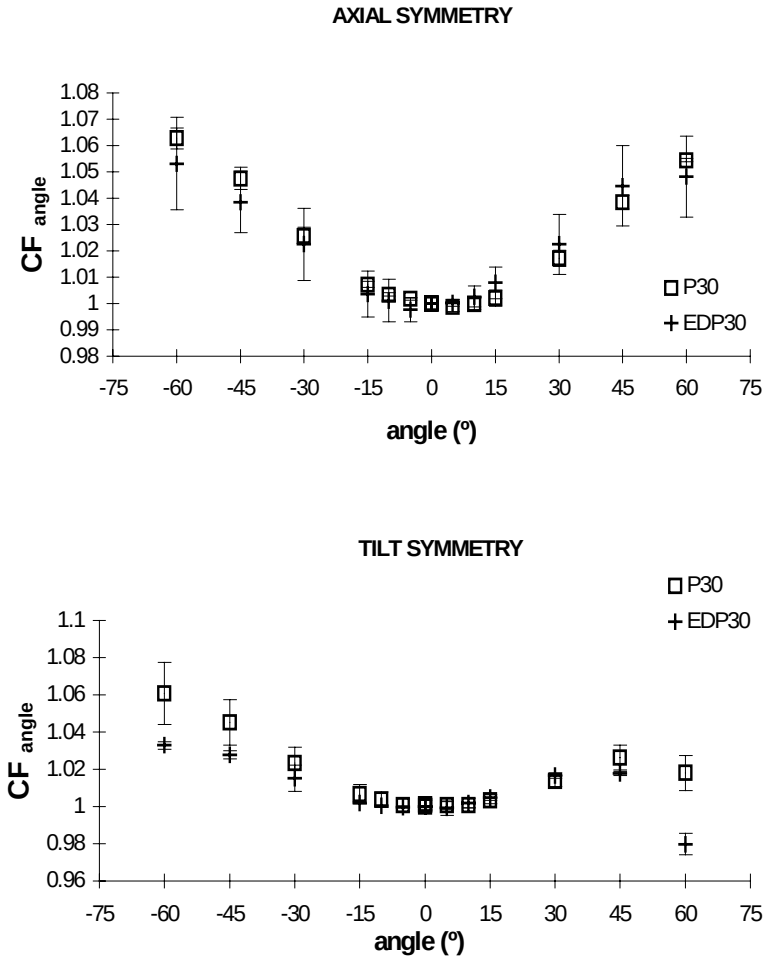

Fig. 5.4 Angular symmetry of both types of diodes. Axial (a) and tilt (b) symmetries are studied. A diagram shows the two symmetry axis. The mean of the correction factors determined for the three diodes of each type is presented. The error bars correspond to 1sd.

5.4.3.5 Wedge correction factor (CF_{wedge})

The effect of wedge filters on diode sensitivity is shown in table 5.3. CF_{wedge} were close to unit for 15º, 30º and 45º wedges for both types of diodes. The 60º wedge correction factor was about 1% for EDP30 while amounted to 4.1% for P30. The uncertainty on the measurement of this factor for the 60º wedge was about 1.6% (1 sd) for EDP30 and 2.4% (1 sd) for P30.

Table 5.3 CF_{wedge}.

Wedge angle	CF_{wedge}

	P30	EDP30
15	0.994±0.003	1.002±0.003
30	0.998±0.008	1.004±0.005
45	0.998±0.009	0.998±0.013
60	1.041±0.025	1.009±0.016

The mean and SD of 5 measurements and for the three diodes of each type is given.

5.4.3.6 Temperature correction factor ($CF_{temperature}$)

The effect of temperature on each diode's response is shown in fig. 5.5. A linear increase of the diode signal with temperature is found. The sensitivity changes by 0.2 % per ºC for P30 and by 0.3 % per ºC for EDP30. As the temperature correction varies significantly within one batch of diodes for both types it is justified determining this factor for each individual diode.

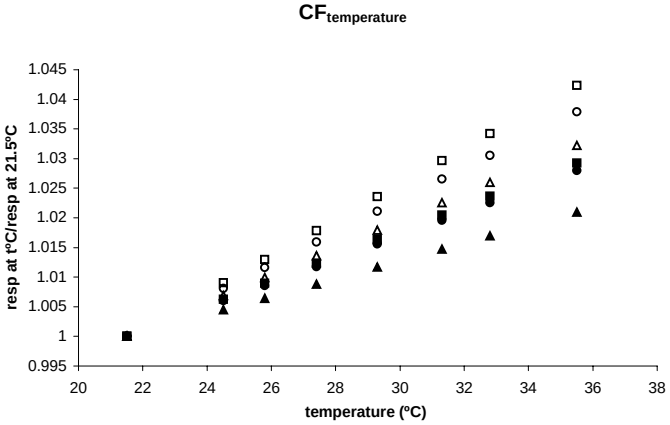

Fig. 5.5 Sensitivity dependence on temperature for EDP30 (empty dots) and for P30 (filled dots). CF for the six diodes is shown.

$CF_{field\ size}$, CF_{tray}, CF_{SSD} and for CF_{wedge} will be the mean of the correction factors determined for the three diodes of each type as the uncertainty on the determination of those factors is of the same order than the difference between the correction factor for diodes of the same type.

5.4.4 *Dose rate dependence*

As it can be seen from Fig. 5.6 the sensitivity variation with dose per pulse is 1% for EDP30 and 3.5% for P30 in the dose per pulse range studied. The uncertainty of the measurements is of the same order of the interdiode variability within the same batch (0.2% 1 sd).

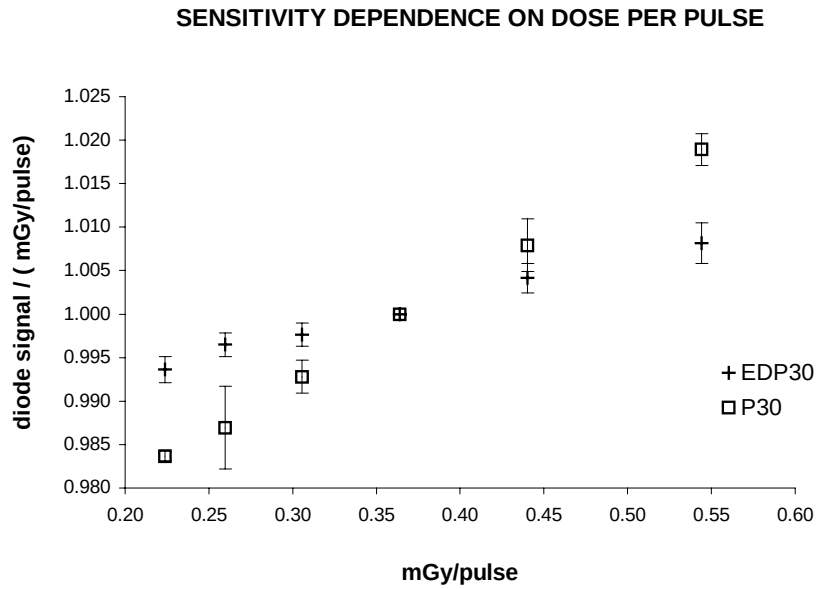

Fig. 5.6 Sensitivity dependence on dose per pulse for EDP30 and for P30.The mean of the correction factors determined for the three diodes of each type is presented. The error bars correspond to 1sd.

5.4.5 *Loss of sensitivity with accumulated dose*

The loss of sensitivity with accumulated radiation dose is shown in Fig. 5.7 The sensitivity of P30 decreases by only 0.2% per 100 Gy while that of EDP30 decreases by 3.4 % per 100 Gy.

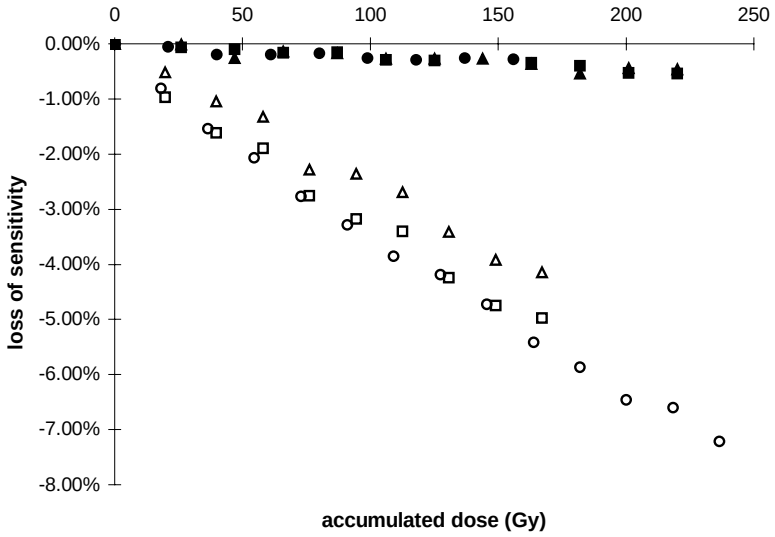

Fig. 5.7 Sensitivity loss with accumulated dose for all EDP30 (empty dots) and for all P30 (filled dots).

5.5 Discussion

5.5.1 **Initial tests** (table 5.2)

All diodes had acceptable signal stability (better than 1%) 5 minutes after irradiation and an acceptable intrinsic precision (better than 0.5%).

The linearity of the diode response with dose was excellent for both types of diodes in the dose ranges studied. As P30 are about 8 times more sensitive than EDP30, when they were connected to DPD510 they saturated with doses higher than 3.5 Gy while no saturation was observed for EDP30 in the range of doses studied. The saturation of P30 with relatively low doses was because the gain of the DPD510 electrometer was not adjusted to the sensitivity of this diode.

Water equivalent build up thickness differs between the two diodes, 1.4 cm for EDP30 and 3 cm for P30. As they are designed to measure in high energy X-ray beams, only P30 measures in conditions of electronic equilibrium in most cases.

The antero-posterior symmetry of P30 is better than that of EDP30. As antero-posterior symmetry is related with the ratio between entrance and exit calibration factors, the overestimation made by using the entrance factor for exit dose measurements will be greater for EDP30 than for P30 (17% and 9% respectively). However, if these diodes have to be used to measure exit doses with accuracy better than 10% an exit calibration factor should be determined. The exit calibration factor is defined as the ratio between the dose measured with an ionisation chamber placed at a depth equal to d_{max} from the exit surface and the reading of the diode tapped on the exit surface of the phantom.

The dose decrease at 5 cm depth under P30 is about 9% while is about 3% for EDP30, making EDP30 more suitable than P30 if the clinic wants to use it in each treatment session. This result is in accordance with the fact that P30 have a thicker build up cap than EDP30. Nevertheless, as both diodes are small no problems would arise if P30 is to be used one or may be few times during the treatment [18].

5.5.2 Calibration factors

There is a factor of 8 between calibration factors of both diodes. This result is in agreement with the difference in sensitivity stated by the manufacturers (a factor of between 4 and 7.5).

5.5.3 Correction factors

5.5.3.1 Field size correction factor (Fig.5.1)

For high-energy photon beams, backscattering is negligible and almost all scattered photons come from the overlying layers [19]. So as the diode is placed on the phantom surface, the reading of the diode is virtually independent of the phantom scatter and only sees the head scatter. Then, the phantom scatter seen by the chamber, placed at 3 cm depth inside the phantom, is higher than the phantom scatter seen by the diode. Therefore, we would expect that diodes underestimated the dose if the diode response was not corrected by field size dependence. However, this only happens for P30 diodes.

EDP30 show the opposite behaviour, they overestimate the dose if no correction is applied. This is because, as the EDP30 build-up cap is not thick enough to guarantee electronic equilibrium, all the electrons scattered from the head of the accelerator reach the diode where as they do not reach the ionisation chamber placed at the depth of dose maximum. This not only compensates for the lack of phantom scatter but overcomes it.

The $CF_{field\ size}$ obtained for EDP30 are in agreement with the results published by Georg et al. [20]. However, for P30 the sensitivity dependence on field size is much lower than that reported for other n-type in vivo diodes [13,15].

5.5.3.2 Tray correction factor (Fig.5.2)

The use of trays to support blocks modifies the incident photon fluency by producing electrons. The block trays used are 6 mm thick, are made of polycarbonate and are placed at 65 cm from the source. P30 and the ionisation chamber, being at the same depth see the same head scatter electron spectrum, therefore no field size dependence on the tray correction factor is expected for P30. For the same reason and

as EDP30 is not measuring under electronic equilibrium, the field size dependence on the tray correction factor can be explained.

5.5.3.3 SSD correction factor (Fig. 5.3)

Georg and al [20] reported an increase in sensitivity by about 3.5 and 4.5% when increasing the SSD from 80 to 120 cm for EDP30 diodes which agrees with our results. However, the results obtained for P30 diodes do not agree with previous published results [15] that reported variations of about 10% when increasing the SSD from 80 to 120 cm for n-type diodes from other manufacturers.

5.5.3.4 Angle correction factor (Fig. 5.4)

For both diodes, having a semi-spherical build-up cap and a ground plate, the directional dependence was expected to be larger than for other diodes having a cylindrical build-up cap. The angle dependence obtained for both types of diodes is larger than it has been reported for Scanditronix diodes [21] (2-3 % for an angle of incidence of 60º). Although both diodes have similar angular dependence, for EDP30 the variation of the dependence within the same batch is not negligible (sd 1.5%) while for P30 the mean of the CF for the three diodes can be used.

5.5.3.5 Wedge correction factor (table 5.3)

The wedges decrease the dose-rate and also change the beam quality; consequently, they change the diode response. This effect is similar for EDP30 and P30 except for the 60º wedge filter. For the 60º-wedge filter the correction factor for P30 is of about 1.040±0.025 while it is 1.009±0.016 for EDP30. These results are in agreement with the dependence on dose rate of both diodes (fig. 5.6). Other authors [2,20,22] suggest correction factors of about 1.5 % for EDP10 and EDP20 and between 1 and 2% for EDP30 which are similar to those obtained for our EDP30.

5.5.3.6 Temperature correction factor (fig. 5.5)

The sensitivity variation with temperature of both types of diodes agrees with the specifications of the manufacturer and for EDP30 it also agrees with the results obtained by other authors [8,10].

The temperature dependence on the diode's sensitivity has been correlated with the dose rate dependence [8] a higher dose rate dependence would mean a higher temperature dependence. However, P30 shows a higher dependence on dose rate than EDP30, which is not in accordance with a lower sensitivity variation with temperature.

5.5.4 Dose rate dependence *(Fig. 5.6)*

From Grussell and Rickner [9,11] hypothesis that dose rate dependence is associated with preirradiated n-type Si diodes, no dose rate dependence would be expected for p-type diodes while for n-type diodes, P30, that have been preirradiated to 25 kGy it would be expected a high sensitivity dependence with dose rate. However from fig. 5.6 it can be seen that both diodes have a dose rate dependence and although P30 has the highest dependence it is only a 2% higher than that of EDP30. These results agree with the sensitivity dependence on SSD (fig. 5.3), where the correction factor is higher for P30 than for EDP30. And also could explain the fact that the 60º wedge correction factor for P30 is a 3% higher than that for EDP30.

5.5.5 Loss of sensitivity with accumulated dose *(fig. 5.7)*

As the preirradiation dose is higher for P30 than for EDP30 the loss of sensitivity obtained for both types of diodes would be in agreement with the hypothesis that the more the diodes accumulate dose the less the sensitivity decreases, reaching a plateau when accumulated doses are high enough. Our results are in disagreement with the thesis that the decrease in sensitivity with irradiation depends on the type of diode [13] (n-type or p-type) and with the 4.5% per 100Gy decrease in sensitivity for an n-type diode reported by Li and al [14].

5.6 Conclusions

Weighing the different correction factors for both types of diodes no conclusions about which type is better can be driven. On one hand, P30 have the highest sensitivity dependence on dose rate and therefore correction factors depending on dose rate as CF_{SSD} and CF_{wedge} for the 60º wedge are higher than for EDP30. On the other hand, EDP30 have an insufficient build up cap and therefore they have a non-negligible tray

correction factor. Moreover, EDP30 also show higher sensitivity dependence with temperature and a greater sensitivity decrease with accumulated dose than P30. Therefore, whether to chose one or the other will depend on the priorities of the user.

However, correction factors that can vary with accumulated dose as CF_{SSD}, CF_{temp}, CF_{wedge} should be redetermined after some time of clinical use to see if they remain constant or not. For n-type diodes a variation of these factors with accumulated dose has been predicted [9]. Recent experiments performed by Lööf [23] et al. show that the dose rate dependence on P30 does not vary with accumulated dose. That would imply that those correction factors would not change after some time of use.

The build up cap should be optimised in both types of diodes in order to make their response more independent of field size keeping the perturbation of the irradiation field as low as possible. Maybe a compromise between the two would be the solution.
Finally, the dependence of diode response on dose rate in a pulsed beam does not seem to be associated with an n-type diode [12,13] but could be associated with the doping level of the diode as has been demonstrated for p-type diodes [11,24].

5.7 References

[1] B.J. Mijnheer, **Possibilities and limitations of in-vivo dosimetry**, in *Radiation dose in radiotherapy from prescription to delivery*, IAEA Report TECDOC-734, edited by IAEA, pp 259-264J.

[2] G. Leunens, J.Van Dam, A. Dutreix and E.van der Schueren.**Quality assurance in radiotherapy by in vivo dosimetry. 1. Entrance dose measurements, a reliable procedure**. Radiother. Oncol. 17, 141-151. 1990.

[3] G. Leunens, J.Van Dam, A. Dutreix and E.van der Schueren. **Quality assurance in radiotherapy by in vivo dosimetry. 2.Determination of the target absorbed dose**. Radiother. Oncol. 19, 73-87. 1990.

[4] J. Van Dam and G. Marinello **Methods for in vivo Dosimetry in External Radiotherapy**. 1st ed. Estro and Garant, Leuven. 1994.

[5] A. Noel, P. Aletti, P. Bey, and L. Malissard. **Detection of errors in individual patients in radiotherapy by systematic in vivo dosimetry**. Radiother. Oncol. 34, 144-151. 1995.

[6] M. Voordeckers, H. Goossens, J. Rutten, W. Van den Bogaert. **The implementation of in vivo dosimetry in a small radiotherapy department**. Radiother. Oncol., 47(1),45-48. 1998.

[7] S. Heukelom, J. H. Lanson and B.J. Mijnheer. **In vivo dosimetry during pelvic treatment**. Radiother. Oncol., 25, 111-126. 1992.

[8] Van Dam, G. Leunens and A. Dutreix. **Correlation between temperature and dose rate dependence of semiconductor response; influence of accumualted dose**. Radiother. Oncol. 19, 345-351. 1990.

[9] G. Rikner and E. Grusell. **Effects of radiation damage on p-type silicon detectors**. Phys. Med. Biol. 28, 1261-1267. 1983.

[10] E.Grusell and G. Rikner. **Evaluation of temperature effects in p-type silicon detectors**. Phys. Med. Biol. 31, 527-534. 1986.

[11] E. Grusell and G. Rickner. **Linearity with dose rate of low resistivity p-type silicon semiconductor detectors**. Phys. Med Biol. 38, 785-792. 1993.

[12] E. Grusell and G. Rickner. **Radiation damage induced dose rate nonlinearity in a n-Type silicon detector**. Acta Radiol. Oncol. 23, 465-469. 1984.

[13] M.Essers, B.J. Mijnheer. **In vivo dosimetry during external photon beam radiotherapy**. Int. J. Radiat. Oncol. Biol. 43**,** 245-249. 1999.

[14] C. Li, L.S. Lamel, D. Tom. **A patient dose verification program using diode detectors**. Med. Dosim. 20**,** 209-214. 1995.

[15] R. J. Meiler, M. B. Podgorsak. **Characterisation of the response of commercial diode detectors used for in vivo dosimetry**. Med. Dosim. 22, 31-37. 1997.

[16] N. Jornet, T. Eudaldo, Mª. D. Carabante, M. Ribas. **Dosimetric Evaluation of a plastic water phantom for high energy photon beam use**. Radiother. Oncol. 51, supplement 1, S40. 1999.

[17] N. Jornet, M. Ribas, and T. Eudaldo. **Calibration of semiconductor detectors for dose assessment in total body irradiation**. Radiother. Oncol. 38, 247-251. 1996.

[18] R. Alecu, J.J. Feldemeier, M. Alecu. **Dose perturbations due to in vivo dosimetry with diodes**. Radiother. Oncol. 42, 289-291. 1997.

[19] J. G. Wierzbicki and D. S. Waid. **Large discrepancies between calculated D_{max} and diode readings for small field sizes and small SSDs of 15 MV photon beams.** Med. Phys. 25(2), 245-246. 1998.

[20] D. Georg, B. De Ost, M.T. Hoornaert, P. Pilette, J.Van. Dam, M. Van Dycke, D. Huyskens. **Build-up modification of commercial diodes for entrance dose measurements in "higher energy" photon beams**. Radiother. Oncol. 51, 249-256. 1999.

[21] S. Heukelom, J. H. Lanson and B. J. Mijnheer. **Comparison of entrance and exit dose measurements using ionization chambers and silicon diodes**.Phys. Med. Biol. 36, 47-59. 1991.

[22] M. Essers, R. Keus, JH. Lanson, et al. **In vivo dosimetry during the treatment of parotid gland tumours.** Radiother. Oncol. 30**,** 154-162. 1994.

[23] M. Lööf, H. Nyström, G. Rikner. **Characterisation of commercial n- and p-type diodes for entrance dose in vivo dosimetry in high energy beams.** Submitted.

[24] D. Wilkins, X. Allen Li, Joanna Cygler, and Lee Gerig. **The effect of dose rate dependence of p-type silicon detectors on linac relative dosimetry**. Med. Phys. 24 (6), 879-881. 1997.

CAPITULO 6

EXPERIENCE OF THE HOSPITAL DE LA SANTA CREU I SANT PAU ON IN VIVO DOSIMETRY (entrance dose)

N. Jornet, M. Ribas.

To be included in the ESTRO BOOKLET: Practical guidelines for the implementation of in vivo dosimetry with diodes in external radiotherapy with photon beams (entrance dose). (under final revission)

R. Boagerts, D. Huyskens (Belgium); M. Lööf, H. Nyström (Denmark); S. Broggi, C. Fiorino (Italy); N. Jornet, M. Ribas (Spain); D. I. Thwaites (United Kingdom). (Authors by alphabetical order of country)

6.1 Tests performed on the diodes before their calibration (Initial tests)

It is not called acceptance test because for some of the tests we have not established acceptance limits.

Due to the way diodes are made, two diodes, even from the same fabrication batch, may not behave the same way when irradiated. Therefore, it is recommended to do some tests before using them in routine. The results of these tests should be contrasted with the technical specifications provided by the manufacturers.

The tests that are performed whenever a new diode is received in our centre are:

6.1.1 Signal stability after irradiation.

6.1.2 Intrinsic precision
6.1.3 Study of the linearity response/dose
6.1.4 Verification of the equivalent water depth of the measuring point (water equivalent thickness of the build-up cap)
6.1.5 Study of the front-back symmetry of the diode
6.1.6 Perturbation of radiation field behind the diode.

All diodes are connected to the same channel of the electrometer to avoid drifts and loss of signal that would depend on the channel where they are connected. All the channels of the electrometer are checked regularly.

All the measurements corresponding to these tests are performed at reference conditions (i.e. collimator opening 10x10 cm^2, phantom surface at the isocenter). For most of the tests the diode is fixed on the surface of a plastic phantom (in our case a polystyrene or a *plastic water* phantom).

6.1.1 Signal stability after irradiation

The display of the signal taken immediately after irradiation is compared with the display of the signal 5 min after the end of the irradiation. Five minutes is considered the average time period of those encountered in clinical practice.

6.1.2 Intrinsic precision

The standard deviation of 10 readings of 100 MU each is calculated.

6.1.3 Study of the linearity response/dose

We verify that the response is proportional (in this case linear) to the absorbed dose for clinical significant doses. As we verify regularly the linearity between M.U and dose, we verify the linearity of the system diode-electrometre between 15 and 600 M.U.

6.1.4 Verification of the water equivalent depth of the measuring point

The diode is fixed on the surface of the *plastic water* phantom and covered with a special *plastic water* slab to avoid air gaps (fig. 6.1). Irradiations with X-rays are performed by adding *plastic water* slabs over the diode until the reading reaches its

maximum. As the depth of dose maximum in water at these irradiation conditions is known, the water equivalent thickness of the build-up cap can be calculated (fig. 6.2).

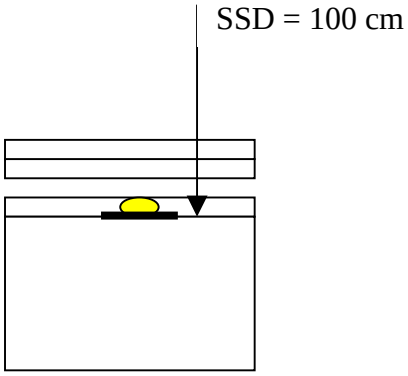

Fig. 6.1 Experimental setting

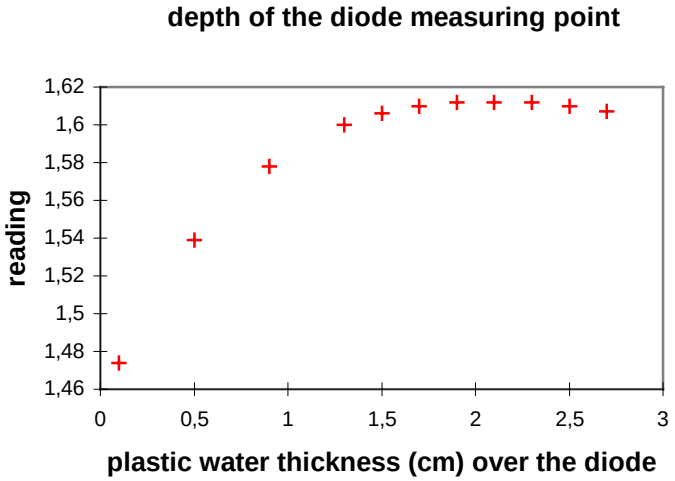

Fig. 6.2 Results for an EDP30 diode. The depth of dose maximum for a 10 x 10 cm^2 and 18 MV X-rays is 3.5 cm, then the water equivalent thickness of the build up cap of EDP30 is 1.4 cm.

6.1.5 Study of the front-back symmetry of the diode

The ratio of the diode reading when irradiated with its round side facing the accelerator collimator, and when irradiated with its flat side facing the collimator, is obtained. The diode measuring point is considered to be on its flat side and is kept at the depth of dose maximum during this test.

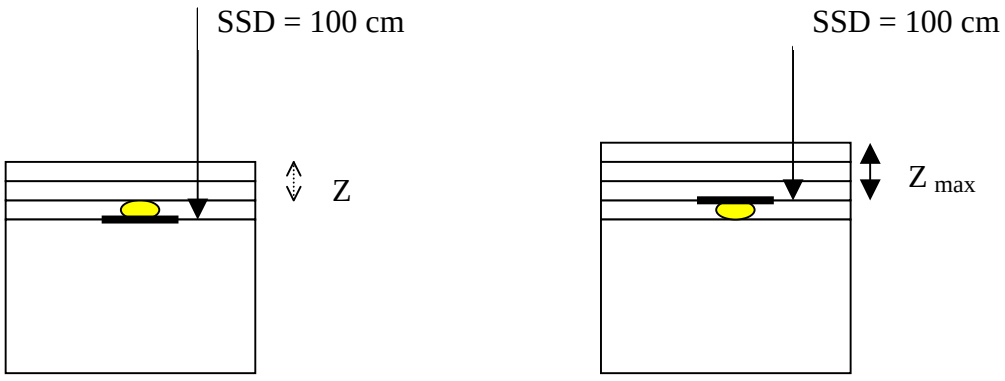

Fig. 6.3 Experimental setting. Z is the thickness of *plastic water* needed to have the measuring point of the diode at the depth of dose maximum (i.e. Z + water equivalent thickness of the build-up-cap of the diode = Z_{max})

6.1.6 Perturbation of radiation field behind the diode: Dose decrease under the diode

First, one X-Omat V Kodak film is placed inside a *plastic water* phantom at 5 cm depth. Then, the diode is fixed on the surface of the phantom. Finally, an irradiation is performed. Another film is exposed under the same conditions but without the diode. The dose decrease at 5 cm depth under the diode is calculated by comparing the two beam profiles at this depth.

We use a film scanner (Scanditronix, as an option of the field analyser RFA-300) to obtain beam profiles. It has a spatial resolution of 0.1 mm.

6.1.7 Results of the initial tests

As an example in table 6.1.a the results of the initial tests for one EDP10 are shown. In table 6.1.b the same is shown for four different types of diodes to be used for high energy X-rays beams (16-25 MV).

Tabla 6.1.a Results of the initial tests (RX-6MV)

	EDP10
Stability after irradiation (5 min)	0.3%
intrinsic precission (sd) (10 irradiations)	0.06%
lineality response/dose (r^2)	1.0000E00 (0.2 Gy-7 Gy)
depth of the diode measurement point (water equivalent depth)	0.80 cm
front back symmetry (ratio[1])	0.989
dose decrease at 5 cm depth	6 %

Tabla 6.1.b Results of the initial tests (RX-18MV)

	EDP30	**P30**	**QED 1116**	**Isorad-p 1164**
Stability after irradiation (5 min)	-0.58%	0.33%	-0.06%	- 0.20%
intrinsic precission (sd) (10 irradiations)	0.16%	0.05%	0.07%	0.10%
lineality response/dose (r^2)	1.0000E00 (0.2 Gy-7 Gy)	1.0000E00 (0.2 Gy-3.5 Gy)	1.0000E0 (0.2 Gy- 7 Gy)	1.0000E00 (0.2 Gy-7 Gy)
depth of the diode measurement point (water equivalent depth)	1.4 cm	3.0 cm	2.2 cm	3.3 cm
front back symmetry (ratio[1])	0.745	0.851	0.941	-
dose decrease at 5 cm depth	2.5%	10.4%	5.6%	14%

[1] ratio refers to the ratio between the dose at the depth of dose maximum with the diode irradiated with its round size facing the collimator and the dose at the depth of dose maximum with the flat size of the diode facing the collimator.

6.2 Methodology for diode's calibration (entrance dose)

Diodes are calibrated against an ionisation chamber placed at the depth of dose maximum inside a plastic phantom (polystyrene *or plastic water*).

The diodes are taped on the surface of the phantom near the field centre, but paying attention that they do not perturb the response of the ionisation chamber (Fig. 6.4). The calibration is performed at reference irradiation conditions (field size at the isocentre 10 x 10 cm^2; SSD = 100 cm) (fig. 6.4). As the accelerator rooms are equipped with air-conditioner the room temperature is always kept between 21ºC and 22ºC.

A 0.6cc cylindrical ionisation chamber (IC) is connected to an electrometer . Their calibration factor is traceable to the National Standard Dosimetry Laboratory in Spain. First, the reading in plastic is converted to reading in water by multiplying the first by a factor determined experimentally (in the case of *plastic water*, this factor is equal to unity). To determine absolute dose to water, the Spanish Dosimetry Protocol is used [1,2]. The Spanish protocol includes the application of a displacement factor, for entrance dose. As the measurements are not performed on the exponential part of the curve but at the depth of dose maximum, this factor is not applied.

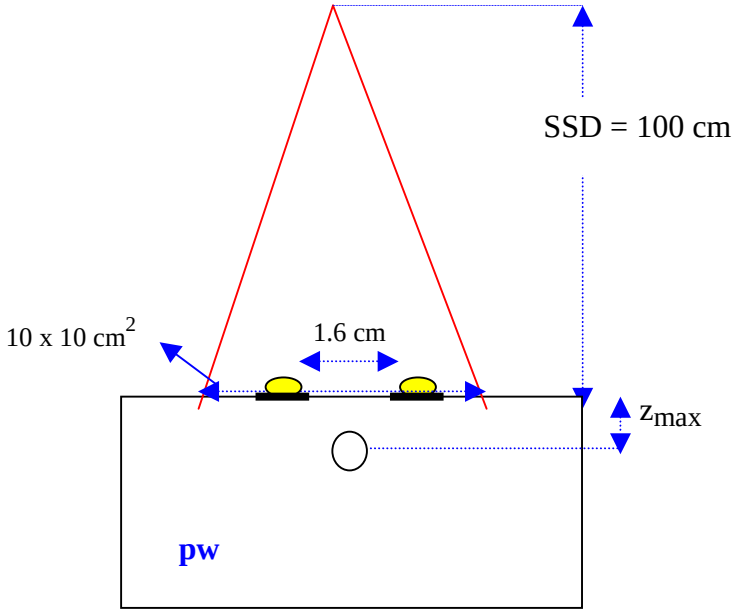

Fig. 6.4 Experimental setting for entrance calibration

The calibration factor F_{cal} is determined as the ratio of the absorbed dose determined with the ionisation chamber and the diode reading (Ec. 6.1).

$$F_{cal} = \frac{\text{absorbed dose IC}}{\text{Diode reading}} \qquad \text{Ec. 6.1}$$

As the sensitivity of the silicon chip of the diodes depends on dose rate, energy and temperature, when measuring conditions differ from calibration conditions some correction factors will have to be applied to the diode reading. Moreover as a diode detector for in vivo dosimetry consists on the chip plus a build-up cap, the design of the latter will have an influence on the diode response when irradiation conditions change. Some of the correction factors depend as well on the diode calibration methodology. In figure 6.5 a schema of the interrelations of the geometrical dependencies of diode's sensitivity with the physical dependencies, build-up cap design and calibration methodology is shown.

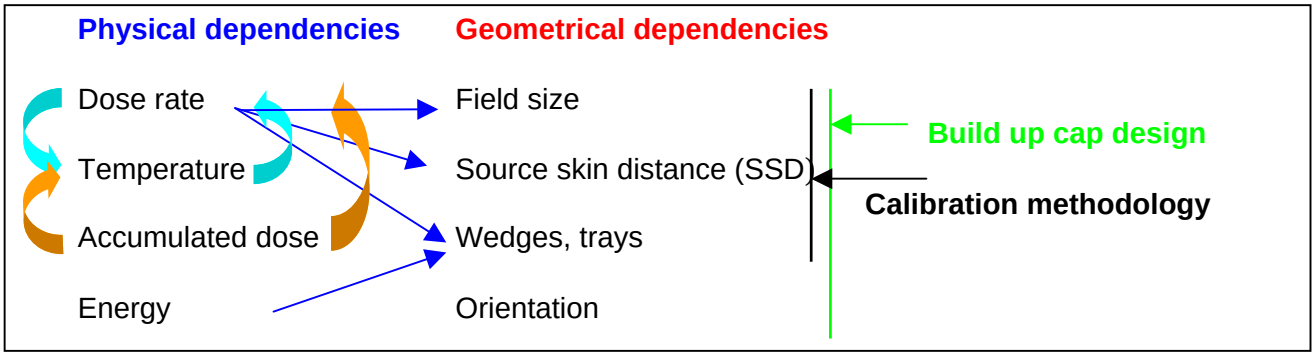

Fig. 6.5 Schema of the relation of the geometrical dependencies of diode's sensitivity (correction factors) with the physical dependencies, build-up cap design and calibration methodology. The arrows show the interrelations.

Let's us take the field size correction factor as an example. The diode is calibrated to give the dose at the depth of dose maximum in standard conditions. When it is taped on the phantom surface the scatter seen by the diode is not the same as that seen by the ionisation chamber (fig. 6.6) so a field correction factor will have to be applied even if the diode build-up cap is thick enough to guarantee electronic equilibrium. Furthermore, as dose rate sensitivity dependence may change with accumulated dose the correction factors that are due to that dependence such as SSD correction factor will have to be checked after some time of use.

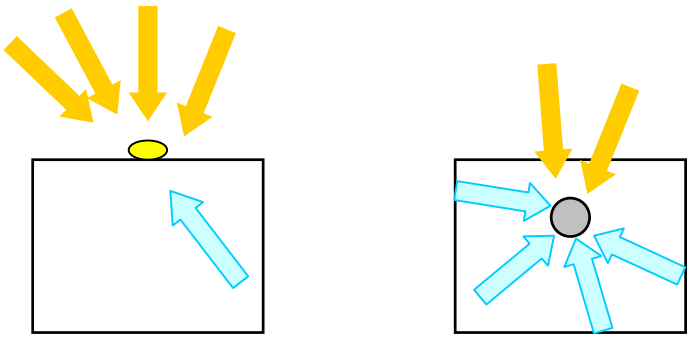

Fig. 6.6 On the left, the diode sees more head scatter than phantom scatter while on the right, the ionisation chamber placed at the depth of dose maximum sees more phantom scatter than head scatter.

The following correction factors are determined:

6.2.1 Field size correction factor ($CF_{field\ size}$)

6.2.2 Tray correction factor (CF_{tray})

6.2.3 SSD correction factor (CF_{SSD})

6.2.4 Wedge correction factor (CF_{wedge})

6.2.5 Angle correction factor (CF_{angle})

6.2.6 Temperature correction factor ($CF_{temperature}$)

In addition, for some types of diodes, the following tests were performed to assess the importance of the following issues:

Influence of the dose rate on the diode's sensitivity
Loss of sensitivity with accumulated dose

6.2.1 Field size correction factor ($CF_{field\ size}$)

Field size correction factor is defined as:

$$CF_{field\,size} = \frac{OF_{ic}(c, z_{max})}{OF_{diode}(c)} \qquad \text{Ec. 6.2}$$

where OF is:

$$OF(c) = \frac{R(c)}{R(10 \times 10)} \qquad \text{Ec. 6.3}$$

and c is the side of the square field in cm, and R applies for reading.

If measures of the OF_{diode} are performed at the same time than OF_{ic} using a plastic phantom, attention should be paid to OF_{ic} because it can differ from OF_{ic} measured in water, so a factor to convert reading-in-plastic to reading-in-water should be applied. This factor will probably depend on field size. To simplify things, you can measure OF_{diode} and compare it with OF_{ic} measured in water at the depth of dose maximum. Field size correction factors for different diodes in different beam qualities are shown in figures 6.7 and 6.8 .

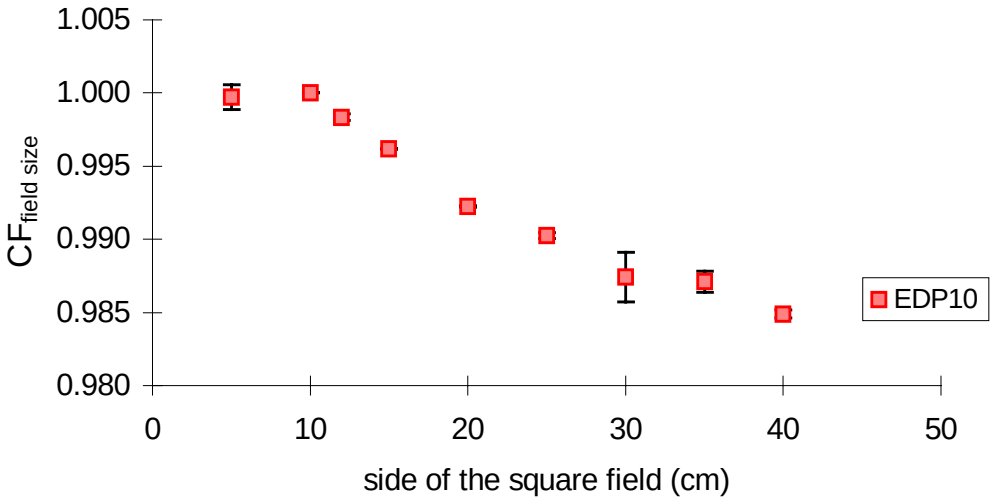

Fig. 6.7 $CF_{field\ size}$ for EDP-10 and 6 MV X-rays. Mean and s.d. of measures performed with 10 diodes is given

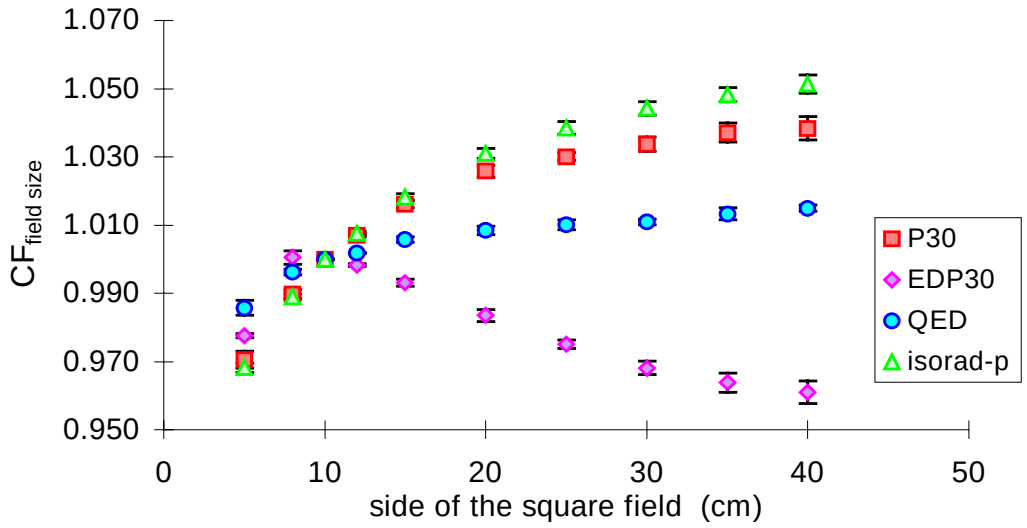

Fig. 6.8 $CF_{field\ size}$ for EDP30, P30, Isorad-p 1164 and QED 1116 for an 18 MV X-ray beam. The mean and standard deviation for three diodes of each type and three measurements is shown.

As mentioned above, even if the diode has an appropriate build up cap (i.e. that guarantees electronic equilibrium) and the equivalent water depth of the measuring point of the diode corresponds to the depth of dose maximum, $CF_{field\ size}$ will be different from unity [3].

6.2.2 Tray correction factor (CF_{tray})

Shielding blocks are positioned on a tray attached to the treatment head. In our hospital, and for Clinac-1800 accelerator, this tray is of PMMA and is 0.5 cm thick. Inserting a tray between the source and the patient increases the amount of electrons that reaches the patient's skin. Therefore, if the diode does not have an appropriate build up cap tray correction factor varies with field size.

To determine CF_{tray}, the tray transmission is first measured with an ionisation chamber for different field sizes at the depth of dose maximum and then with the diodes taped to the surface of the plastic phantom. The transmission factors measured with the ionisation chamber and the diodes are compared, and CF_{tray} as a function of field size is obtained (fig. 6.9 and fig. 6.10).

$$CF_{tray} = \frac{\text{transmission}_{ic}\ (c, \text{water})}{\text{transmission}_{diode}\ (c)} \qquad \text{Ec. 6.4}$$

Where the transmission is defined as:

$$\text{transmission} = \frac{R(c, \text{tray})}{R(c)} \qquad \text{Ec. 6.5}$$

with c is the side of the square field in cm, and R the reading.

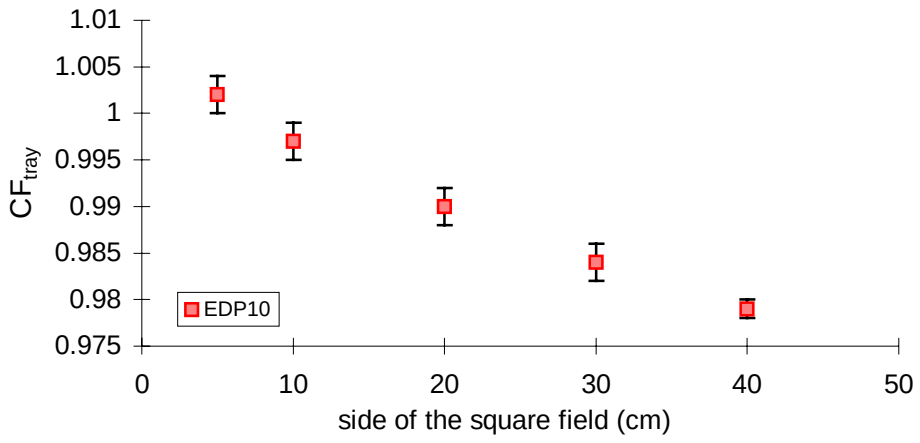

Fig. 6.9 CF_{tray} for EDP10 and 6 MV X-rays. The mean and the s.d. of CF_{tray} determined for 10 EDP10 diodes.

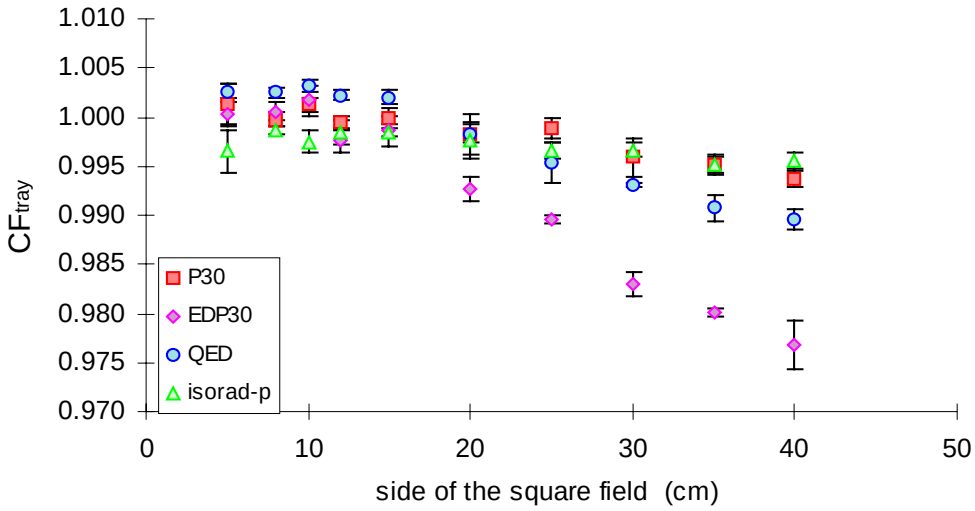

Fig. 6.10 CF_{tray} for EDP30, P30, QED 1116 and Isorad-p 1164 for an 18 MV X-ray beam. The mean and standard deviation for three diodes of each type and three measurements is shown.

6.2.3 SSD correction factor (CF_{SSD})

When the source surface distance is changed, the dose per pulse and the electronic contamination change. First, the sensitivity of the diodes depends on the dose per pulse. Secondly, if the build-up cap of the diode isn't thick enough an overestimation of dose at short SSD can also be due to electronic contamination that would be "seen" by the diode but not by the ionisation chamber placed at the depth of dose maximum. Therefore, a SSD correction factor different from unity is expected.

The correction factor for SSD is defined:

$$CF_{SSD} = \frac{\dfrac{R_{ic}(z_{max}, 10\,x\,10, SSD)}{R_{ic}(z_{max}, 10x10, SSD = 100)}}{\dfrac{R_{diode}(z_{max}, 10\,x\,10, SSD)}{R_{diode}(z_{max}, 10x10, SSD = 100)}} \qquad \text{Ec. 6.7}$$

The diode is taped to the surface of a *plastic water* phantom. The field size is fixed to 10x10 cm^2 at the isocentre. The reading of the diode measured at different SSD normalised to the reading of the diode at 100 cm SSD is compared to the same ratio measured with an ionisation chamber placed inside a *plastic water* phantom at the depth of dose maximum.

In figure 6.11 CF_{SSD} for different types of diodes and for 18 MV X-rays is shown.

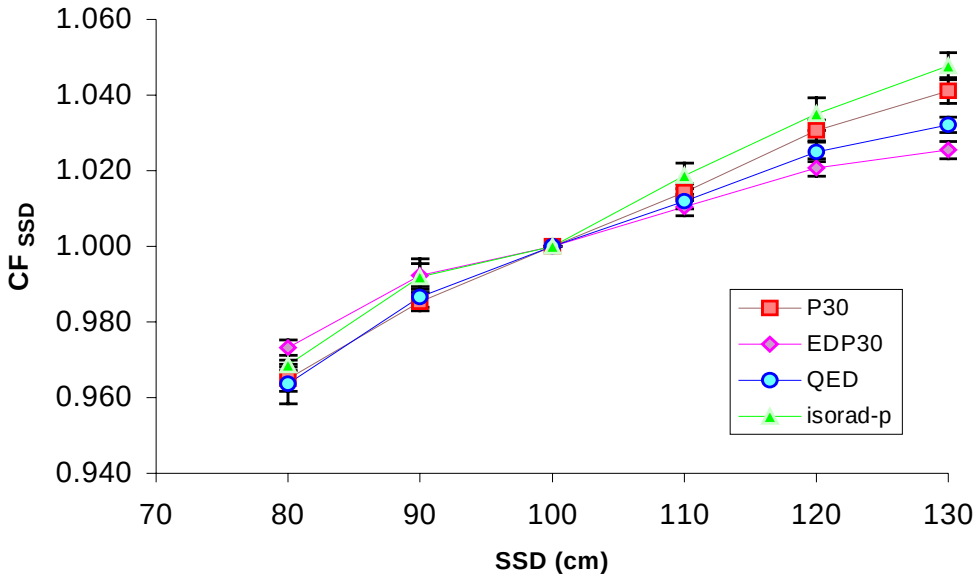

Fig. 6.11 CF_{SSD} for EDP30, P30, QED 1116 and Isorad-p 1164 for an 18 MV X-ray beam. The mean and standard deviation for three diodes of each type and three measurements is shown

6.2.4 Wedge correction factor (CF_{wedge})

Inserting a wedge in the beam results in a decrease of the dose rate and a modification of the spectrum of the beam. Therefore, as the sensitivity of the diode depends on both, dose rate and energy, a correction factor different from unity is expected when using wedges.

The wedge correction factor is defined as the ratio between the transmission factor for a 10 x 10 cm^2 field size, measured with the ionisation chamber placed at the depth of dose maximum, and the transmission factor for the same field size, measured with the diode placed at the field centre taped on the surface of the plastic phantom.

$$CF_{wedge} = \frac{\text{transmission}(w,10\,x\,10,z_{max})_{ic}}{\text{transmission}(w,10\,x\,10)_{diode}} \qquad \text{Ec. 6.6}$$

with w the wedge angle.

For 6 M V X-rays CF_{wedge} was determined for ten EDP10 diodes, three times each and for different field sizes. In this case the estimated uncertainties associated to the determination of this factor are indicated in table 6.1 for the different wedges. These uncertainties correspond to 1sd of 5 measurements performed with the same diode on different days. Therefore, as for EDP10 and 6 MV X-rays beams the dependence on field size of CF_{wedge} is of the same order of the uncertainty of the factor itself, CF_{wedge} is considered independent of field size and the correction factor determined for a 10x10 cm^2 field size is used.

Table 6.1 Uncertainties associated to the determination of the wedge correction factor for EDP10 and 6 MV X-Rays.

Wedge angle (º)	15	30	45	60
Uncertainty (%)	0.2	0.7	0.4	1.0

In table 6.2, the correction factors for the different diodes EDP10, EDP30, P30, QED 1116 and isorad-p 1164 are shown for the different wedges. The mean of 5 measurements for three different diodes of the same type is given.

Table 6.2 CF_{wedge} for different wedges for a 10x10 cm^2 and for 6 MV X-Rays (EDP10) and for 18 MV X-Rays (EDP30 , P30 , QED 1116 and Isorad-p 1164).

Wedge angle (º)	**15**	**30**	**45**	**60**
CF_{wedge} EDP10	1.009	1.013	1.018	1.035
CF_{wedge} EDP30	1.002	1.004	0.998	1.009
CF_{wedge} P30	0.994	0.998	0.998	1.041
CF_{wedge} QED 1116	1.005	0.999	1.012	1.015
CF_{wedge} Isorad-p 1164	0.993	0.989	0.978	1.010

6.2.5 Angle correction factor (CF_{angle})

To measure the directional dependence of the diodes they where placed with the measuring point (considered to be at the basis of the diode) at the isocentre on the surface of the plastic phantom. The variation of the diode response with gantry angle for a 10x10 cm^2 field size was measured with the diode long axis perpendicular (axial symmetry) and parallel (tilt symmetry) to the axis of gantry rotation (fig. 6.12). The results of the measurements are shown in figures 6.13 and 6.14.

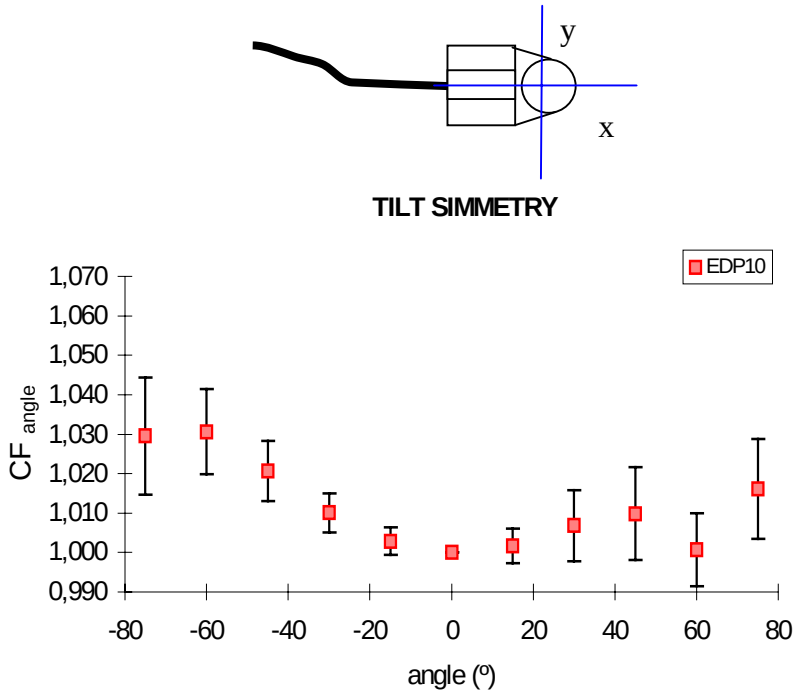

Fig. 6.12 The plane containing x: TILT. The plane containing y: AXIAL.

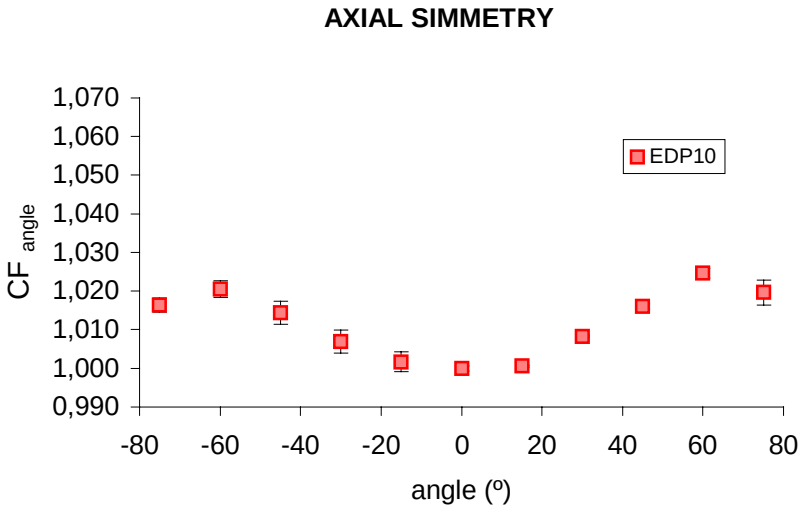

Fig. 6.13 Axial and Tilt symmetry for EDP10, for 6 MV X-Rays.

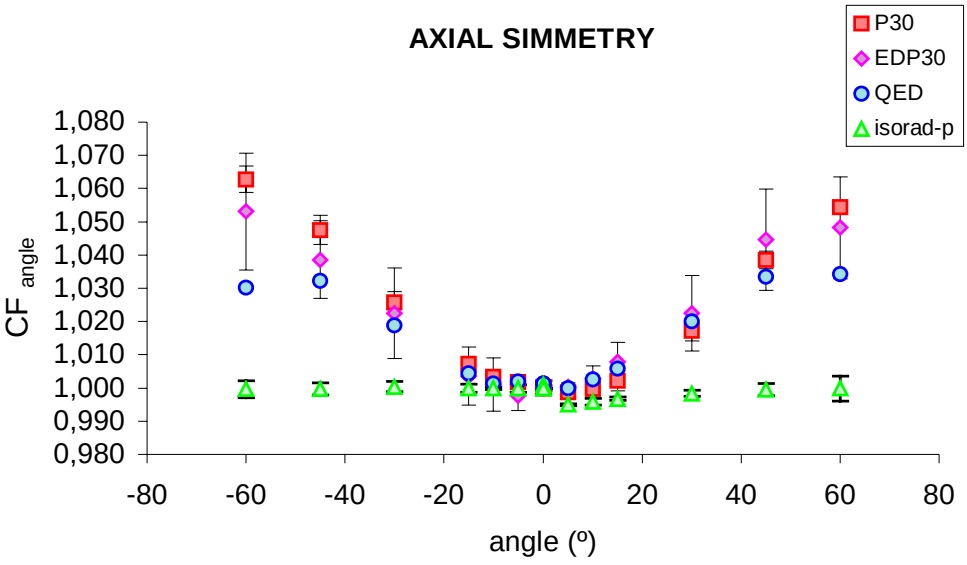

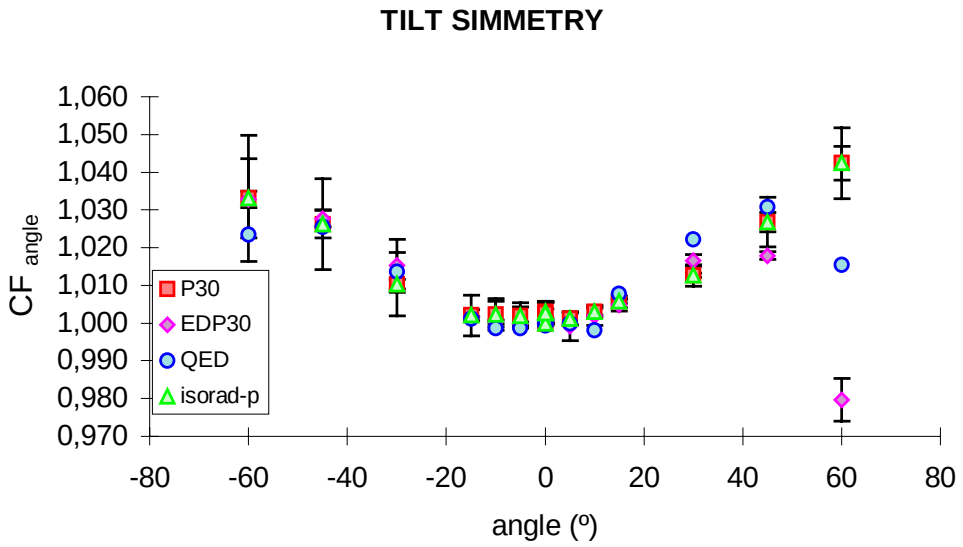

Fig. 6.14 Axial and Tilt symmetry for P30, EDP30, QED 1116 and Isorad-p 1164 for 18 MV X-Rays.

6.2.6 Temperature correction factor ($CF_{temperature}$)

To study the influence of temperature on the diode signal, a water phantom equipped with a thermostat is used. The diodes are taped on a thin slab of Perspex, which is in contact with the water. The temperature, measured with a digital thermistor provided with an immersion probe, is slowly increased from 22ºC to 32ºC. Readings of the diodes are determined at different temperatures and expressed relative to that at 22.5ºC. Each temperature value is maintained approximately 20 minutes in order to reach full thermal equilibrium between the surface of the phantom and the diodes. The variation of the reading of the diode is a linear function of temperature. Then, we can define the sensitivity variation with temperature (SVWT) as the slope of the linear ajust (%/ºC).

The temperature correction factor is defined as:

$$CF_{temperature} = 1 - SVWT \cdot [T(^oC) - 22.5^oC] \qquad \text{Ec. 6.8}$$

if the temperature at which the diodes have been calibrated (T_{cal}) is 22.5. If T_{cal} differs from 22.5ºC the temperature correction factor is defined as:

$$CF_{temperature} = \frac{1 - SVWT \cdot [T(^oC) - 22.5^oC]}{1 - SVWT \cdot [22.5^oC - T_{cal}(^oC)]} \qquad \text{Ec. 6.9}$$

For 10 EDP10 SVWT varies from 0.26 %/ºC to 0.34 %/ºC.

The procedure is done twice, when the diodes are received and after some time of use. In table 6.3 the variation of sensitivity per ºC for one EDP30 diode, new and after some time of clinical use (accumulated dose should be estimated) is shown.

Table 6.3 Variation of sensitivity in % per ºC for one EDP30 diodes. When they are new and after some time of use.

Diode number	New (%/ºC)	Post-irradiation (%/ºC)
1	0. 290	0. 275
2	0. 293	0. 291
3	0. 320	0. 340
4	0. 216	0. 274
5	0. 281	0. 273

In Fig. 6.15 variation of sensitivity of P30, EDP30, Isorad-p 1164 and QED 1116 is shown.

(a)

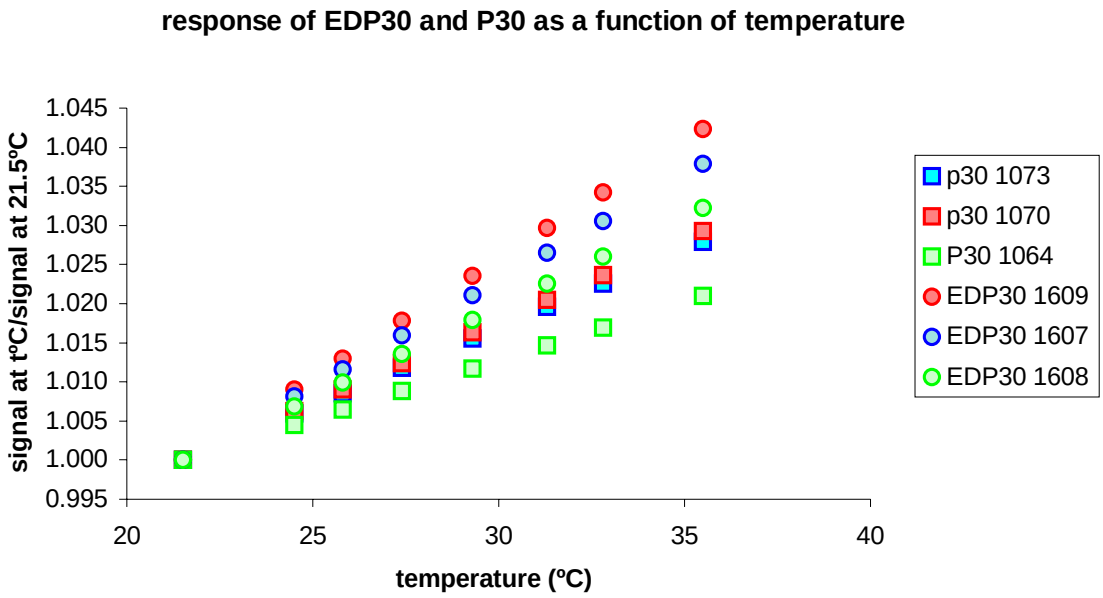

(b)

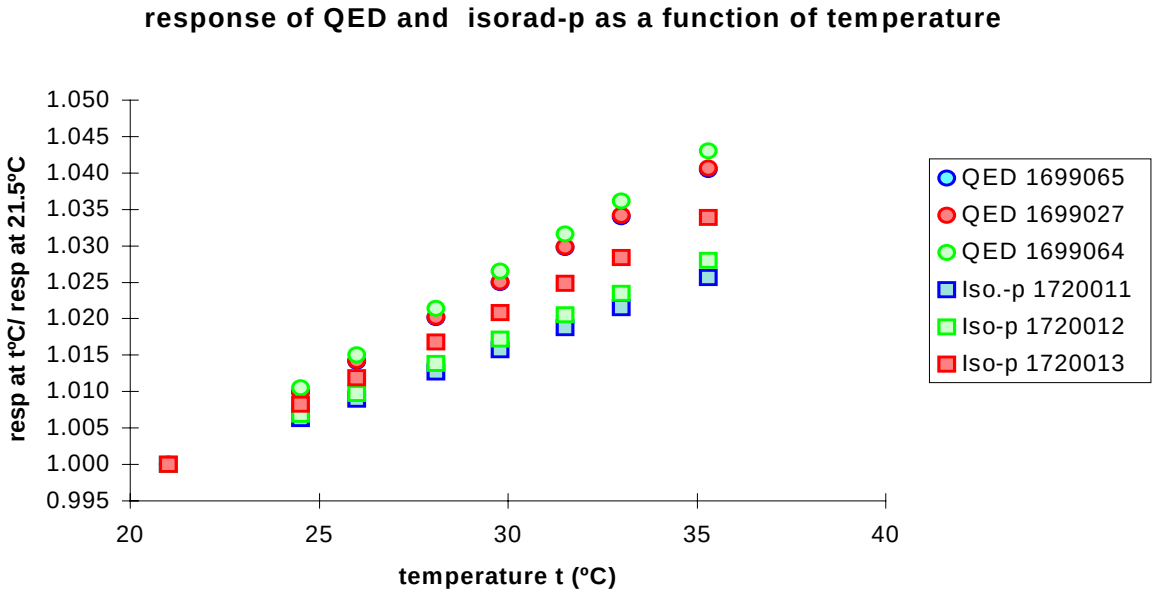

Fig. 6.15 Variation of sensitivity with temperature for (a) three EDP30 and three P30 diodes, and (b) three QED 1116 and three Isorad-p 1164 diodes. Here, we chose 21.5ºC as normalisation temperature, as we are only interested in comparing the different types of diodes.

6.3 Influence of dose-rate on the diode's sensitivity

A Clinac 1800 accelerator (Varian) changes the dose rate by varying the number of pulses per unit of time and not the dose per pulse. Therefore, to test the influence of dose per pulse on the diode sensitivity the following experiment was designed. The diodes are inserted in a *plastic water* phantom at the depth of dose maximum with their flat surface facing the beam. The source surface distance is then varied from 80 cm (0.76 mGy/pulse) to 130 cm (0.29 mGy/pulse). The field size is chosen in such a way that the phantom is completely irradiated at any distance.

No wedges are used to reduce dose rate as by doing so, not only dose-rate would be modified but also the energy spectrum. Then, the results of the experiment would mix up dose rate dependence with energy dependence.

This test has been performed for EDP30, P30, QED 1116 and Isorad-p 1164. Results are shown in fig. 6.16.

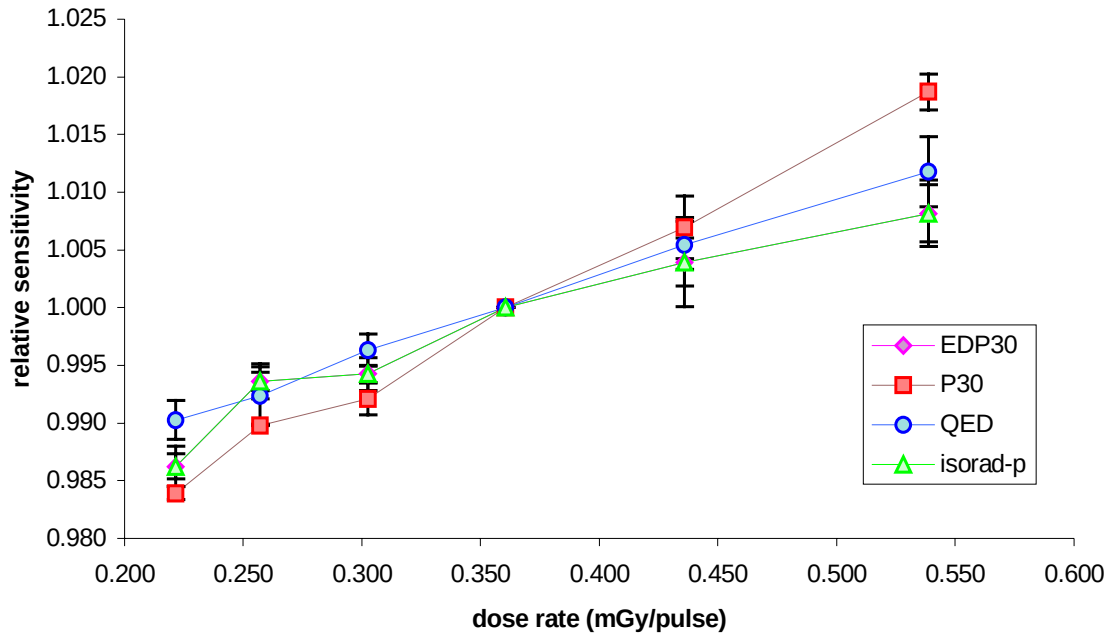

Fig. 6.16 Influence of dose-rate. Relative sensitivity is defined as the ratio of the response of the diode at any dose per pulse to the response at the dose per pulse corresponding to a SSD of 100 cm.

6.4 Loss of sensitivity with accumulated dose (SVWAD)

The loss of sensitivity with accumulated dose has been studied for EDP30, P30, QED 1116 and Isorad-p 1164 diodes. Readings of 177 MU (2 Gy) have been taken after irradiations of 1500 MU (17 Gy) at 240 MU/min (dose-rate used in the clinical practice). An 18 MV X-ray beam has been used. A monitoring ionisation chamber is used to avoid accelerator fluctuations influencing the results of the study.

Fig. 6.17 shows the loss of sensitivity with accumulated dose for the different types of diodes.

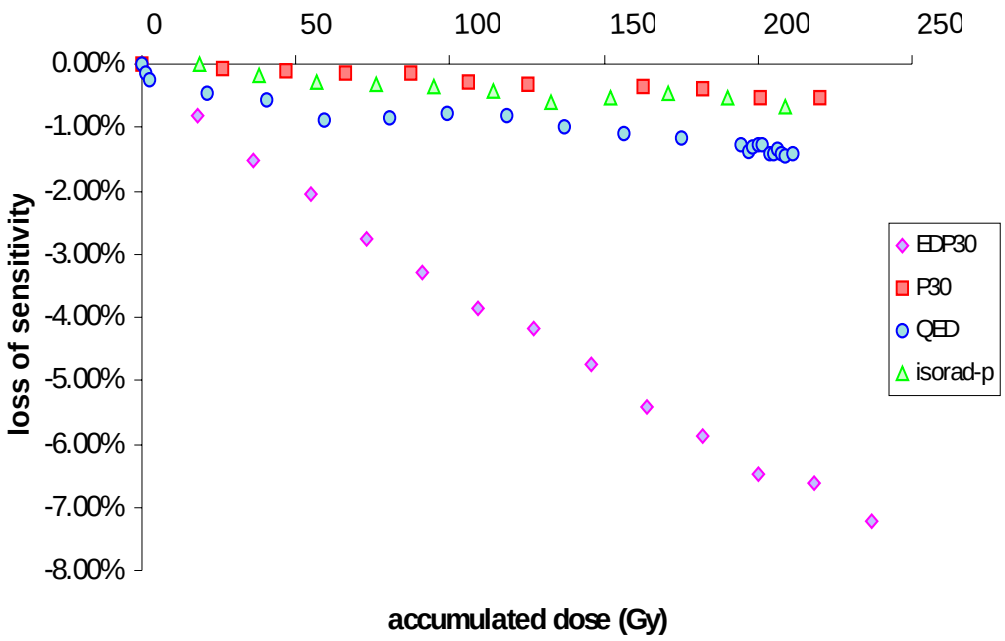

Fig. 6.17 Sensitivity loss with accumulated dose for P30, EDP30, QED 1116 and Isorad-p 1164.

6.5 Summary of correction factors.

The mean and standard deviation of the correction factors for ten EDP10 diodes is given in table 6.4.

Table 6.4 Summary of entrance correction factors for edp10 for 6 MV X-Rays.

CF **field size** SSD =100cm Open field	**Field size (cm)** **5 x 5** **10 x 10** **15 x 15** **20 x 20** **30 x 30** **40 x 40**	 1.000 ± 0.001 1.000 ± 0.000 0.996 ± 0.000 0.992 ± 0.000 0.987 ± 0.002 0.985 ± 0.000

CF_{tray}	**Field size (cm)**	
SSD =100cm	**5 x 5**	1.002 ± 0.002
	10 x 10	1.000 ± 0.002
	15 x 15	0.996 ± 0.002
	20 x 20	0.992 ± 0.002
	30 x 30	0.987 ± 0.002
	40 x 40	0.985 ± 0.001
CF_{angle} (Axial symmetry)	**Angle**	
	0º	1.000 ± 0.000
SSD =100cm	**10º**	1.002 ± 0.001
Field size	**30º**	1.008 ± 0.007
10 x10cm^2	**45º**	1.015 ± 0.010
Open field	**60º**	1.023 ± 0.010
CF_{wedge}	**Wedge angle**	
SSD =100cm	**15º**	1.009 ± 0.002
Field size	**30º**	1.013 ± 0.007
10 x10 cm^2	**45º**	1.018 ± 0.004
	60º	1.035 ± 0.010
SVWT		0.26-0.34%/ºC

For EDP30, P30 and Isorad-p (1164) the mean and the standard deviation of three diodes of each type and three determinations for diode is given. For QED (1116) the mean and standard deviation of one measurement and three diodes is given, with the exception of CF_{wedge} and $CF_{angle.}$, for which the results of one diode and one measurement are given (table 6.4).

Table 6.5 Summary of entrance correction factors for EDP30, P30, QED 1116 and Isorad-p 1164 for 18 MV X-Rays.

$CF_{field\ size}$	**Field size (cm)**	**EDP30**	**P30**	**QED**	**Isorad-p**
SSD =100cm	**5 x 5**	0.978± 0.001	0.970± 0.002	0.986± 0.002	0.968± 0.001
Open field	**10 x 10**	1.000± 0.000	1.000± 0.000	1.000± 0.000	1.000± 0.000
	15 x 15	0.993± 0.001	1.016± 0.001	1.006± 0.001	1.018± 0.001
	20 x 20	0.984± 0.002	1.026± 0.002	1.008± 0.001	1.031± 0.001
	30 x 30	0.968± 0.002	1.034± 0.002	1.011± 0.001	1.044± 0.002
	40 x 40	0.961± 0.003	1.038± 0.003	1.015± 0.001	1.051± 0.003
CF_{tray}	**Field size (cm)**	**EDP30**	**P30**	**QED**	**Isorad-p**
SSD =100cm	**5 x 5**				

	10 x 10	1.000± 0.001	1.001± 0.001	1.003± 0.001	0.997± 0.002
	15 x 15	1.002± 0.002	1.001± 0.001	1.003± 0.001	0.997± 0.001
	20 x 20	0.999± 0.001	1.000± 0.001	1.002± 0.001	0.999± 0.002
	30 x 30	0.993± 0.001	0.998± 0.002	0.998± 0.002	0.998± 0.002
	40 x 40	0.983± 0.001	0.996± 0.000	0.993± 0.000	0.997± 0.001
		0.977± 0.002	0.994± 0.001	0.990± 0.001	0.996± 0.001
CF $_{SSD}$	**SSD (cm)**	**EDP30**	**P30**	**QED**	**Isorad-p**
Field size = 10x10 cm^2	**80**	0.973± 0.002	0.965± 0.003	0.964± 0.005	0.969± 0.001
	90	0.992± 0.004	0.985± 0.002	0.987± 0.003	0.992± 0.003
	100	1.000± 0.000	1.000± 0.000	1.000± 0.000	1.000± 0.000
Open field	**110**	1.010± 0.002	1.014± 0.002	1.012± 0.002	1.019± 0.003
	120	1.021± 0.002	1.031± 0.003	1.025± 0.003	1.035± 0.004
	130	1.025± 0.002	1.041± 0.003	1.032± 0.002	1.048± 0.004
CF $_{angle}$ (Axial symmetry)	**Angle**	**EDP30**	**P30**	**QED**	**Isorad-p**
	0º	1.000± 0.000	1.000± 0.000	1.000	1.000± 0.000
SSD =100cm	**10º**	1.002± 0.006	1.002± 0.002	1.002	1.000± 0.001
Field size	**30º**	1.022± 0.011	1.022± 0.003	1.020	1.000± 0.001
10 x10 cm^2	**45º**	1.042± 0.015	1.044± 0.003	1.033	1.000± 0.001
	60º	1.050± 0.015	1.058± 0.003	1.033	1.000± 0.002
Open field					
CF $_{wedge}$	**Wedge angle**	**EDP30**	**P30**	**QED**	**Isorad-p**
SSD =100cm	**15º**	1.002± 0.003	0.994± 0.003	1.005	0.993± 0.001
Field size	**30º**	1.004± 0.005	0.998± 0.008	0.999	0.989± 0.003
10 x10 cm^2	**45º**	0.998± 0.013	0.998± 0.009	1.012	0.978± 0.011
	60º	1.009± 0.016	1.041± 0.025	1.015	1.010± 0.007
SVWT (%/ºC)		**EDP30**	**P30**	**QED**	**Isorad-p**
		0.23-0.30	0.15-0.21	0.29-0.30	0.19-0.25
SVWAD (%/100Gy)		**EDP30**	**P30**	**QED**	**Isorad-p**
		3.4	0.2	0.8	0.3

6.6 How in vivo dosimetry is performed in routine in our hospital

At this moment an in vivo dosimetry check of entrance dose is performed on the second treatment session of every treatment performed at the linear accelerator (Clinac 1800, 6 MV and 18 MV X-rays). The expected entrance dose (reference dose in next table) is that from the 3D treatment planning system (TPS). In our case CadPlan (Varian-Dosetek Oy, vs. 2.7, 6.2.7).

The dosimetrist is asked to fill the following table:

Patient's name:
Identification number:
Dosimetry number:
Cadplan identification number:
Date of simulation:
Anatomical localisation:
Energy:
CT planning (Y/N):

Dose per fraction to ICRU point (Gy):

	Field identification			
Gantry angle				
SSD (cm)				
Equivalent field size (cm x cm)				
Wedge (º)				
Tray (Y/N)				
diode angle (º)				
Reference dose (CadPlan)				
ICRU point dose				

Where **diode angle** refers to the angle between the perpendicular to the diode basis and the angle of incidence of the beam and **reference dose** corresponds to the dose at 1.5 or at 3.5 cm depth from the entrace surface for 6 MV and 18 MV X-rays respectively.

From this table the expected reading of the diode can be easily calculated by dividing the reference dose by all the correction factors. This value is used to give the range inside which the in vivo measurement should be.

Then the radiation therapists, at the treatment unit, on the second treatment fraction are asked to fill in the following table (in vivo chart):

Date:

Field identification				
DFD (cm) (detector focus distance)				
Acceptance limits	Filled in by the physicist			
Diode reading				

If the entrance dose is out of limits	Energy	Cerrobend blocks
You should **CHECK**	Field size	MU
	SSD	wedge
	Diode position (has it turned? has it fallen down?)	
	Error with the SET	

The acceptance limits (that's to say the limits within which the in vivo dose measuremet should be so that no action would be taken) at this moment are ±5% of the expected entrance dose when no wedges are used and ±7% when wedges are used.

Once the in vivo dosimetry has been performed, on the same day or the day after, a physicist evaluates the results.

If the entrance dose differs with the prescribed dose in more than a 5 %, an immediate check of the patient set-up and the diode position is performed. If the radiation therapists detect any anomaly on those parameters, they are asked to repeat the in vivo measurements during the next treatment session. If they don't find any reason for the difference two situations have to be distinguished:

1. The differences are for most of the patients that day. If several in vivo entrance doses do not match with the expected entrance doses during the same day the calibration of the beam should be checked as well as the calibration factors of the diodes.

2. The differences are for only one patient. In that case, the physicist should go over the in vivo chart, the dosimetry chart, to check the monitor unit calculation and finally to perform a phantom simulation.

The flow diagram showing what it is done when the action levels are exceeded for entrance dose is shown in figure 6.18.

Since now, we have found an explanation for all the deviations. The most frequent reasons for deviations greater than 5% in the entrance dose were:

- The diode has turned or fallen down.
- There has been a set up error (SSD, field size, cerrobend blocks)
- There has been a mistake when introducing the calibration factors of the diodes in the electrometer.
- For isocentric techniques the SSD during the treatment is not the same that it was planned due to a change in the diameter of the patient.

Some times, due to the patient position or immobilisation device the diode can not be placed directly on the patient's skin. Only on these cases the reading of the diode is corrected by the inverse square law.

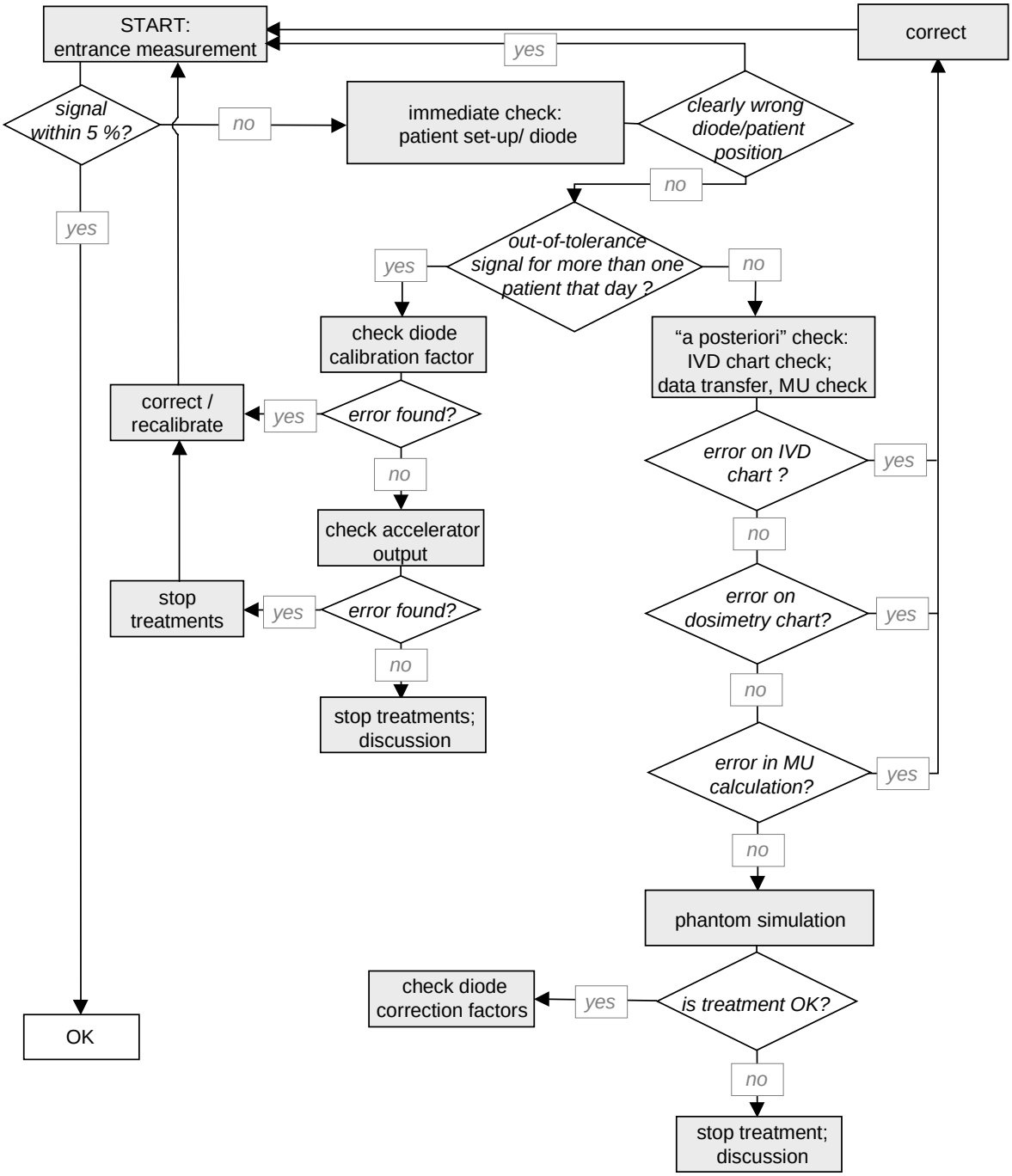

Fig. 6.18 Decision flow chart for entrance in vivo dosimetry.

6.6.1 How entrance in vivo dose is calculated from entrance in vivo measurements

$$D_{ent,diode} = L_{ent,\,diode} \times F_{cal,ent} \times CF_{ent} \qquad \text{Eq. 6.10}$$

$$CF_{ent} = CF_{field} \times CF_{tray} \times CF_{angle} \times CF_{SSD} \times CF_{wedge} \qquad \text{Eq. 6.11}$$

$$F_{cal,ent} = \frac{D_{ic,}(z_{max},10x10)}{L_{diode}} \qquad \text{Eq. 6.12}$$

Equation 6.12 corresponds to equation 6.1 for entrance calibration.

6.6.2 Results

An "in vivo dosimetry" Excel book manages all patients and gives "on line" the mean and s.d. of all treatments that have been evaluated. As an example in table 6.6 the deviation in % between expected and measured entrance dose for all evaluated pelvic treatments is shown.

In our department, pelvis are treated with 18 MV X-rays using a four conformed field box technique. We treat at a SSD = 100 cm, i.e we do not use an isocentric technique.

Table 6.6 Deviations between entrance doses measured by in vivo measurements and predicted by CadPlan (3D and 2D dosimetries).

	C2 left	C4 right	C2+C4 lateral	C3 post	C1 Ant	C1+C3 A/P	All fields
Mean	0.965%	0.328%	0.646%	1.828%	1.273%	1.551%	1.098%
Sd	2.026%	2.630%	2.37%	1.982%	2.38%	2.207%	2.333%
N	706	706	1412	706	706	1412	2824

Mean and s.d. refer to the mean and the standard deviation of the deviations in % between expected (CadPlan) and measured dose for each field. N is the number of treatments evaluated (in this case large fields and boost fields are considered together).

Table 6.7 Deviations between entrance doses measured by in vivo measurements and predicted by CadPlan (3D dosimetries).

	C2 left	C4 right	C3 post	C1 Ant	All fields
Mean	0.349%	-0.330%	1.250%	1.505%	0.694%
Sd	2.520%	2.220%	1.971%	2.660%	2.430%
N	22	22	22	22	88

Mean and s.d. refer to the mean and the standard deviation of the deviations in % between expected (CadPlan) and measured dose for each field. N is the number of treatments evaluated (in this case large fields and boost fields are considered together).

The uncertainty in the measured entrance dose in these kind of treatments has been estimated in 1.6% (1 s.d.).

The accuracy of the entrance dose measured with the diodes will depend on the accuracy of F_{cal} and CF that has been estimated to be 0.5% (1 s.d.) and on the reproducibility and accuracy of diode's positioning 1.5% (1 s.d.).

So we are evaluating the possibility of changing the tolerance level to 3% for entrance doses and pelvic treatments.

6.7 References

[1] SEFM (Sociedad Española de Física Médica). **Procedimientos recomendados para la dosimetría de fotones y electrones de energías comprendidas entre 1 MeV y 50 MeV en radioterapia de haces externos**. 1984.

[2] SEFM (Sociedad Española de Física Médica). **Suplemento al documento SEFM nº 1: Procedimientos recomendados para la dosimetría de fotones y electrones de energías comprendidas entre 1 MeV y 50 MeV en radioterapia de haces externos**. 1987.

[3] N. Jornet, M. Ribas, T. Eudaldo. **In vivo dosimetry: Intercomparison between p-type and n-type based diodes for 16 to 25 MV energy range**. Med. Phys., vol 27 nº6, 1287-1293. 2000.

CAPÍTULO 7

DISCUSIÓN DE LOS RESULTADOS

7.1 Introducción

En este estudio se pone a punto un sistema de dosimetría *in vivo* con diodos que permite, por un lado, determinar la dosis en distintos puntos en la técnica de irradiación corporal total (ICT), y por otro, verificar la dosis administrada en tratamientos estándar con haces de fotones de alta energía.

Dado que se calibran los diodos con dos finalidades distintas, se ha optado por dividir la discusión en dos apartados. El primero corresponderá a la determinación de la dosis en la técnica de ICT y el segundo a la dosimetría *in vivo* como herramienta de la garantía de calidad en los tratamientos con radioterapia.

7.2 La dosimetría *in vivo* en la técnica de ICT

En nuestro centro, un paciente sometido a una irradiación corporal total se trata en bipedestación a 405 cm de la fuente de irradiación y con un haz de RX de 18 MV [1,2]. Para conseguir que la piel esté correctamente irradiada, se interpone una lámina de metacrilato de 1 cm de grosor entre la fuente y el paciente con la finalidad de degradar el haz. Los pulmones se protegen con bloques de *cerrobend* que atenúan parcialmente el haz. De esta forma, el pulmón recibe una dosis de radiación más baja durante todo el tratamiento. Todos estos parámetros hacen que no sea posible planificar el tratamiento de forma estándar, es decir, mediante un sistema de planificación 3D utilizando imágenes de TC. Para ello, sería necesario, en primer lugar, introducir en el planificador los perfiles, rendimientos en profundidad, la tasa de dosis y

demás parámetros requeridos por el planificador en condiciones de ICT y en segundo lugar, obtener imágenes TC con el paciente en bipedestación. Dada la dificultad de la primera condición y la imposibilidad en estos momentos de obtener imágenes TC en bipedestación, se optó por la dosimetría *in vivo* con diodos para determinar la dosis *on line* en diversos puntos de interés en el paciente (cabeza/cuello, pulmones, abdomen, extremidades inferiores).

Los diodos escogidos con esta finalidad fueron los EDP30 que acababan de ser comercializados por Scanditronix para ser utilizados en haces de RX de energías comprendidas entre 16 y 25 MV. Scanditronix indicaba que estos diodos estaban provistos de un capuchón de equilibrio electrónico de 3 cm equivalentes agua de grosor.

En primer lugar, previa a su calibración para ICT, se sometieron los diodos a un test inicial o de aceptación (capítulo 3). En él se comprobaba la estabilidad de la respuesta de los diodos post-irradiación, la linealidad de la respuesta con la dosis, la reproducibilidad de las medidas, el grosor equivalente agua del capuchón de equilibrio electrónico, la simetría antero-posterior de la respuesta y la perturbación del haz en profundidad debida al diodo.

De estos tests cabe destacar dos resultados: 1) el grosor del capuchón de equilibrio electrónico y 2) la asimetría de la respuesta antero-posterior.

1. A partir de la tabla 3.1 se constata que el grosor equivalente agua del capuchón de los EDP30 es igual a 14 mm para fotones de 18 MV. Este resultado ha sido corroborado por Meijer et al. [3]. Este capuchón es insuficiente para garantizar el equilibrio electrónico en el punto de medida del diodo. Sjören y Karlsson [4] cuantificaron la contaminación electrónica en un haz de RX de 20 MV para distintas condiciones de irradiación (distintas DFS, distintos tamaños de campo, interponiendo filtros y bandejas entre la fuente y la superficie, etc). Concluyeron que el capuchón de equilibrio electrónico de los EDP30 es suficiente para absorber todos los electrones secundarios pero sería necesario añadir un capuchón adicional para aumentar el número de fotones dispersados cerca de la parte sensible del detector.

2. El diodo presenta una asimetría entre la respuesta anterior (diodo con la superficie curva mirando al foco de irradiación) y posterior (diodo con la superfície plana mirando al foco de irradiación) de aproximadamente un 25%. En este test, la parte sensible del detector está a 100 cm de la fuente y está cubierta por el mismo espesor equivalente agua cuando se mide la respuesta anterior y posterior (3.5 cm equivalentes agua). Esta asimetría tiene como consecuencia que el diodo subestima la dosis en este porcentaje si se utiliza el factor de calibración entrada cuando el diodo mide dosis salida.

La calibración de los diodos se hace en condiciones de ICT. Se realizan cuatro calibraciones independientes, entrada sin y con bloque de *cerrobend* de transmisión parcial ($F_{cal,en}$, $F_{cal,en,cer}$) y salida sin y con bloque de transmisión parcial ($F_{cal,ex}$, $F_{cal,ex,cer}$). Si se utilizara el factor de calibración entrada para las medidas a la entrada detrás de un bloque de 3 cm de grosor se infraestimaría la dosis en un 30-35%. Este porcentaje aumenta a medida que el grosor del bloque aumenta (tabla 3.2). En la tabla 3.2 también se puede ver que si se añade un capuchón de equilibrio electrónico adicional de tal manera que el grosor total del capuchón sea igual a 3 cm y se calibra comparando la lectura del diodo con la de la cámara de ionización a 3 cm de profundidad, la dependencia del cociente $F_{cal,en,cer}/ F_{cal,en}$ con el grosor del bloque y el valor absoluto de este cociente disminuyen.

En el capítulo 3 también se estudia la dependencia de la sensibilidad de los diodos con la temperatura. En este caso se obtienen resultados muy similares a los obtenidos por otros autores [5-7]. Un diodo calibrado a 22.5ºC (temperatura ambiente de la sala) sobrestimaría la dosis en aproximadamente un 3% cuando se fija sobre el paciente. Este resultado se corrobora en el capítulo 4 en donde se presentan los resultados de las medidas *in vivo* sobre una serie de 60 pacientes sometidos a ICT. Si no se aplicara el factor de corrección por temperatura existiría una desviación sistemática entre la dosis prescrita y la dosis calculada a partir de las medidas *in vivo* de un 2-3%.

Una vez se han calibrado los diodos, es necesario desarrollar e implementar algoritmos de cálculo para que a partir de las dosis medidas a la entrada y a la salida del haz de radiación se pueda calcular la dosis a plano medio. En el capítulo 4 se ponen a punto dos algoritmos, uno desarrollado en el propio centro, muy simple, que

consiste en la media entre la dosis entrada y la dosis salida corregida por un factor, CF (ec. 4.1), que depende del grosor real del paciente en los puntos de interés y otro más complejo que fue desarrollado por Rizzotti [8].

Antes de utilizar estos algoritmos en rutina y para calcular dosis en pacientes, se verifican en maniquíes regulares y homogéneos y en maniquíes antropomórficos contrastando los resultados obtenidos con medidas a plano medio realizadas con cámaras de ionización y detectores termoluminiscentes. No se encuentran diferencias significativas entre los dos métodos de cálculo y los valores obtenidos coinciden dentro de un 2% con las medidas con cámara de ionización y en un 3 % con las medidas con detectores termoluminiscentes para un maniquí homogéneo. Estos porcentajes se corresponden con las incertidumbres (1 DE) en las medidas de ambos métodos. En el maniquí antropomórfico, ambos algoritmos coinciden y la dosis calculada es igual, dentro de la incertidumbre de la medida, a la dosis determinada con los detectores termoluminiscentes.

El algoritmo simple resulta también útil para calcular la dosis a plano medio de pulmón con y sin bloques de transmisión parcial. Cuando no se utilizan estos bloques de protección, dado que CF no varía demasiado con el grosor (de 1.015 a 0.985 entre 7 y 32 cm), no es necesario calcular el grosor equivalente agua para determinar CF utilizando la gráfica de la figura 4.1 (a). Al interponer las protecciones a pulmón, para el cálculo de la dosis a plano medio de pulmón se ha de utilizar una calibración especial de los diodos (capítulo 3) y un factor de corrección CF' determinado en estas condiciones (fig. 4.1 (b)). Este factor depende fuertemente del espesor, principalmente durante los 10 primeros centímetros. Por lo tanto, cuando se interponen las protecciones a pulmón, debe utilizarse el grosor equivalente que se obtiene a partir de la transmisión y del rendimiento en profundidad en un maniquí equivalente agua (fig. 4.2). El algoritmo propuesto por Rizzotti resulta útil en este caso ya que el grosor equivalente agua está implícito. La determinación de CF' y de las curvas de Rizzotti en el caso de que las protecciones se utilicen, conlleva más incertidumbre que cuando se determinan sin ellas. Por esto, la dosis a pulmón detrás de las protecciones se da con una incertidumbre de aproximadamente $\pm$10%.

De las medidas sobre la serie de pacientes se puede ver que la dosis esperada a la entrada sobre el eje central del haz coincide con la dosis medida (fig. 4.4 a). Para el

campo anteroposterior (A/P), con la excepción de un caso, en que existe una desviación de un 4% respecto a la dosis esperada, todas las medidas tienen desviaciones respecto a la dosis esperada inferiores al 2 %. Para el campo posteroanterior (P/A) todas las desviaciones están dentro del 4 % a excepción de 5 medidas que corresponden al paciente más grueso de la serie (35 cm). La dispersión de resultados cuando se compara la dosis medida a la salida en el eje central con la dosis esperada es mucho mayor que la obtenida cuando se valora la dosis entrada (fig. 4.4 b). Los histogramas, en este caso, están centrados sobre –1.3% para el campo A/P y sobre –3.6% para el campo P/A. Esta desviación sistemática de las medidas se asocia al hecho de que el diodo de salida está en contacto con el soporte de la ICT. En este caso, cualquier movimiento del paciente puede mover el diodo de tal manera que se pierda la perpendicularidad entre el eje del haz y la base del diodo. En la irradiación P/A el diodo que mide la dosis a la salida del haz está fijado sobre el abdomen del paciente y en pacientes con diámetros superiores a 25 cm, la movilidad de éste es importante. Este hecho justifica que en este caso la media de las desviaciones sea superior para el campo P/A que para el A/P. Las dosis a plano medio calculadas a partir de las medidas *in vivo* con el algoritmo simple coinciden con las dosis prescritas para ambos campos.

En la figura 4.5 se puede ver que no existen diferencias significativas entre las dosis a plano medio en el eje central del haz calculadas a partir de las medidas *in vivo* por los dos métodos. Dado que los factores CF (sin bloque de *cerrobend*) (fig.4.1(a)) son muy próximos a la unidad, el método simple permite conocer de forma inmediata la dosis a plano medio a partir de las dosis entrada y la dosis salida. Esta es la principal razón por la que en nuestro centro se ha optado por utilizarlo en rutina.

7.3 La dosimetria *in vivo* como control de calidad en un tratamiento

El éxito de un tratamiento con radioterapia depende, entre otros parámetros, de que la dosis administrada sea realmente la prescrita por el radioterapeuta. La dosimetría *in vivo* nos permite monitorizar la administración de la dosis de forma independiente a los sistemas de planificación y a los programas que calculan las unidades de monitor. Es pués, un sistema único para verificar toda la cadena dosimétrica, desde la calibración del haz, pasando por la planificación del paciente, hasta la sesión de tratamiento.

Dependiendo de la magnitud de los errores que se quieran detectar, la calibración de los diodos deberá ser más o menos exhaustiva.

En el capítulo 6, se describen ampliamente los procedimientos para calibrar los diodos. Para verificar la metodología de calibración ésta se aplicó en la calibración de un conjunto de diez diodos EDP10 ya que los factores de corrección para este tipo de diodos han sido publicados por distintos grupos de investigación [9,10]. Dado que los resultados obtenidos eran coherentes con los publicados se adoptó esta metodología en la calibración de distintos tipos de diodos (EDP30, P30, QED 1116 y Isorad-p 1164) diseñados para medir la dosis *in vivo* en haces de RX de energías comprendidas entre 16 y 25 MV.

Se calibraron 3 diodos de cada tipo. Los factores de corrección se determinaron 3 veces para cada diodo.

El factor de corrección por tamaño de campo para campos mayores que el de 10 x 10 cm^2 es inferior a la unidad para los EDP30 mientras que supera la unidad para los restantes. El hecho de tener un capuchón de equilibrio electrónico de 3 cm equivalentes agua no implica que el factor de corrección sea igual a la unidad. De hecho, el tipo de diodo que presenta el mayor factor de corrección (5%) es el Isorad-p (geometría cilíndrica) que tiene un capuchón de 3.3 cm equivalentes agua. Este factor de corrección significativamente más alto, corrobora la hipótesis de que dicho factor de corrección está relacionado con la metodología de calibración. Este diodo detecta muchos menos fotones dispersos que la cámara situada a 3 cm de profundidad. El diodo QED 1116 es el que tiene los valores menores de este factor de corrección, ya que al tener un capuchón de grosor intermedio entre los EDP30 y los Isorad- p 1164, es el que mejor compensa la falta de contribución de los fotones dispersos por el maniquí, con la contaminación fotónica y electrónica que proviene del cabezal.

El factor de corrección por bandeja está relacionado con el grosor del capuchón, siendo prácticamente despreciable (para todos los tamaños de campo a excepción del 40 x 40 cm^2) para los diodos con el capuchón más grueso (Isorad-p 1164 y P30).

El factor de corrección por la distancia foco superficie (DFS) está relacionado con la dependencia de la respuesta del diodo en función de la tasa de dosis y con la contaminación electrónica y fotónica de baja energía. La dependencia de la respuesta en función de la tasa de dosis también se ha relacionado con el tipo de diodo (n o p) [11]. A partir de la figura 6.16 se observa que el diodo que presenta más dependencia es el P30, siendo la diferencia respecto al resto de los diodos más significativa para las altas tasas. Sería de esperar, por ejemplo, que los diodos EDP30 tuviesen un factor de corrección a DFS pequeñas mucho menor que los P30. Sin embargo, los valores del factor de corrección para distancia foco superficie igual a 80 cm para los distintos tipos de diodos no son tan diferentes, siendo esto compatible con el hecho de que debido a su capuchón de equilibrio electrónico, los EDP30 detectan más contaminación electrónica y fotónica de baja energía. El mismo razonamiento se puede aplicar para DFS mayores de 100 cm.

La dependencia de la respuesta del diodo con la tasa de dosis y con el espectro energético son los responsables del factor de corrección por cuña (tabla 6.4).

El factor de corrección por ángulo de incidencia depende exclusivamente de la geometría del capuchón. Sólo es igual a la unidad cuando el diodo tiene simetría cilíndrica (Isorad-p) (tabla 6.5). Sin embargo, este tipo de diodos presentan el inconveniente de crear una perturbación del campo de irradiación en profundidad mucho mayor (tabla 6.1b).

La variación de la sensibilidad con la temperatura varía entre 0.15%/ºC hasta 0.30%/ºC, siendo los diodos P30 los que presentan menor variación. Sólo debe corregirse la respuesta cuando los diodos permanecen sobre el paciente un tiempo suficiente (5 min. mínimo) para que alcancen el equilibrio térmico.

La pérdida de sensibilidad con la dosis acumulada es significativamente mayor para los EDP30 (tabla 6.5), ya que son los diodos que han recibido una dosis de preirradiación menor (tabla 6.1b). Este tipo de diodos, por tanto, deben recalibrarse con una frecuencia 7 veces mayor que los otros tipos de diodos estudiados.

Si se aplican todos los factores de corrección a la lectura del diodo se puede determinar la dosis entrada con una precisión de un 0.2% -0.3%(1DE) dependiendo

del tipo de diodo y cuando no se utilizan filtros en cuña. Si se utilizan filtros de 60º esta precisión disminuye hasta un 2.5% para los P30. Puesto que los límites de tolerancia en las dosis entrada determinadas *in vivo* deben estar de acuerdo con la precisión de las medidas, el límite de tolerancia en campos con cuña debe ser mayor que para los campos sin cuña. Sin embargo, se está trabajando para mejorar la precisión en la determinación del factor de corrección por filtro en cuña. La definición de los límites de tolerancia, y de las acciones a seguir cuando se superan éstos es de extrema importancia. Un número elevado de repeticiones de las dosimetrías *in vivo* pondrán en duda la utilidad de estos controles y en consecuencia puede inducir al desencanto entre el personal técnico de las unidades de tratamiento. El límite de tolerancia debe definirse en función de la precisión con la que se mide la dosis in vivo y de la reproducibilidad de las medidas en el paciente. Por tanto, no será el mismo para un campo tangencial de mama (angulación, filtros en cuña) que para un campo directo sin protecciones ni filtros en cuña.

7.4 Bibliografía

[1] R. Miralbell, M. Rouzaud, E. Grob, P. Nouet, S. Bieri, S. Majno, P. Botteron, M. Montero y J.C. Precoma. **Can an optimized total body irradiation technique be fast and reproducible?** Int. J. Radiat. Oncol. Biol. Phys., vol 29: 1167-1173. 1994.

[2] M. Ribas, N. Jornet, T. Eudaldo et al. **Midplane dose determination during total body irradiation using *in vivo* dosimetry**. Radiother. Oncol. 49: 91-98, 1998.

[3] G. J. Meijer, A. W. H. Minken, M. Karel et al. **Accurate *in vivo* dosimetry of a randomized trial of porstate cancer irradiation**. Int. J. Radiat. Oncol. Biol. Phys. 49, nº 5: 1409-1418, 2001.

[4] R. Sjögren, M. Karlsson. **Influence of electron contamination on *in vivo* surface dosimetry for high-energy photon beams**. Med. Phys., 25; 916-921, 1998.

[5] B. Nilsson, B.I. Rudén y B. Sorcini. **Characteristics on silicon diodes as patients dosemeters in external radiation therapy.** Radiother. Oncol., 11: 279-288. 1988.

[6] G. Rikner, E. Grussell. **Evaluation of temperature effects in p-type silicon detectors.** Phys. Med. Biol. vol 31: 527-534. 1986.

[7] J. Van Dam, G. Leunens y A. Dutreix. **Correlation between temperature and dose rate dependence of semiconductor response; influence of accumulated dose.** Radiother. Oncol., 19: 345-351. 1990.

[8] A. Rizzotti, C. Compri, G.F. Garussi. **Dose evaluation to patients irradiatied by Co-60 beams, by means of direct measurements on the incident and on the exit surfaces.** Radiother. Oncol. 34: 144-151. 1985.

[9] G. Leunens, A. Dutreix, E. Van der Schueren. **Quality assurance in radiotherapy by *in vivo* dosimetry. 1. Entrance dose measurements, a reliable procedure**. Radiother. Oncol. 17; 141-151, 1990.

[10] S. Heukelom, J.H. Lanson y B.J. Mijnheer. **Comparison of entrance and exit dose measurements using ionization chambers and silicon diodes**. Phys. Med. Biol. 36: 47-59, 1991.

[11] G. Rikner y E. Grusell. **Effects of radiation damage on p-type silicon detectors. Phys. Med. Biol.**, 28: 1261-1267, 1983.

CAPÍTULO 8

CONCLUSIONES

8.1 Introducción

El objetivo de este trabajo ha sido la puesta a punto de la técnica de dosimetria *in vivo* con detectores de semiconductor (diodos) para medir la dosis en una técnica especial, la irradiación corporal total (ICT), y como control de calidad sobre la dosis administrada en técnicas estándar con haces de RX de alta energía.

Para ello, se ha establecido una metodología de calibración de diodos y se han implementado algoritmos de cálculo para determinar la dosis en el punto ICRU a partir de la medida de la dosis *in vivo* en la entrada y en la salida del haz. Aunque en esta tesis se aplican estos algoritmos al cálculo de la dosis en distintos puntos de interés en el paciente para la técnica de ICT, estos algoritmos son también aplicables a técnicas estándar de tratamiento una vez determinados los factores de corrección y las curvas de Rizzotti en estas condiciones. Se estudia la aplicabilidad de estos algoritmos en presencia de heterogeneidades (pulmón) en la técnica de ICT y detrás de protecciones de *cerrobend* de distinto espesor.

A medida que la energía de RX aumenta, se hace necesario un capuchón de equilibrio electrónico más grueso para que el diodo mida bajo condiciones de equilibrio electrónico. Esto conlleva un aumento de la perturbación del haz de radiación y por tanto una infradosificación del volumen que se quiere tratar. Algunos fabricantes de diodos han optado por no dotar a sus diodos del grosor de capuchón electrónico necesario. En esta tesis se han caracterizado y calibrado 4 tipos distintos de diodos comercializados para altas energías de RX y se relacionan las características estos diodos con los valores de los factores de corrección obtenidos.

8.2 Conclusiones

1. Debido a la asimetría antero-posterior de la respuesta de los diodos de geometría semiesférica es necesario calibrar los diodos a la entrada y a la salida del haz. En el caso de los diodos EDP30 y en condiciones de ICT, utilizar el factor de calibración entrada para diodos colocados a la salida del haz implicaría una sobrestimación de la dosis de un 25%.

2. La técnica de ICT escogida en nuestro centro conlleva la utilización de protecciones de *cerrobend* de transmisión parcial para reducir la dosis a pulmón. Los diodos que miden la dosis *in vivo* detrás de estas protecciones necesitan una calibración específica. Si se utilizara el factor de calibración entrada sin protecciones cuando se mide detrás de protección, la dosis se infraestimaría en un 30-35%. Esta infraestimación es debida a que detrás de la protección hay una disminución de tasa de dosis y un cambio en la calidad del haz de radiación y por tanto el diodo tiene menor sensibilidad.

3. Al interponer los bloques los bloques de *cerrobend* para proteger el pulmón en la técnica de ICT, el factor de calibración entrada ($F_{en,cer}$) depende del grosor de los bloques. A medida que el grosor aumenta, la sensibilidad del diodo disminuye y por tanto, el factor de calibración entrada aumenta. Esta dependencia se puede evitar añadiendo un capuchón de equilibrio adicional sobre el diodo de manera que en total tenga un capuchón de 3 cm equivalentes agua y calibrando respecto a la medida de dosis con cámara de ionización colocada a 3 cm de profundidad dentro del maniquí.

4. El algoritmo simple propuesto en nuestro centro para calcular la dosis a plano medio en ICT (media aritmética entre la dosis entrada y la dosis salida corregida por un factor determinado experimentalmente) es igual de preciso que el método de Rizzotti. Este algoritmo simple presenta la ventaja de ser más fácil de aplicar y dado que el factor de corrección (CF) es muy próximo a 1 (fig. 4.1(a)), la dosis a plano medio es de cálculo inmediato a partir de las dosis entrada y salida.

5. El algoritmo simple permite calcular la dosis en pulmón.). En el caso de que se utilicen las protecciones de transmisión parcial para el pulmón, debe utilizarse el

grosor equivalente agua para determinar el factor de corrección CF'. Este factor se determina detrás de las protecciones. En este caso también es necesaria una calibración especial de los diodos.

6. Dado que el factor de corrección para calcular la dosis a partir de la media entre la dosis entrada y la dosis salida detrás de las protecciones de *cerrobend* (CF') no es despreciable y que se debe calcular el grosor tejido equivalente, el método de Rizzotti seria, en este caso, más conveniente.

7. No aplicar el factor de corrección por temperatura a las lecturas de los diodos, en la técnica de ICT, representaría una sobreestimación de la dosis de aproximadamente 3%.

8. Existen diferentes tipos de diodos disponibles comercialmente que difieren en el nivel de preirradiación, el tipo y nivel de dopaje, diseño y grosor del capuchón de equilibrio electrónico. Es necesario conocer como cada una de estas características influyen en la respuesta del diodo para poder utilizar los diodos para dosimetria *in vivo* de una forma adecuada dentro la práctica clínica.

9. El grosor equivalente agua del capuchón de equilibrio electrónico de los EDP30 determinado experimentalmente (14 mm) no coincide con el especificado por el fabricante (30 mm).

10. La metodología utilizada para calibrar los diodos es responsable de algunos de los factores de corrección. Es decir, aunque el diseño del capuchón y la naturaleza del diodo tienen influencia sobre el valor de los factores de corrección, el hecho de que la respuesta del diodo, fijado sobre la superficie del maniquí, se compare con la respuesta de una cámara de ionización dentro del maniquí y a la profundidad del máximo de dosis hace que el valor de algunos factores de corrección nunca puedan ser 1.

11. Los nuevos diodos tipo n (P30) no presentan una diferencia significativa en la dependencia de su respuesta con la tasa de dosis con respecto a los diodos tipo p. Esta dependencia, descrita para los Isorad-n (antiguos diodos tipo n), podría estar asociada al nivel de dopaje de los diodos y no al tipo de dopaje.

12. Así mismo, la pérdida de sensibilidad con la dosis acumulada no depende tanto del tipo de diodo, como de la dosis de preirradiación.

13. En la implementación en la rutina clínica de la dosimetría *in vivo* como control de calidad de los tratamientos, es esencial definir en primer lugar, los límites de tolerancia de las medidas *in vivo* y en segundo lugar, que acciones deben seguirse cuando las dosis medidas no están dentro de estos límites. Estos límites deben fijarse en función del tipo de errores que se quieren detectar y de la precisión que se puede alcanzar en las medidas *in vivo*.

8.3 Investigaciones futuras

A partir de esta tesis, se abren dos líneas de investigación. La primera pretende profundizar en la calibración de los diodos no sólo en haces de fotones sino también en haces de electrones. La segunda se focaliza en el desarrollo de algoritmos de cálculo para determinar la dosis en presencia y dentro de heterogeneidades a partir de dosis entrada y dosis salida determinadas *in vivo*, tanto en la técnica de ICT como en técnicas estándar.

Dentro de la primera línea se están realizando estudios sobre la independencia de los factores de corrección, sobre si es necesaria la aplicación de factores de corrección cuando se conforman los campos y, si lo es, cómo deberían aplicarse y, por último se están poniendo a punto protocolos de calibración de los diodos para dar la dosis a la salida. También se ha finalizado la calibración de diodos para medir la dosis *in vivo* en tratamientos con haces de electrones y actualmente se están analizando los resultados.

Dentro de la segunda línea, se pretende en primer lugar determinar la dosis dentro del tejido blando en el punto de prescripción de dosis cuando el haz atraviesa heterogeneidades simétricas o asimétricas a partir de la dosis entrada y la dosis salida determinadas *in vivo*. En segundo lugar, se pretende determinar la dosis dentro de las heterogeneidades con medidas ionométricas y posteriormente utilizar la dosimetría *in vivo* para calcularla.

CURRICULUM VITAE

Nacida en Barcelona el 11 de Setiembre de 1968. Licenciada en Ciencias Físicas por la Universidad Autónoma de Barcelona en Junio del año 1991. En 1992 obtuvo el título de tercer ciclo “Diplôme d’Études Approfondis en Physique Radiologique et Médicale” en el Centro de Energía Atómica de la Universidad Paul Sabatier de Toulouse y la Universidad París III de París. Magister en ciencias Físicas de la Universidad Autónoma de Barcelona en 1997.

Es físico adjunto del Servicio de Radiofísica y Radioprotección del Hospital de la Santa Creu i Sant Pau desde Marzo del año 1993. Desde 1999 es especialista en Radiofísica Hospitalaria. Ha participado como investigadora en dos proyectos del Fondo de Investigación Sanitaria: “Optimización de la evaluación de la dosis en tratamientos de terapia de alta energía mediante el desarrollo de técnicas de dosimetría in vivo y de simulación por Montecarlo” y “Dosimetría in vivo en terapia de alta energía. Intercomparación mediante detectores semiconductores y termoluminiscentes”. Coautora de 25 trabajos presentados en congresos de Física Médica nacionales e internacionales.

Lista de publicaciones :

Intercomparison between two different in vivo dosimetry diodes for 16 to 25 MV energy range. N. Jornet, M. Ribas, T. Eudaldo. Med. Phys. Vol. 27-6, 1287-1293, 2000.

Characteristics of LiF:Mg,Cu,P for clinical application M. Ginjaume, X. Ortega, M. A. Duch, N. Jornet y A. Sánchez-Reyes. Radiat. Prot. Dosim. Vol. 85, nº 1-4, 389-391, 1999.

Dosimetric evaluation of a *plastic water* phantom for high energy photon beam use. N. Jornet, T. Eudaldo, M.D. Carabante, M. Ribas. Radiother. Oncol. Vol.51 supplement 1, 155, 1999.

Midplane dose determination using in vivo dosimetry in total body irradiation technique. M. Ribas, N. Jornet, T. Eudaldo, D. Carabante, M.A. Duch, M. Ginjaume, G. Gomez de Segura, F. Sanchez Doblado. Radiother. Oncol. 335, 91-98, 1998.

Test de aceptación de diodos para ser utilizados en dosimetría in vivo. N. Jornet, M. Ribas, T. Eudaldo, M.D. Carabante. Boletín S.E.F.M. nº 7, 1998.

A comparison of two in vivo dosimetry procedures in total body irradiation technique. M.A. Duch, N. Jornet, M. Ginjaume, M. Ribas, X. Ortega. Med. Biol. Eng. Com. Vol. 35, supplement part 2: 1038, 1997.

Quality assurance in radiotherapy by in vivo dosimetry with diodes during prostatic treatments. N. Jornet, M. Ribas, T. Eudaldo et al. Med. Biol. Eng. Com. Vol. 35, supplement part 2: 1082, 1997.

Calibration of semiconductor detectors for dose assessment in total body irradiation. N. Jornet, M. Ribas, T. Eudaldo. Radiother. Oncol. 38: 247-251, 1996.